

---

---

---

**CHAPTER****6**

---

---

---

---

# Perturbation Formalism

---

In Chapter 4, we studied the various instability mechanisms using highly simplified models in which the particle beam was modeled either as a single point charge without any internal structure, or as two point charges interacting with each other through wake fields. This approach offers intuitive pictures of the physics of several collective instabilities encountered in high intensity circular accelerators. Similar simplified models were applied in Chapter 3 to the case of linear accelerators.

However, these simplified macroparticle models have their limitations. One limitation is that their quantitative predictions can be rather crude. Another is that the instabilities are treated one by one, and it may be desirable to have a more formal treatment that allows them to be cast into one framework. Still another limitation, which is perhaps more serious, is the fact that some instabilities observed in circular accelerators involve higher oscillation modes in the longitudinal structure of the beam that are not properly treated by the simplified models.

Figure 6.1 gives sketches of a few of the collective modes of the beam motion. We use the symbol  $l$  to denote the longitudinal mode number. In contrast, we have been using the index  $m$  to denote the transverse modes. Two-particle models clearly do not suffice for studying any mode with mode number higher than  $l = 2$ .

**Exercise 6.1** Extend Figure 6.1 to include the  $m = 2$  modes.

The mode frequencies depend on the beam intensity. Figure 6.2 is a sketch of what is expected of this dependence. The  $(m, l)$  mode has an

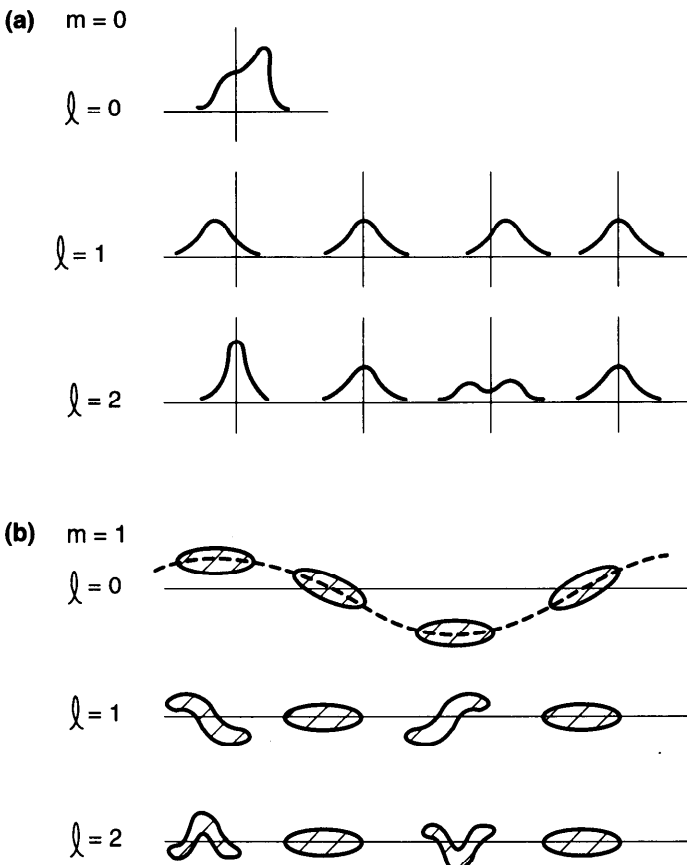


**Figure 6.1.** Sketches of the lowest few modes in the longitudinal structure of the beam. Successive snapshots are taken for each mode as the beam executes collective (a) longitudinal ( $m = 0$ ) and (b) transverse ( $m = 1$ ) motions. These sketches depict the behavior at low beam intensities. The mode patterns become more complicated as the beam intensity increases. The mode with  $m = 0$  and  $\ell = 0$  is a static mode.

unperturbed frequency of  $m\omega_B + l\omega_s$  at zero beam intensity  $N = 0$ . As  $N$  increases, the mode frequencies shift. There are a few general rules—reflected in Figure 6.2—for how these mode frequencies shift with beam intensity. These are: (i) The ( $m = 0, l = 0$ ) mode frequency stays zero for all beam intensities. (ii) For short bunches, the ( $m = 1, l = 0$ ) and the ( $m = 2, l = 0$ ) modes shift down with increasing beam intensity. (iii) For short bunches, the ( $m = 1, l \neq 0$ ) modes tend to shift up with increasing beam intensity. For long bunches, these modes tend to shift down. (iv) The ( $m = 0, l = \pm 1$ ) modes do not shift for small to medium beam intensities. These facts will be explained as we proceed.

We assume in general that  $\omega_B \gg \omega_s$ . As a result, when we consider the mode coupling effects in Sections 6.5 and 6.7, we do not consider coupling

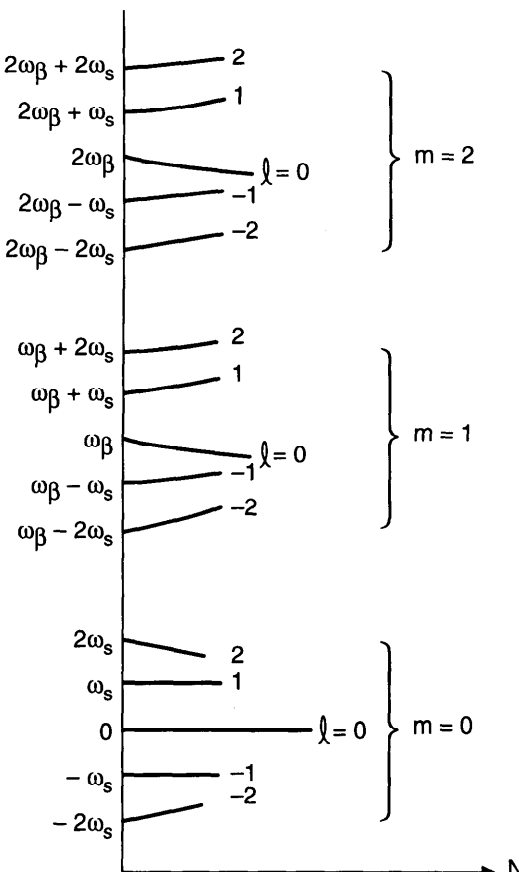


**Figure 6.2.** Sketch of the dependence of the mode frequencies on the intensity  $N$  for a short bunched beam. Ignoring the radial modes, a mode is specified by its transverse mode index  $m$  and longitudinal index  $\ell$ . When  $N = 0$ , the mode frequencies are given by  $m\omega_\beta + l\omega_s$ . As  $N$  increases, the mode frequencies shift, obeying some general rules mentioned in the text.

among modes with different  $m$ 's. The modes in Figure 6.2 therefore form three disjoint clusters, specified by  $m = 0, 1$ , and  $2$ , respectively. Figure 6.2 also does not include the radial modes, which are the subject of Section 6.4. The consideration of radial modes would result in a splitting of each mode frequency in Figure 6.2 into a family of frequencies.

One could, of course, increase the number of macroparticles in the simplified model, but when there are more than two macroparticles in the system, the analysis along this line becomes cumbersome. A computer simulation may be used to extend the model to anywhere from three to several thousand macroparticles, but then dealing with  $10^{12}$  particles this way seems hopeless.

The solution to this difficulty is to go to the other extreme, in which ideally one would have an infinite number of particles, and then apply the result to

our  $10^{12}$ -particle system. In this approach, the motion of the beam is described by a superposition of modes, rather than a collection of individual particles.

In principle, the mode representation and the particle representation of the beam motion are identical. To describe fully  $10^{12}$  particles, one needs  $10^{12}$  modes, and vice versa. The detailed methods of analysis in the two approaches are different—the particle representation usually is conveniently treated in the time domain, while in the mode representation the frequency domain is more convenient—but, in principle, they necessarily give the same final results.

In practice, the mode representation offers a formalism that can be used systematically to treat the instability problem and, in many cases, can be used to obtain analytic results for arbitrarily high mode numbers (at least when the mode order is much lower than  $10^{12}$ ). The advantage over the particle representation in these respects will become clear as we proceed.

In Section 6.1, the basic mathematical tool, namely the Vlasov equation,<sup>1</sup> used for the mode representation of the beam motion, will be derived. This technique is applied in all following sections. In Section 6.2, we describe a phenomenon in which the longitudinal wake field distorts the parabolic potential well formed by the accelerating rf voltage, and as a result the longitudinal beam distribution is deformed. Such a phenomenon is depicted as the static mode with  $m = 0$  and  $l = 0$  in Figure 6.1(a).

From Section 6.3 on, a perturbation treatment of the Vlasov equation that leads to the evaluation of the mode frequencies and mode patterns will be presented. The stability of the beam requires that all modes be stable; if any one of the modes shows the potential of growing exponentially, the beam will be unstable. A critical analysis of the modes, therefore, leads to the stability criterion for the beam. The mode analysis that we will follow was largely developed by Sacherer<sup>2</sup> and extended by others.<sup>3</sup> We will also mention work using other approaches when appropriate.<sup>4</sup>

<sup>1</sup>A. A. Vlasov, J. Phys. USSR **9**, 25 (1945). See also, for example, S. Chandrasekhar, *Plasma Physics*, Univ. of Chicago, 1960; Francis F. Chen, *Introduction to Plasma Physics*, Plenum, New York, 1977; J. D. Lawson, *The Physics of Charged-Particle Beams*, Clarendon, Oxford, 1977.

<sup>2</sup>F. Sacherer, CERN Report SI-BR/72-5 (1972); F. Sacherer, IEEE Trans. Nucl. Sci. **NS-20**, 825 (1973); F. J. Sacherer, 9th Int. Conf. High Energy Accel., Stanford, 1974, p. 347; F. J. Sacherer, IEEE Trans. Nucl. Sci. **NS-24**, 1393 (1977); B. Zotter and F. Sacherer, Proc. Int. School Part. Accel., Erice, 1977, CERN Report 77-13, p. 175.

<sup>3</sup>See for example G. Besnier, Nucl. Instr. Meth. **164**, 235 (1979); J. L. Laclare, Proc. 11th Int. Conf. High Energy Accel., Geneva, 1980, p. 526; B. Zotter, CERN Reports SPS/81-18, SPS/81-19, SPS/81-20 (1981); Toshio Suzuki and Kaoru Yokoya, Nucl. Instr. Meth. **203**, 45 (1982); Kohtaro Satoh and Yongho Chin, Nucl. Instr. Meth. **207**, 309 (1983); Toshio Suzuki, Yongho Chin, and Kohtaro Satoh, Part. Accel. **13**, 179 (1983); G. Besnier, D. Brandt, and B. Zotter, Part. Accel. **17**, 51 (1985).

<sup>4</sup>In addition to references mentioned elsewhere, see C. Pellegrini and A. M. Sessler, Nuovo Cimento **3A**, 116 (1971); A. N. Lebedev, *Physics with Intersecting Storage Rings*, Academic Press,

Strictly speaking, in a complete treatment of the beam-surroundings system, an oscillation mode  $\lambda$  is specified by the quantities

$$\psi^{(\lambda)}, \vec{E}^{(\lambda)}, \vec{B}^{(\lambda)}, \text{ and } \Omega^{(\lambda)}, \quad (6.1)$$

where  $\psi^{(\lambda)}$  is the beam distribution function,  $\vec{E}^{(\lambda)}$  and  $\vec{B}^{(\lambda)}$  are the electromagnetic wake fields, and  $\Omega^{(\lambda)}$  is the mode frequency that describes the time dependence of  $\psi^{(\lambda)}$ ,  $\vec{E}^{(\lambda)}$ , and  $\vec{B}^{(\lambda)}$ . To study such a problem would require setting up and solving the "Vlasov-Maxwell" equations in which  $\vec{E}^{(\lambda)}$  and  $\vec{B}^{(\lambda)}$  appear in the Vlasov equation as the force terms and  $\psi^{(\lambda)}$  appears in the Maxwell equation as the source term. This solution scheme is difficult to handle, but fortunately it is also not necessary for our purpose. What we have done previously has allowed us to express  $\vec{E}^{(\lambda)}$  and  $\vec{B}^{(\lambda)}$  directly in terms of  $\psi^{(\lambda)}$  through the wake functions for relativistic beams. By doing so, the number of variables of the problem is greatly reduced, and one needs then only to solve the Vlasov equation for  $\psi^{(\lambda)}$  without having to pay attention to  $\vec{E}^{(\lambda)}$  and  $\vec{B}^{(\lambda)}$ .

The Vlasov equation obtained is nonlinear in  $\psi^{(\lambda)}$ , and we need to linearize it in order to search for the beam oscillation modes. This will be done in Section 6.3. Modes will be found and their stability conditions discussed in Sections 6.4 and 6.5. It turns out that when the beam is unstable, particles will not immediately be lost from the beam, but the bunch length and the energy spread of the beam will increase; we will describe this phenomenon also in Section 6.5.

Sections 6.2 through 6.5 treat the longitudinal motions. The Sacherer formalism also applies to the transverse dipole motion of the beam. This will be treated in Sections 6.6 and 6.7. The remaining two sections of the chapter, Sections 6.8 and 6.9, deal with the special case of beams with multiple bunches and the case of unbunched beams, respectively.

## 6.1 THE VLASOV EQUATION

The Vlasov equation describes the collective behavior of a multiparticle system under the influence of electromagnetic forces. To construct the Vlasov equation, one starts with the single-particle equations of motion

$$\begin{aligned}\dot{q} &= f(q, p, t), \\ \dot{p} &= g(q, p, t),\end{aligned}\quad (6.2)$$

---

New York, 1971, p. 184; R. D. Kohaupt, DESY Report 80/22 (1980); R. D. Ruth, Ph.D. Thesis, BNL Report 51425 (1981); C. Pellegrini, *AIP Proc.* **87**, *Phys. High Energy Part. Accel.*, Fermilab, 1981, p. 77; Jiunn-Ming Wang, *AIP Proc.* **153**, *Phys. Part. Accel.*, Fermilab 1984 and SLAC 1985, p. 697; S. Y. Lee and J. M. Wang, *IEEE Trans. Nucl. Sci.* **NS-32**, 2323 (1985).

where  $q$  and  $p$  are the coordinate and momentum variables, respectively, and the  $(q, p)$  plane is the phase space. The state of a particle at a given time  $t$  is represented by a point in the phase space. The motion of a particle is described by the motion of its representative point. For a particle executing a simple harmonic motion, for example, its representative point in phase space traces out an ellipse. We often do not distinguish between the representative point in phase space and the particle itself in real space; although somewhat ambiguous, this should not cause much confusion.

In a conservative deterministic system, the particle trajectory in phase space is completely determined by the initial conditions  $(q_0, p_0)$  at time  $t = t_0$ .<sup>5</sup> Two particles having the same initial conditions must have exactly the same trajectory in phase space. It follows that the only way for two trajectories to meet at a given time is for them to coincide at all times. In other words, trajectories either completely coincide or never intersect.

Consider now a distribution of particles occupying an area in the phase space. Because they cannot intersect with particles on the boundary of the distribution as the distribution evolves in time, particles inside the distribution cannot leak out by crossing the boundary. Similarly, no particles from outside can penetrate into the distribution.

If the system is conservative, i.e., if the system is not influenced by any damping or diffusion effects due to external sources,<sup>6</sup> we have the conditions that

$$f = \frac{\partial H}{\partial p} \quad \text{and} \quad g = -\frac{\partial H}{\partial q}, \quad (6.3)$$

where  $H$  is the Hamiltonian. It follows that

$$\frac{\partial f}{\partial q} + \frac{\partial g}{\partial p} = 0. \quad (6.4)$$

As will be seen in Eq. (6.10), the condition (6.4) leads to an area conservation property: as the particle distribution evolves in the phase space, its shape may be distorted but its area remains constant. In fact, in a nonconservative system, the left hand side of Eq. (6.4) has the physical meaning of the rate of area shrinkage.

<sup>5</sup>In particular, one does not need to know  $\ddot{q}_0$ ; this follows from the fact that Newton's equation is a second order differential equation in time.

<sup>6</sup>It is possible that the degrees of freedom of the system are coupled among themselves *internally* so that motions in some degrees of freedom grow exponentially at the expense of having some other motions damped. In fact, this possibility of damping and antidamping through internal couplings is the origin of beam instability we are studying. One way of telling whether the damping and antidamping come from an external source or an internal source is to sum over the growth rates of all modes (provided they can be found); the sum should vanish for an internal source. See Eqs. (4.120) and (6.217).

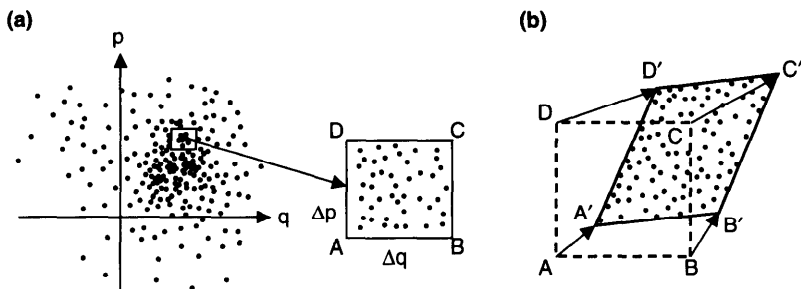


**Figure 6.3.** (a) Phase space distribution of particles at time  $t$ . A rectangular box  $ABCD$  with area  $\Delta q \Delta p$  is drawn and magnified. (b) At a later time,  $t + dt$ , the box moves and deforms into a parallelogram with the same area as  $ABCD$ . All particles inside the box move with the box.

In Figure 6.3(a) we have sketched the distribution of a group of particles in the phase space at time  $t$ . A rectangular  $\Delta q \Delta p$  box is then drawn:

$$\begin{aligned} & A(q, p), \\ & B(q + \Delta q, p), \\ & C(q + \Delta q, p + \Delta p), \\ & D(q, p + \Delta p). \end{aligned} \quad (6.5)$$

The box is small enough so that the numbers of particles contained in adjacent boxes of the same size—if drawn—are about equal. The box is also large enough so that it contains at least several particles.

Let the number of particles enclosed by the box be

$$\psi(q, p, t) \Delta q \Delta p, \quad (6.6)$$

where  $\psi$  is the phase space distribution density depending on  $q$ ,  $p$ , and  $t$  and is normalized by

$$\int_{-\infty}^{\infty} dq \int_{-\infty}^{\infty} dp \psi(q, p, t) = N, \quad (6.7)$$

with  $N$  the total number of particles in the system.

At time  $t + dt$ , the box has moved to  $A'B'C'D'$  as shown in Figure 6.3(b). We have used  $\Delta q$  and  $\Delta p$  (rather than  $dq$  and  $dp$ ) to denote the dimensions of the box, but have used  $dt$  to denote the time increment. This is because we do not want the box size to be vanishingly small, but  $dt$  should be considered truly infinitesimal.

In general, the rectangular box deforms into a parallelogram. (The only case in which the rectangular box remains rigid in shape as time evolves is

simple harmonic motion.) The vertices of the parallelogram are

$$\begin{aligned} A' &[q + f(q, p, t) dt, p + g(q, p, t) dt], \\ B' &[q + \Delta q + f(q + \Delta q, p, t) dt, p + g(q + \Delta q, p, t) dt], \\ C' &[q + \Delta q + f(q + \Delta q, p + \Delta p, t) dt, \\ &\quad p + \Delta p + g(q + \Delta q, p + \Delta p, t) dt], \\ D' &[q + f(q, p + \Delta p, t) dt, p + \Delta p + g(q, p + \Delta p, t) dt]. \end{aligned} \quad (6.8)$$

The condition that no particles leak into or out of the box gives

$$\psi(q, p, t) \text{ area}(ABCD) = \psi(q + f dt, p + g dt, t + dt) \text{ area}(A'B'C'D'). \quad (6.9)$$

For a Hamiltonian system, the condition (6.4) implies the area of the box is conserved:

$$\begin{aligned} \text{area}(A'B'C'D') &= \left| \overrightarrow{A'B'} \times \overrightarrow{A'D'} \right| \\ &= \Delta q \Delta p \left[ 1 + \left( \frac{\partial f}{\partial q} + \frac{\partial g}{\partial p} \right) dt \right] \\ &= \Delta q \Delta p = \text{area}(ABCD). \end{aligned} \quad (6.10)$$

Equation (6.9) then gives

$$\begin{aligned} \psi(q, p, t) &= \psi(q + f dt, p + g dt, t + dt) \\ &= \psi + \frac{\partial \psi}{\partial q} f dt + \frac{\partial \psi}{\partial p} g dt + \frac{\partial \psi}{\partial t} dt, \end{aligned} \quad (6.11)$$

or, after canceling out  $\psi$  on both sides,

$$\frac{\partial \psi}{\partial t} + f \frac{\partial \psi}{\partial q} + g \frac{\partial \psi}{\partial p} = 0. \quad (6.12)$$

Equation (6.12) is the *Vlasov equation*—particularly when the forces involved are electromagnetic in origin. It can also be put in the form

$$\frac{d\psi}{dt} = 0, \quad \text{or} \quad \psi = \text{const in time.} \quad (6.13)$$

Equation (6.13), sometimes loosely referred to as the *Liouville theorem*,<sup>7</sup> states that the local particle density does not change if (an important if) the observer moves with the flow of boxes, but it does not tell how the boxes flow. The Vlasov form (6.12), on the other hand, does not have this ambiguity, since it contains explicitly the single-particle information  $f$  and  $g$ .

Strictly speaking,  $f$  and  $g$  are given by external forces. Collisions among discrete particles in the system, for example, are excluded. However, if a particle interacts more strongly with the *collective* fields of the other particles than with its nearest neighbors, the Vlasov equation still applies if one treats the collective fields on the same footing as the external fields. This in fact forms the basis of treating the collective instabilities using the Vlasov technique.

One special case where the Vlasov equation (6.12) can be solved exactly is when the system is described by a Hamiltonian  $H(q, p)$  which does not have an explicit time dependence. Using the properties (6.3), a stationary solution to Eq. (6.12) is found to be

$$\psi(q, p) = \text{any function of } H(q, p). \quad (6.14)$$

In this system, individual particles stream along constant-Hamiltonian contours in the phase space in such a way that the overall distribution is stationary.

**Exercise 6.2** Solve the Vlasov equation for a system of particles subject to simple harmonic motions with Hamiltonian  $H = \omega(q^2 + p^2)/2$ . Show that the Vlasov equation can be written as

$$\frac{\partial\psi}{\partial t} + \omega \frac{\partial\psi}{\partial\phi} = 0 \quad (6.15)$$

and its general solution is

$$\psi(q, p, t) = \text{any function of } (r, \phi - \omega t), \quad (6.16)$$

where  $r$  and  $\phi$  are the polar coordinates defined by  $q = r \cos \phi$  and  $p = -r \sin \phi$ . Once the initial distribution of the beam is given at  $t = 0$ , Eq. (6.16) means that the distribution at time  $t$  is obtained by rigidly rotating the initial distribution in phase space angle  $\phi$  at a constant angular speed of  $\omega$ . A stationary distribution is any function of  $r$  without dependence on  $\phi$ , or equivalently, any function of the Hamiltonian  $H$ .

<sup>7</sup>The Vlasov equation applies to a system of many particles. Strictly, the Liouville theorem applies to an *ensemble* of many systems, each containing many particles. It describes the conservation of density of the ensemble in the  $2N$ -dimensional  $\Gamma$ -space and applies to situations much more general than that considered here, such as when collisions among discrete particles are included.

**Exercise 6.3** Consider a damped simple harmonic motion with  $f = \omega p$  and  $g = -\omega q - 2\alpha p$ , where  $\alpha > 0$  is the damping rate. The Vlasov equation needs to be modified here because the conservation of phase space area is violated. Following the derivation from Eq. (6.9) to Eq. (6.12), show that the modified Vlasov equation reads

$$\frac{\partial \psi}{\partial t} + \omega p \frac{\partial \psi}{\partial q} - (\omega q + 2\alpha p) \frac{\partial \psi}{\partial p} = 2\alpha \psi. \quad (6.17)$$

Note that a straightforward substitution of  $f$  and  $g$  into the form (6.12) would lose the term on the right hand side of Eq. (6.17). Note also that  $\partial f / \partial q + \partial g / \partial p = -2\alpha$  is negative, which means the area of phase space boxes shrinks with time according to Eq. (6.10). Show that the general solution of Eq. (6.17) is

$$\psi(q, p, t) = e^{2\alpha t} \times (\text{any function of } A \text{ and } \Phi), \quad (6.18)$$

where

$$\begin{aligned} A^2 &= e^{2\alpha t} \left( q^2 + p^2 + \frac{2\alpha}{\omega} qp \right), \\ \Phi &= \tan^{-1} \left( \frac{\omega p + \alpha q}{q\sqrt{\omega^2 - \alpha^2}} \right) + \sqrt{\omega^2 - \alpha^2} t. \end{aligned} \quad (6.19)$$

Equation (6.18) is that of a distribution peaking up while spiraling inward with time.

In the derivation of the Vlasov equation, we have assumed that there are no significant diffusion or external damping effects. This is usually a good approximation for proton beams. For electron beams, synchrotron radiation contributes to both damping and diffusion,<sup>8</sup> and one needs to modify the Vlasov equation accordingly to obtain another equation called the *Fokker-Planck equation*.<sup>9</sup> Strictly speaking, our results obtained using the Vlasov equation apply only to protons and not electrons. However, when the instability occurs in a time shorter than the damping or diffusion times, the Vlasov treatment can apply also to electrons. The treatment of collective instabilities using the Fokker-Planck equation is beyond our scope here.<sup>10</sup>

<sup>8</sup>Matthew Sands, *The Physics of Electron Storage Rings, an Introduction*, SLAC Report 121 (1970).

<sup>9</sup>See for example, S. Chandrasekhar, Rev. Mod. Phys. **15**, 1 (1943).

<sup>10</sup>A. Renieri, Frascati Laboratory Report LNF-76/11(R) (1976); Toshio Suzuki, Part. Accel. **14**, 91 (1983).

## 6.2 POTENTIAL-WELL DISTORTION

As a first application of the Vlasov technique, we will study the effect of longitudinal wake fields on a distortion of the equilibrium shape of a beam bunch.<sup>11</sup> The mechanism is a static one; no part of the beam bunch is executing collective oscillation. The extent of the bunch shape distortion depends on the beam intensity; higher beam intensities cause larger distortions. The dynamics of the bunch shape oscillations will be treated in later sections of this chapter.

Consider a bunched beam that travels along the axis of the vacuum chamber pipe in a circular accelerator. We assume the beam does not have any transverse dimension, i.e., the beam has the shape of an infinitesimally thin thread. Such a beam does not generate transverse wake fields; only the  $m = 0$  wake is excited.

Consider now a particle in the beam executing longitudinal synchrotron oscillation. The physical quantities of interest are the longitudinal displacement  $z$  of the particle relative to the bunch center and the relative energy error  $\delta$ . The phase space coordinates  $q$  and  $p$  of the previous section are related to these quantities by

$$q = z \quad \text{and} \quad p = -\frac{\eta c}{\omega_s} \delta, \quad (6.20)$$

where  $\eta$  is the slippage factor defined in Eq. (1.10) and  $\omega_s$  is the synchrotron oscillation frequency.

As mentioned, the Vlasov equation is constructed by first writing down the single-particle equations of motion. In the present case, the equations are

$$z' = -\eta \delta \quad \text{and} \quad \delta' = K(z), \quad (6.21)$$

where a prime means taking derivative with respect to the distance  $s$  along the accelerator circumference. In contrast with Eq. (1.9), we have left the  $\delta'$ -equation open for the time being, except that we do know the function  $K$  cannot depend on  $\delta$ , because the system is conservative. [See Eq. (6.4).]

The Vlasov equation corresponding to Eq. (6.21) is<sup>12</sup>

$$\frac{\partial \psi}{\partial s} - \eta \delta \frac{\partial \psi}{\partial z} + K(z) \frac{\partial \psi}{\partial \delta} = 0, \quad (6.22)$$

<sup>11</sup>C. Pellegrini and A. M. Sessler, Nuovo Cimento **3A**, 116 (1971); B. Zotter, Proc. 4th Advanced ICFA Beam Dynamics Workshop on Collection Effects in Short Bunches, Tsukuba, 1990, KEK Report 90-21.

<sup>12</sup>A subtlety arises if one (incorrectly) uses time  $t$ , instead of  $s$ , as the independent variable here. The point is that the impedance is an object localized in  $s$ , not  $t$ . The difference, however, is negligibly small. What happens is that the quantity  $Z_0^{\parallel}(\omega')/\omega'$  of Eq. (6.74) later will be replaced by  $Z_0^{\parallel}(\omega')/p\omega_0$ , where  $\omega' = p\omega_0 + \omega_s$ . See Toshio Suzuki, Part. Accel. **12**, 237 (1982).

where we will set  $\partial\psi/\partial s = 0$ , since we are looking for a stationary distribution. The general stationary solution can be written as

$\psi(z, \delta) = \text{any function of the Hamiltonian } H,$

$$H = \frac{\eta^2 c^2}{\omega_s} \left[ \frac{\delta^2}{2} + \frac{1}{\eta} \int_0^z K(z') dz' \right]. \quad (6.23)$$

The second integral term in the Hamiltonian is the potential-well term. A simple harmonic system would have a parabolic potential well.

If the potential well is provided by an external rf voltage  $V_{\text{rf}}(z)$ , we have

$$K(z) = \frac{eV_{\text{rf}}(z)}{CE} = \frac{\omega_s^2}{c^2 \eta V'_{\text{rf}}(0)} V_{\text{rf}}(z), \quad (6.24)$$

where  $E$  is the particle energy,  $C$  is the accelerator circumference,  $V'_{\text{rf}}$  is the derivative of  $V_{\text{rf}}$  with respect to  $z$ , and we have used the expression

$$\omega_s^2 = \frac{e\eta c^2 V'_{\text{rf}}(0)}{CE}. \quad (6.25)$$

A practical case is given by  $V_{\text{rf}} = \hat{V} \sin(\omega_{\text{rf}} z/c)$ . The deviation of  $V_{\text{rf}}(z)$  from a linear dependence on  $z$  is a cause of potential-well distortion. The general stationary distribution (6.23) is given by any function of the Hamiltonian

$$H = \frac{\eta^2 c^2}{2\omega_s} \delta^2 + \frac{\omega_s c^2}{\omega_{\text{rf}}^2} \left[ 1 - \cos\left(\frac{\omega_{\text{rf}} z}{c}\right) \right]. \quad (6.26)$$

This Hamiltonian also describes the form of the rf bucket. A stationary distribution must conform to the contours of constant Hamiltonian (6.26) inside the bucket. For small oscillation amplitudes, we have  $K = \omega_s^2 z / \eta c^2$ , the case of simple harmonic motion.

One noteworthy special case of the stationary beam distribution is that given by  $\exp(-\text{const} \times H)$ . This distribution is always Gaussian in  $\delta$ . In case the bunch length is much shorter than the rf wavelength ( $z \ll c/\omega_{\text{rf}}$ ), the familiar quadratic form of the Hamiltonian is reestablished, and the distribution is also Gaussian in  $z$ . As the bunch length increases, the bunch shape deviates from Gaussian; the potential well is distorted by the rf bucket, although the distribution remains Gaussian in  $\delta$ .

There is another reason for the Hamiltonian to deviate from the quadratic form, and thus to cause potential-well distortion, namely, the wake fields of high intensity beams. To illustrate this, consider a bunch that is short compared with the rf wavelength. Let the wake fields be characterized by a wake function  $W_0'(z)$  (integrated over the accelerator circumference), and

assume that the wake has dissipated before the beam completes one revolution. Then the single-particle motion can be described by Eq. (6.21) with

$$K(z) = \frac{\omega_s^2}{\eta c^2} z - \frac{r_0}{\gamma C} \int_z^\infty dz' \rho(z') W'_0(z - z'), \quad (6.27)$$

where the second term is the retarding voltage seen by a particle at longitudinal location  $z$  due to the wake force produced by all particles in front of it;  $\rho(z')$  is the particle density at location  $z'$  and is normalized by

$$\int_{-\infty}^\infty dz \rho(z) = N. \quad (6.28)$$

The corresponding Hamiltonian is

$$H = \frac{\eta^2 c^2}{2\omega_s} \delta^2 + \frac{\omega_s}{2} z^2 - \frac{\eta c^2 r_0}{\omega_s \gamma C} \int_0^z dz'' \int_{z''}^\infty dz' \rho(z') W'_0(z'' - z'). \quad (6.29)$$

The stationary solution to the Vlasov equation must be a function of  $H$ . The complication here, compared with the case of rf bucket distortion, is that the complicated  $z$ -dependence of  $H$  now involves the beam density  $\rho$ , which in turn is determined by the stationary distribution itself. Clearly some self-consistency requirement is involved in solving the problem. Below we will give a few explicit examples of this procedure.

Continuing the Gaussian example mentioned above, even though the  $z$ -dependence is complicated, the stationary distribution maintains its gaussian distribution in  $\delta$ ,

$$\psi(z, \delta) = \frac{1}{\sqrt{2\pi}\sigma_\delta} \exp\left(-\frac{\delta^2}{2\sigma_\delta^2}\right) \rho(z), \quad (6.30)$$

where  $\sigma_\delta$  is the rms beam energy spread.

The Gaussian form and the value of  $\sigma_\delta$  in Eq. (6.30) are arbitrary as long as the collective beam behavior is governed by the Vlasov equation, as in the case of a proton beam. However, if the beam behavior is governed, as for an electron beam, by the Fokker-Planck equation, then Eq. (6.30) with a specific value for  $\sigma_\delta$  will be the unique solution of the stationary beam distribution.

Equation (6.30) matches the stationary solution

$$\psi(z, \delta) \propto \exp\left(-\frac{\omega_s}{\eta^2 c^2 \sigma_\delta^2} H\right). \quad (6.31)$$

Substituting Eq. (6.29) into Eq. (6.31), we obtain a transcendental equation

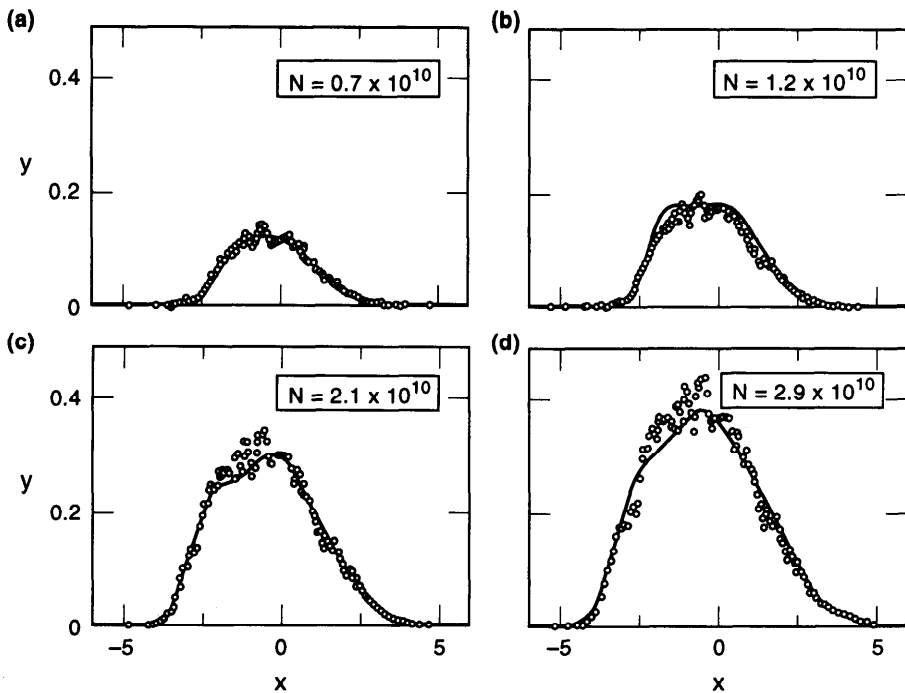


**Figure 6.4.** Potential-well distortion of bunch shape for various beam intensities for the SLC damping ring. The open circles are the measured results. The horizontal axis is  $x = -z / \sigma_{z0}$ , where  $\sigma_{z0}$  is the unperturbed rms bunch length. The vertical scale gives  $y = 4\pi e\rho(z) / V_{rf}(0)\sigma_{z0}$ . (Courtesy Karl Bane, 1992.)

for the line density  $\rho(z)$ ,<sup>13</sup>

$$\rho(z) = \rho(0) \exp \left[ -\frac{1}{2} \left( \frac{\omega_s z}{\eta c \sigma_\delta} \right)^2 + \frac{r_0}{\eta \sigma_\delta^2 \gamma C} \int_0^z dz'' \int_{z''}^\infty dz' \rho(z') W'_0(z'' - z') \right]. \quad (6.32)$$

In the limit of zero beam intensity, the solution reduces to the bi-Gaussian form, where the rms bunch length is related to  $\sigma_\delta$  by  $\sigma_z = \eta c \sigma_\delta / \omega_s$ .

For high beam intensities,  $\rho(z)$  deforms from Gaussian shape. Together with Eq. (6.28), Eq. (6.32) can in principle be solved numerically for  $\rho(z)$  once the wake function  $W'_0(z)$  is known and  $\sigma_\delta$  specified. Figure 6.4 shows the result of one such attempt for the electron damping ring for the SLAC Linear Collider.<sup>14</sup> The bunch shape is Gaussian at low beam intensities, and

<sup>13</sup>J. Haissinski, Nuovo Cimento **18B**, 72 (1973).

<sup>14</sup>Karl L. F. Bane and Ronald D. Ruth, Proc. IEEE Conf. Part. Accel., Chicago, 1989, p. 789.

it distorts as the beam intensity is increased. The calculated bunch shapes agree well with the measured results<sup>15</sup> shown as open circles in Figure 6.4.

One feature of Figure 6.4 is that the distribution leans forward ( $z > 0$ ) as the beam intensity increases. This effect comes from the parasitic loss of the beam bunch, and is a consequence of the real (resistive) part of the impedance. Since the SLC damping ring is operated above transition, the bunch moves forward so that the parasitic energy loss can be compensated by the rf voltage.<sup>16</sup>

Another feature of Figure 6.4 is that the bunch length increases as the beam intensity increases. As we will elaborate later, the bunch shape distortion comes mainly from the imaginary part of the impedance. That the bunch lengthens in Figure 6.4 is a consequence of the fact that the imaginary part of the impedance seen by the beam is mostly inductive.

Another example allowing closed-form solution of Eq. (6.29) occurs when the wake function has the special form

$$W'_0(z) = S\delta'(z), \quad (6.33)$$

where  $\delta(z)$  is the  $\delta$ -function. Under this condition, the retarding wake at location  $z$  can be related to the local derivative of the line density,

$$\int_z^\infty dz' \rho(z') W'_0(z - z') = S\rho'(z). \quad (6.34)$$

The wake field (6.33) can be produced by a purely imaginary impedance

$$Z_0^{\parallel}(\omega) = i \frac{S\omega}{c^2}. \quad (6.35)$$

The quantity  $S$  can be related to the familiar quantity  $Z_0^{\parallel}/n$  by  $S = -i(c^2/\omega_0)(Z_0^{\parallel}/n)$ . Strictly speaking, the frequency dependence of the impedance (6.35) says it is inductive with an inductance  $L = -S/c^2$ , and one has  $S < 0$ ; but we will extend the meaning of this impedance to capacitive impedances by including  $S > 0$ . One physical effect that produces such a wake function is that due to the space charge Coulomb repulsion [see Eq. (2.80)] with

$$S = \frac{2C}{\gamma^2} \left( \ln \frac{b}{a} + \frac{1}{2} \right), \quad (6.36)$$

<sup>15</sup>L. Rivkin et al., *Proc. Euro. Part. Accel. Conf.*, Rome, 1988, p. 634.

<sup>16</sup>In fact, one way to measure the parasitic loss is by measuring the position of the bunch center as a function of beam intensity. And a measurement of parasitic loss as a function of the bunch length is a way to measure the real part of the impedance as a function of frequency. See P. B. Wilson et al., *IEEE Trans. Nucl. Sci.* **NS-24**, 1211 (1977).

where  $b$  is the vacuum chamber pipe radius, and  $a$  is the transverse beam radius.

In the present example, we will not assume a Gaussian solution, but will write the stationary distribution of the beam bunch in the ansatz form

$$\psi(z, \delta) = \begin{cases} \frac{3\eta c N}{2\pi\omega_s \hat{z}_0^3} \sqrt{\hat{z}_0^2 - \frac{1}{\kappa} \left( \frac{\eta c}{\omega_s} \delta \right)^2 - \kappa z^2} & \text{if } \frac{1}{\kappa} \left( \frac{\eta c}{\omega_s} \delta \right)^2 + \kappa z^2 < \hat{z}_0^2, \\ 0 & \text{otherwise,} \end{cases} \quad (6.37)$$

where the dimensionless parameter  $\kappa$ , yet to be found as a function of beam intensity, specifies the degree of distortion of the beam distribution due to the wake fields. The unperturbed beam would have  $\kappa = 1$ . The form (6.37) is such that the unperturbed beam has an elliptical distribution in the phase space; and when perturbed by the wake field, the beam distribution remains elliptical but distorted in such a way that its phase space area (the emittance) is independent of  $\kappa$ , i.e., independent of the beam intensity. The fact that the bunch centroid is located at  $z = 0$  assumes there is no net parasitic loss of the bunch, and this is a consequence of the wake (6.33) being considered.

The distribution (6.37) has a parabolic line density

$$\rho(z) = \frac{3N\sqrt{\kappa}}{4\hat{z}_0^3} (\hat{z}_0^2 - \kappa z^2) \quad \text{if } z < \frac{\hat{z}_0}{\sqrt{\kappa}}. \quad (6.38)$$

The unperturbed beam has a total length  $2\hat{z}_0$ ; the perturbed beam has a total length  $2\hat{z} = 2\hat{z}_0/\sqrt{\kappa}$ .

To be self-consistent, the distribution has to be a function of the Hamiltonian (6.29). Using Eqs. (6.34) and (6.38), we have

$$H = \frac{\eta^2 c^2}{2\omega_s} \delta^2 + \frac{\omega_s}{2} (1 + D\kappa^{3/2}) z^2, \quad (6.39)$$

where

$$D = \frac{3Nr_0\eta c^2 S}{2\omega_s^2 \gamma C \hat{z}_0^3}. \quad (6.40)$$

Comparing Eq. (6.39) with the ansatz (6.37) indicates that the stationary distribution must have the form

$$\psi = \frac{3\eta c N}{2\pi\omega_s \hat{z}_0^3} \sqrt{\hat{z}_0^2 - \frac{2}{\kappa\omega_s} H} \quad (6.41)$$

and that self-consistency requires

$$\kappa^2 - 1 - D\kappa^{3/2} = 0, \quad (6.42)$$

or, in terms of the beam length  $\hat{z}$ , a fourth order equation<sup>17</sup>

$$\left(\frac{\hat{z}}{\hat{z}_0}\right)^4 + D \frac{\hat{z}}{\hat{z}_0} - 1 = 0. \quad (6.43)$$

In the limit of weak beam intensity,  $D = 0$ , we have  $\hat{z} = \hat{z}_0$ . As the beam intensity increases, the beam shape remains parabolic, but its length changes—either shortens or lengthens according to the sign of  $D$ . Figure 6.5(a) illustrates the phase space distributions of the unperturbed ( $D = 0$ ), the shortened ( $D > 0$ ), and the lengthened ( $D < 0$ ) bunches. The solid curve in Figure 6.6 gives the dependence of  $\hat{z}/\hat{z}_0$  on the wake strength parameter  $D$ . For any given value of  $D$ , there is a solution of  $\hat{z}$ . The bunch lengthens below transition and shortens above transition if the impedance is capacitive. The opposite holds if the impedance is inductive.

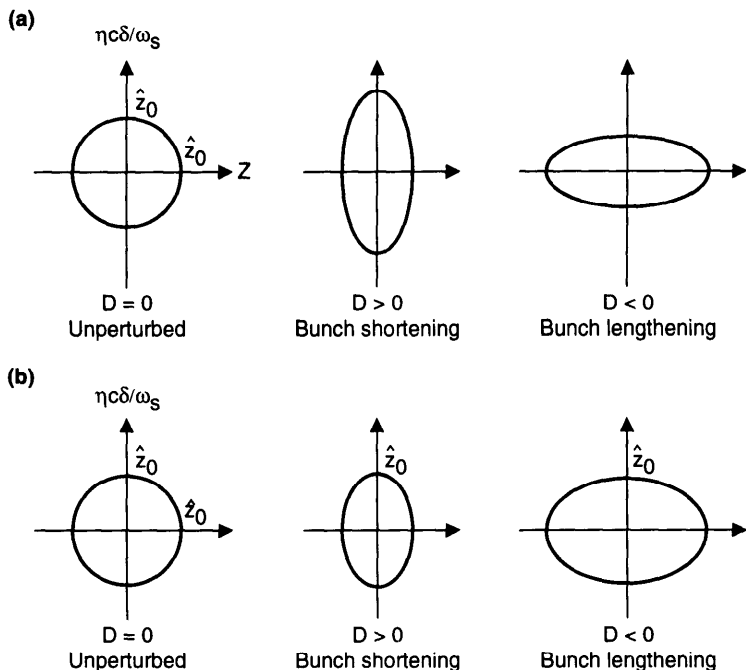


**Figure 6.5.** (a) The unperturbed and the potential-well distorted beam distributions in phase space for model (6.37) with the wake function (6.33). (b) Same as (a), but for the model (6.44). The phase space area is held fixed in (a). The maximum extent of  $\delta$  is held fixed in (b).

<sup>17</sup>A. Hoffman, *Frontiers of Particle Beams*, Lecture Notes in Phys., 296, Springer-Verlag, 1986, p. 99.

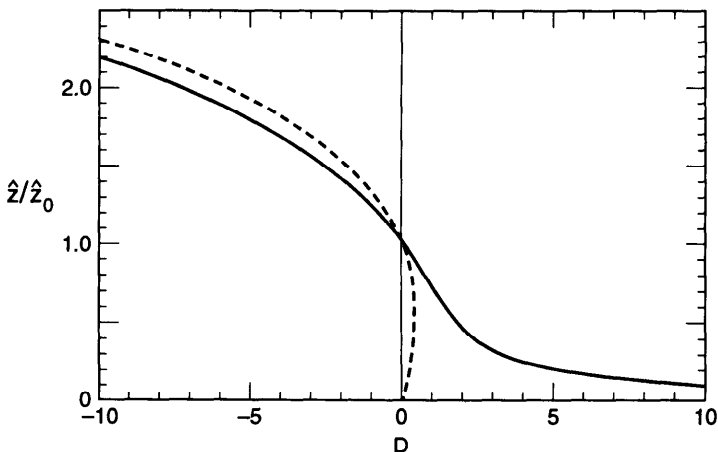


**Figure 6.6.** Bunch length  $\hat{z}/\hat{z}_0$  as a function of wake strength  $D$  for two models. The solid curve is the solution to Eq. (6.43). The dashed curve is the solution to Eq. (6.45). There is no physical solution to Eq. (6.45) when  $D > 2/3^{3/2}$ .

In the previous model, the beam area in phase space is kept constant as the beam intensity is varied. As we have just seen, this leads to a fourth order algebraic equation for the parabolic bunch length. The condition of constant phase space area applies to a proton beam when the accelerator operator carefully matches the injected beam (a different beam intensity requires a different matching) to the distorted potential well so that there is no increase in emittance.

As mentioned, for an electron beam, the stationary distribution has to assume a Gaussian form (6.30–6.32), and its  $\delta$ -distribution is unperturbed by the potential-well distortion. However, to obtain a qualitative illustration of potential-well distortion of an electron beam, one could compromise the requirement of a Gaussian distribution and modify Eq. (6.37) slightly to obtain

$$\psi(z, \delta) = \begin{cases} \frac{3N\eta c\sqrt{\kappa}}{2\pi\omega_s \hat{z}_0^3} \sqrt{\hat{z}_0^2 - \left(\frac{\eta c}{\omega_s} \delta\right)^2 - \kappa z^2} & \text{if } \left(\frac{\eta c}{\omega_s} \delta\right)^2 + \kappa z^2 < \hat{z}_0^2, \\ 0 & \text{otherwise.} \end{cases} \quad (6.44)$$

The distribution (6.44) maintains a constant spread in  $\delta$ , while the bunch length varies with the beam intensity.

The line density  $\rho(z)$  is still given by Eq. (6.38) with the total bunch length  $2\hat{z}_0/\sqrt{\kappa}$ . The total spread in  $\delta$  is equal to  $2\hat{z}_0\omega_s/|\eta|c$ , independent of the beam intensity. The Hamiltonian, which involves the line density  $\rho(z)$ , is still

given by Eq. (6.39). Following a procedure like the one in the previous model, we obtain a self-consistency condition that leads to a cubic equation for  $\hat{z}/\hat{z}_0$ ,

$$\left(\frac{\hat{z}}{\hat{z}_0}\right)^3 - \frac{\hat{z}}{\hat{z}_0} + D = 0, \quad (6.45)$$

where  $D$  is given in Eq. (6.40).

Again,  $\hat{z} = \hat{z}_0$  when  $N = 0$ , and the bunch lengthens or shortens as  $D < 0$  or  $D > 0$ . The phase space distribution of this beam is illustrated in Figure 6.5(b). Bunch length as a function of wake strength  $D$  is shown in Figure 6.6 as the dashed curve. One difference from the model (6.37) is that the model (6.44) does not allow a stationary solution for  $D > 2/3^{3/2}$ . At  $D = 2/3^{3/2}$ , the bunch assumes a length of  $\hat{z}_0/\sqrt{3}$ . In the region  $D > 2/3^{3/2}$ , the beam cannot maintain an unperturbed  $\delta$ -spread in its stationary state. A similar observation is made in Exercise 6.4. See also the discussion following Eq. (6.160).

### Exercise 6.4

- (a) For the wake (6.33), show that the potential-well distorted beam distribution in the Gaussian form (6.31) satisfies

$$f(z) = f(0)e^{-z^2/2\sigma_z^2}, \quad (6.46)$$

where  $f(z) = \alpha\rho(z)e^{-\alpha\rho(z)}$  with  $\alpha = r_0S/\eta\sigma_\delta^2\gamma C$ .

- (b) Given  $\alpha$ , find  $\rho(z)$  numerically as a function of  $N = \int_{-\infty}^{\infty} dz \rho(z)$ . Is there always a solution for any value of  $N$ ? Figure 6.7 gives the result. Give an approximate expression for the bunch length when  $|\alpha| \ll 1$ .
- (c) Show that the bunch lengthens if  $\alpha < 0$ , and shortens if  $\alpha > 0$ . Give a physical reason why this is so. Show that  $\rho(z) < 1/\alpha$  for all  $z$  if  $\alpha > 0$ .
- (d) Repeat the study for the wake  $W'_0(z) = S\delta(z)$ . Observe that in this case there is a shift of the beam centroid, which is absent in the previous case. Explain the physical origin of this shift.

**Exercise 6.5** For the wake  $W'_0(z) = S\delta(z)$ , or equivalently a purely resistive impedance  $Z_0^\parallel = S/c$ , show that a closed form solution for the Gaussian form (6.31) is given by<sup>18</sup>

$$\rho(z) = \frac{\sqrt{2/\pi} e^{-z^2/2\sigma_z^2}}{\alpha\sigma_z [\coth(\alpha N/2) - \operatorname{erf}(z/\sqrt{2}\sigma_z)]}, \quad (6.47)$$

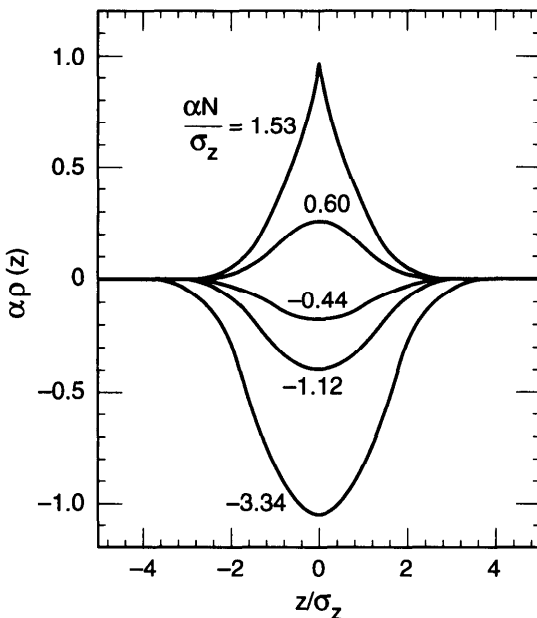


**Figure 6.7.** A Gaussian beam potential well distorted by the wake (6.33). The graph shows  $\alpha\rho(z)$  as a function of  $z/\sigma_z$  for five values of  $\alpha N/\sigma_z$ , where  $\alpha$  is defined after Eq. (6.46). The bunch lengthens if  $\alpha < 0$ , and shortens if  $\alpha > 0$ . There is no solution if  $\alpha\rho(0) > 1$ , corresponding to  $\alpha N/\sigma_z > 1.53$ .

where  $\text{erf}(x) = (2/\sqrt{\pi}) \int_0^x e^{-t^2} dt$  is the error function,  $\sigma_z = |\eta|c\sigma_\delta/\omega_s$ , and  $\alpha = r_0 S / \eta\sigma_\delta^2\gamma C$ . Show that for a weak beam with  $|\alpha N| \lesssim 1$ , the peak beam density occurs at

$$z \approx \frac{\alpha N}{\sqrt{2\pi}} \sigma_z. \quad (6.48)$$

This peak location moves forward above transition and backward below transition as the beam intensity increases. Figure 6.8 shows the bunch shape for various beam intensities. Does a Gaussian form solution exist for any beam intensity?

### Exercise 6.6

(a) Consider the following ansatz distribution for a proton beam:

$$\psi(z, \delta) = \frac{N\eta c}{2\pi\omega_s \hat{z}_0} \frac{1}{\sqrt{\hat{z}_0^2 - \frac{1}{\kappa} \left(\frac{\eta c}{\omega_s} \delta\right)^2 - \kappa(z - \bar{z})^2}}, \quad (6.49)$$

<sup>18</sup>A. G. Ruggiero, IEEE Trans. Nucl. Sci. NS-24, 1205 (1977).

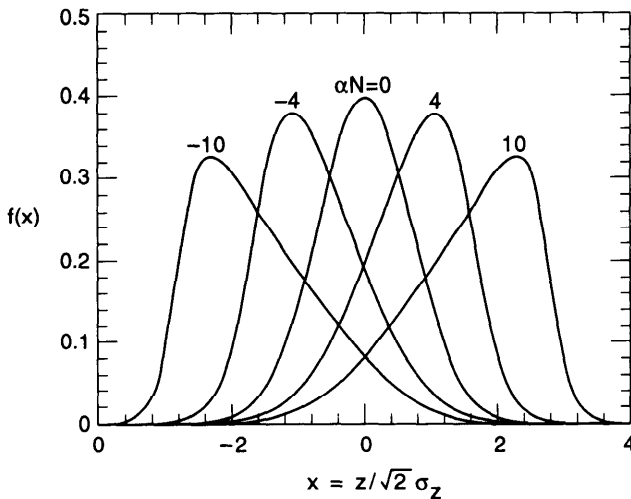


**Figure 6.8.** Bunch shape for different beam intensities according to Eq. (6.47), where  $\rho(z) = Nf(x)/\sigma_z$  and  $x = z/\sqrt{2}\sigma_z$ . The  $\alpha N = 0$  case is Gaussian. The beam peak density is located approximately according to Eq. (6.48). Cases with  $\alpha N > 0$  are above transition; those with  $\alpha N < 0$  are below transition. The head of the bunch is toward the right.

where  $\kappa$  parametrizes the potential-well distortion and  $\bar{z}$  gives the bunch centroid shift due to the parasitic beam loss. This beam has a uniform distribution in  $z$ . For a constant wake function  $W'_0(z < 0) = -W_0$ , show that a self-consistent condition gives,

$$\left(\frac{\hat{z}}{\hat{z}_0}\right)^4 - D\left(\frac{\hat{z}}{\hat{z}_0}\right)^3 - 1 = 0, \quad (6.50)$$

where

$$D = \frac{Nr_0\eta c^2 W_0}{2\omega_s^2 \gamma C \hat{z}_0}. \quad (6.51)$$

The same self-consistency condition also gives the bunch centroid shift

$$\bar{z} = -D\hat{z}_0. \quad (6.52)$$

Above transition,  $D > 0$ , the bunch centroid shifts forward and the bunch lengthens. Below transition, the opposite occurs.

- (b) Repeat (a) for electrons. Show that Eq. (6.52) still holds, but Eq. (6.50) becomes

$$\left(\frac{\hat{z}}{\hat{z}_0}\right)^2 - D\left(\frac{\hat{z}}{\hat{z}_0}\right) - 1 = 0 \quad \text{or} \quad \frac{\hat{z}}{\hat{z}_0} = \sqrt{1 + \frac{D^2}{4}} + \frac{D}{2}. \quad (6.53)$$

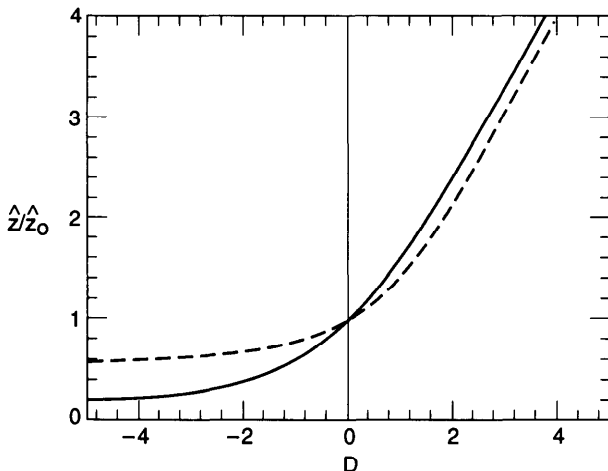


**Figure 6.9.** Bunch length versus beam intensity for the models (6.50) (dashed curve) and (6.53) (solid curve).

Figure 6.9 gives the bunch length dependence on the strength parameter  $D$  for cases (6.50) and (6.53).

- (c) Repeat (a) and (b) for the wake function  $W'_0(z) = S\delta(z)$  as in Exercise 6.5. Does the bunch shape distort? Explain the result obtained. Show that the bunch centroid shifts to the location

$$\bar{z} = \frac{Nr_0\eta c^2 S}{2\omega_s^2 \gamma C \hat{z}_0}. \quad (6.54)$$

The synchrotron frequency of single-particle motion in the potential well can be derived from the potential-well distorted Hamiltonian (6.39). For both models (6.37) and (6.44), the incoherent synchrotron frequency shift  $\Delta\omega_s$  satisfies

$$\left( \frac{\omega_s + \Delta\omega_s}{\omega_s} \right)^2 = 1 + \frac{3Nr_0\eta c^2 S}{2\omega_s^2 \gamma C \hat{z}^3}. \quad (6.55)$$

For small frequency shifts, we have

$$\Delta\omega_s \approx \frac{3Nr_0\eta c^2 S}{4\omega_s \gamma C \hat{z}^3}. \quad (6.56)$$

For the space charge wake,  $S$  is given by Eq. (6.36); Eq. (6.56) reproduces Eq. (1.48) obtained in Chapter 1.

Consider the numerical example that followed Eq. (1.48) for a 1 GeV proton synchrotron with  $N = 10^{10}$ ,  $C/2\pi = 60$  m,  $b = 5$  cm,  $a = 0.38$  cm,  $\eta = -0.45$ , and  $\nu_s = 0.04$ . We find  $S = 1100$  m and  $D = -0.83(\hat{z}/\hat{z}_0)^3$ . The bunch lengthens because  $D < 0$ . If we further assume the model (6.37) with unperturbed bunch length  $\hat{z}_0 = 0.30$  m,<sup>19</sup> we find a lengthened bunch with  $\hat{z} = 0.47$  m. Equation (6.55) then predicts a perturbed synchrotron tune of  $\nu_s + \Delta\nu_s = 0.016$ .

Equation (6.55) is established by combining Eqs. (6.3), (6.20), and (6.39). Instead of using Eq. (6.39), one may repeat the calculation using the more general Hamiltonian (6.29). By Taylor expanding the Hamiltonian to second order in  $z$ , one finds the perturbed synchrotron frequency

$$\Delta\omega_s \approx -\frac{\eta c^2 r_0}{2\omega_s \gamma C} \int_0^\infty dz' \rho(z') W_0''(-z'), \quad (6.57)$$

where  $W_0''$  is the second derivative of  $W_0$ . In terms of the impedance, we have

$$\Delta\omega_s \approx -i \frac{\eta c^2 r_0}{4\pi\omega_s \gamma C} \int_{-\infty}^\infty d\omega \tilde{\rho}(\omega) \frac{\omega}{c} Z_0^{\parallel}(\omega). \quad (6.58)$$

If the process is repeated taking into account the wake fields for multiple turns, the result becomes

$$\Delta\omega_s \approx -i \frac{\eta c^2 r_0}{2\omega_s \gamma C^2} \sum_{p=-\infty}^{\infty} \tilde{\rho}(p\omega_0) p\omega_0 Z_0^{\parallel}(p\omega_0). \quad (6.59)$$

For a point bunch with  $\tilde{\rho} = N$ , we have reproduced the potential-well distortion term (the first term on the right hand side) of Eq. (4.9) obtained for the one-particle model of Robinson instability.

When  $\Delta\omega_s > 0$ , the bunch length shortens due to the tighter focusing. Similarly,  $\Delta\omega_s < 0$  means the bunch lengthens. From Eq. (6.58), the sign of  $\Delta\omega_s$  is determined by the overlap integral of the bunch spectrum  $\tilde{\rho}(\omega)$  and the function  $\omega \operatorname{Im} Z_0^{\parallel}(\omega)$ . Consider a resonator impedance;  $\omega \operatorname{Im} Z_0^{\parallel}(\omega)$  is negative at low frequencies (inductive) and positive at high frequencies (capacitive). For a long bunch, the spectrum is limited to low frequencies; the overlap integral gives a  $\Delta\omega_s$  that has the same sign as  $-\eta$ , according to Eq. (6.58). Conversely, for a short bunch,  $\Delta\omega_s$  tends to have the same sign as  $\eta$ . It follows that, above transition, a long bunch tends to become longer and a short bunch tends to become shorter. Below transition, the tendencies are reversed.

<sup>19</sup>We do not assume model (6.44), because this is for a proton beam.

**Exercise 6.7** Find the incoherent synchrotron tune shift due to a resonator impedance (2.82). Substitute the Gaussian bunch spectrum (2.193) to show that

$$\Delta\nu_s = \frac{\Delta\omega_s}{\omega_0} \approx \sqrt{\frac{\pi}{2}} \frac{Nr_0\eta c^2}{4\pi^2\gamma\omega_s\sigma_z^2} \frac{R_s}{Q} \begin{cases} -c/\omega_R\sigma_z, & \text{long bunch,} \\ \omega_R\sigma_z/c, & \text{short bunch,} \end{cases} \quad (6.60)$$

where the long and short bunches are compared with  $c/\omega_R$ . Above transition, a long bunch lengthens and a short bunch shortens. Perform the integration numerically for various parameter values. Show that the bunch keeps its length when  $\sigma_z \approx 1.2c/\omega_R$  if  $Q = 1$ .

### 6.3 LINEARIZATION OF THE VLASOV EQUATION

On top of the static potential-well distorted bunch shape, particles in a beam execute accidental collective motions. Although they may have only infinitesimal amplitudes initially, these motions grow exponentially under unfavorable conditions. When this happens, the beam is unstable. Some of these instabilities were examined in Chapter 4, using simplified beam models. In this and the following sections, the Vlasov technique will be applied to treat this subject. The approach basically follows Sacherer's. The result contains all the instabilities of Chapter 4 as special cases.

Consider again a thread beam as we did in the previous section. At first, let us switch off the wake field and let the beam have an initial phase-space distribution  $\psi_0$ . Being an equilibrium distribution,  $\psi_0$  is only a function of  $r$ , i.e.,

$$\psi_0 = \psi_0(r), \quad (6.61)$$

where we have introduced the polar coordinates

$$\begin{aligned} z &= r \cos \phi, \\ \frac{\eta c}{\omega_s} \delta &= r \sin \phi. \end{aligned} \quad (6.62)$$

Note that  $r$  is related to the unperturbed Hamiltonian by  $H = \omega_s r^2/2$ , and Eq. (6.61) follows from the fact that the stationary distribution must be a function of the Hamiltonian. The coordinate system is indicated in Figure 6.10.

Now we turn on the wake fields and suppose there is a disturbance in the distribution, so that now we have

$$\psi(r, \phi, s) = \psi_0(r) + \psi_1(r, \phi) e^{-i\Omega s/c}. \quad (6.63)$$

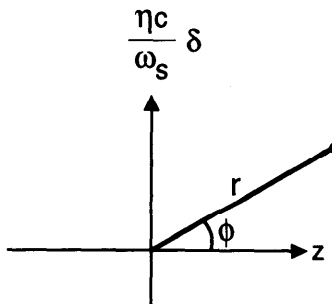


**Figure 6.10.** Coordinate system in the longitudinal phase space.

We have assumed the disturbance has a single frequency  $\Omega$ , i.e., it contains only one single mode of oscillation. We will consider the disturbance to be small.

The mode frequency  $\Omega$  and the mode distribution  $\psi_1$  are not arbitrary. The disturbance  $\psi_1$  first generates a wake field. Being an oscillation mode, the additional disturbance in the beam distribution caused by this wake field must have the same pattern as the original disturbance  $\psi_1$ . The beam-wake system, therefore, has to be solved self-consistently. As a result, only a discrete set of values are possible for  $\Omega$ , and associated with each value of  $\Omega$  there is a well-defined distribution  $\psi_1$ . Below, we will show how to obtain these solutions for  $\Omega$  and  $\psi_1$  using the Vlasov technique.

If we project  $\psi_1$  onto the  $z$ -axis, we obtain the longitudinal distribution

$$\rho_1(z)e^{-i\Omega s/c} = \int_{-\infty}^{\infty} d\delta \psi_1(r, \phi) e^{-i\Omega s/c}. \quad (6.64)$$

This  $\rho_1(z)$  is the distribution observed at a fixed location in the accelerator; it is the distribution that a localized impedance responds to, and is slightly different from the snapshot beam disturbance observed as a function of  $z$  at a given time. See Figure 6.11. The snapshot distribution is given by

$$\rho_1(z)|_{\text{snapshot}} = \rho_1(z)e^{-i\Omega z/c}. \quad (6.65)$$

One revolution before, the beam observed at the same location has a distribution  $\rho_1(z) \exp[-i\Omega(s/c - T_0)]$ , with  $T_0$  the revolution period.

The wake field excited by  $\rho_1$  produces a retarding voltage. The voltage seen by a particle at  $z$  (relative to the bunch center) as it passes by the location  $s$  in the accelerator is

$$V(z, s) = e \int_{-\infty}^{\infty} dz' \sum_{k=-\infty}^{\infty} \rho_1(z') e^{-i\Omega[(s/c) - kT_0]} W'_0(z - z' - kcT_0). \quad (6.66)$$

In writing down this expression, we have included the multturn wake fields and have used the causality property that  $W'_0(z) = 0$  if  $z > 0$ .

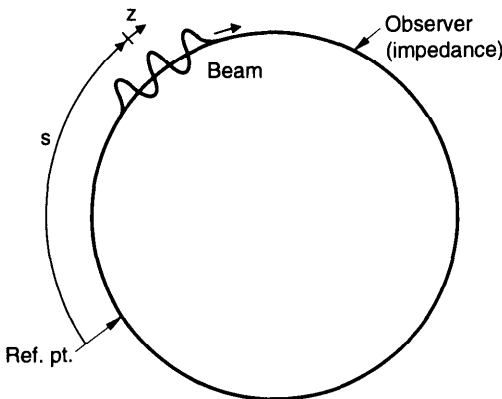


**Figure 6.11.** Snapshot of a disturbance on the beam in a circular accelerator. The signal seen by a localized impedance is slightly different. The disturbance shown is that of an  $l = 4$  mode.

As we anticipate solving the problem in the frequency domain, we will now introduce the Fourier transform of  $\rho_1$  according to Eq. (2.104) and the impedance  $Z_0^{\parallel}(\omega)$  according to Eq. (2.72). Equation (6.66) then becomes

$$V(z, s) = \frac{e}{T_0} e^{-i\Omega s/c} \sum_{p=-\infty}^{\infty} \tilde{\rho}_1(p\omega_0 + \Omega) e^{i(p\omega_0 + \Omega)z/c} Z_0^{\parallel}(p\omega_0 + \Omega), \quad (6.67)$$

where  $\omega_0 = 2\pi/T_0$  and we have made use of the identity (2.210).

Note that the snapshot frequency spectrum is related to  $\tilde{\rho}_1(\omega)$  by

$$\tilde{\rho}_1(\omega)|_{\text{snapshot}} = \tilde{\rho}_1(\omega + \Omega). \quad (6.68)$$

If we used the snapshot spectrum in Eq. (6.67), the frequency offset in the argument of  $\tilde{\rho}_1$  would have dropped out.

Having obtained  $V(z, s)$ , the Vlasov equation reads

$$\frac{\partial \psi}{\partial s} - \eta \delta \frac{\partial \psi}{\partial z} + \frac{\omega_s^2}{\eta c^2} z \frac{\partial \psi}{\partial \delta} - \frac{e}{T_0 E c} V(z, s) \frac{\partial \psi}{\partial \delta} = 0, \quad (6.69)$$

where  $E$  is the design energy of the beam particles. The two middle terms can be simplified if we use polar coordinates (6.62), yielding

$$\frac{\partial \psi}{\partial s} + \frac{\omega_s}{c} \frac{\partial \psi}{\partial \phi} - \frac{e}{T_0 E c} V(z, s) \frac{\partial \psi}{\partial \delta} = 0. \quad (6.70)$$

We now substitute Eqs. (6.63) and (6.67) into the above equation, and linearize it by keeping only the first order terms in  $\psi_1$ . Remembering that  $V$

is already first order and that  $\psi_0$  depends only on  $r$ , we obtain the linearized Vlasov equation

$$\begin{aligned} -i\Omega\psi_1 + \omega_s \frac{\partial\psi_1}{\partial\phi} - \frac{\eta r_0 c}{\gamma T_0^2 \omega_s} \sin\phi \psi'_0(r) \\ \times \sum_{p=-\infty}^{\infty} \tilde{\rho}_1(p\omega_0 + \Omega) e^{i(p\omega_0 + \Omega)z/c} Z_0^{\parallel}(p\omega_0 + \Omega) = 0. \end{aligned} \quad (6.71)$$

Actually,  $\psi_0$  also produces a wake field, which means  $V$  contains a zeroth order term, which has been ignored here. Inclusion of such a term is equivalent to imposing a perturbed potential well on the motion of  $\psi_1$ ; it is dropped because it is not essential to the illustration of the mechanism of collective beam instabilities. However, the potential-well distortion does contribute to a redefinition of  $\omega_s$ . As a result, all  $\omega_s$ 's from here on should be regarded as potential-well shifted, as given by Eqs. (6.57–6.59). The coordinates (6.62) are redefined accordingly. The “unperturbed” distribution  $\psi_0$  is thus a function of this redefined, perturbed  $r$ .

In the procedure leading to Eq. (6.71), we have linearized with respect to the perturbation  $\psi_1$ , not with respect to the impedance or the beam intensity. The impedance and the beam intensity do not have to be small in this linearization procedure. On the other hand, the linearization with respect to  $\psi_1$  poses an important limitation in our analysis. For a given unperturbed distribution  $\psi_0(r)$ , Eq. (6.71) describes the behavior of an infinitesimal deviation from it. If this deviation grows in time, the beam is unstable; otherwise it is stable. The analysis does not give any information on other unperturbed distributions. Showing the beam is unstable with a certain  $\psi_0$  does not prove the beam is necessarily unstable, because it may stabilize with a different  $\psi_0$ . This point will be illustrated further by Figure 6.16.

Having linearized the Vlasov equation, we are now ready to discuss the collective modes of beam motion under the influence of beam-impedance interaction. To do so, we first Fourier expand  $\psi_1$  according to

$$\psi_1(r, \phi) = \sum_{l=-\infty}^{\infty} \alpha_l R_l(r) e^{il\phi}. \quad (6.72)$$

This is possible because  $\psi_1$  must be periodic in  $\phi$  with period  $2\pi$ . We have used  $l$  as the summation index in anticipation that it actually is the longitudinal model index used in Figure 6.1 in the limit of weak beam intensities.

Substituting Eq. (6.72) into Eq. (6.71), we obtain

$$\begin{aligned} -i \sum_{l'} \alpha_{l'} R_{l'}(r) e^{il'\phi} (\Omega - l' \omega_s) - \frac{\eta r_0 c}{\gamma T_0^2 \omega_s} \sin\phi \psi'_0(r) \\ \times \sum_p \tilde{\rho}_1(\omega') Z_0^{\parallel}(\omega') e^{i(\omega'r/c)\cos\phi} = 0, \end{aligned} \quad (6.73)$$

where  $\omega'$  in the summation over  $p$  is an abbreviation for  $p\omega_0 + \Omega$ . Multiply the equation by  $\exp(-il\phi)$  and integrate over  $\phi$  from 0 to  $2\pi$ , and repeat for all values of  $l$ . We obtain an infinite set of equations,

$$-i(\Omega - l\omega_s)\alpha_l R_l(r) + \frac{\eta r_0 c^2}{\gamma T_0^2 \omega_s} l i^l \frac{\psi'_0(r)}{r} \sum_p \tilde{\rho}_1(\omega') \frac{Z_0^{\parallel}(\omega')}{\omega'} J_l\left(\frac{\omega' r}{c}\right) = 0, \\ l = 0, \pm 1, \pm 2, \dots, \quad (6.74)$$

where  $J_l(x)$  is the Bessel function. Some properties of the Bessel functions that we will use later in the text are given in Table 6.1.<sup>20</sup> Note the appearance of the quantity  $Z_0^{\parallel}(\omega')/\omega'$  in Eq. (6.74).

We still need an expression for  $\tilde{\rho}_1(\omega')$  in Eq. (6.74). This is found below:

$$\begin{aligned} \tilde{\rho}_1(\omega') &= \int_{-\infty}^{\infty} dz e^{-i\omega' z/c} \rho_1(z) \\ &= \int_{-\infty}^{\infty} dz \int_{-\infty}^{\infty} d\delta e^{-i\omega' z/c} \psi_1(r, \phi) \\ &= \frac{\omega_s}{\eta c} \int_0^{\infty} r dr \int_0^{2\pi} d\phi \exp\left(-i\frac{\omega' r}{c} \cos \phi\right) \sum_{l'} \alpha_{l'} R_{l'}(r) e^{il'\phi} \\ &= \frac{2\pi\omega_s}{\eta c} \sum_{l'} \int_0^{\infty} r dr \alpha_{l'} R_{l'}(r) i^{-l'} J_{l'}\left(\frac{\omega' r}{c}\right). \end{aligned} \quad (6.75)$$

When Eq. (6.75) is substituted into Eq. (6.74), we obtain the integral equation

$$(\Omega - l\omega_s)\alpha_l R_l(r) = -i \frac{2\pi r_0 c}{\gamma T_0^2} l \frac{\psi'_0(r)}{r} \sum_{l'=-\infty}^{\infty} \int_0^{\infty} r' dr' \alpha_{l'} R_{l'}(r') i^{l-l'} \\ \times \sum_{p=-\infty}^{\infty} \frac{Z_0^{\parallel}(\omega')}{\omega'} J_l\left(\frac{\omega' r}{c}\right) J_{l'}\left(\frac{\omega' r'}{c}\right). \quad (6.76)$$

The fact that Bessel functions appear prominently in Eq. (6.76) has been addressed in Eq. (4.19). Given the impedance  $Z_0^{\parallel}$  and the unperturbed distribution  $\psi_0$ , we have to find the  $R_l(r)$ 's and  $\alpha_l$ 's to satisfy Eq. (6.76). This is obviously not easy to do in general. Below we will first proceed by choosing a simplified model of  $\psi_0$ , namely,

$$\psi_0(r) = \begin{cases} 0 & \text{if } r > \hat{z}, \\ \frac{N\eta c}{\pi \hat{z}^2 \omega_s} & \text{if } r < \hat{z}. \end{cases} \quad (6.77)$$

<sup>20</sup>I. S. Gradshteyn and I. M. Ryzhik, *Table of Integrals, Series and Products*, Academic Press, 1980.

**Table 6.1. Some properties of Bessel functions.**

$$\frac{1}{2\pi} \int_0^{2\pi} d\phi e^{il\phi - ix \cos \phi} = i^{-l} J_l(x)$$

$$e^{-ix \cos \phi} = \sum_{l=-\infty}^{\infty} i^{-l} J_l(x) e^{il\phi}$$

$$J_l(-x) = (-1)^l J_l(x) = J_{-l}(x)$$

$$J_l(x) \approx \frac{1}{l!} \left( \frac{x}{2} \right)^l \quad \text{for } |x| \ll 1$$

$$J_l(0) = \delta_{l0}$$

$$\sum_{l=-\infty}^{\infty} J_l^2(x) = 1$$

$$\frac{1}{2\pi} \int_0^{2\pi} d\phi \sin \phi e^{-il\phi + ix \cos \phi} = -i^l \frac{l}{x} J_l(x)$$

$$J'_l(x) = \frac{1}{2}[J_{l-1}(x) - J_{l+1}(x)]$$

$$\int_0^{\infty} \frac{dx}{x} J_{\nu+2l}(x) J_{\nu+2l'}(x) = \frac{\delta_{ll'}}{2(\nu+2l)} \quad (\nu > 0)$$

$$\int_0^{\infty} x dx J_l(kx) J_l(k'x) = \frac{1}{k} \delta(k - k')$$

$$\int_0^{\infty} x^{-\alpha} dx J_{\mu}(x) J_{\nu}(x) = \frac{\Gamma(\alpha) \Gamma[\frac{1}{2}(\mu + \nu + 1 - \alpha)]}{2^{\alpha} \Gamma[\frac{1}{2}(-\mu + \nu + 1 + \alpha)] \Gamma[\frac{1}{2}(\mu + \nu + 1 + \alpha)] \Gamma[\frac{1}{2}(\mu - \nu + 1 + \alpha)]} \\ (\mu + \nu + 1 > \alpha > 0)$$

$$\int_{-\infty}^{\infty} dy e^{iyx} J_l(x) = \frac{2i^l}{\sqrt{1-y^2}} \cos(l \cos^{-1} y) H(1 - |y|)$$


---

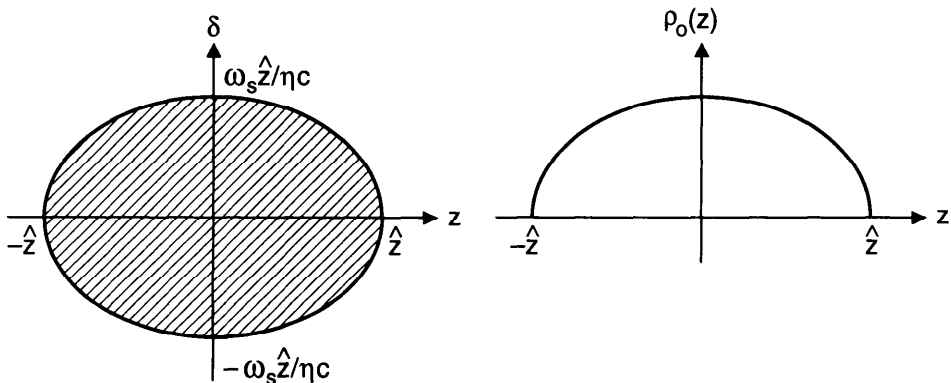


**Figure 6.12.** Phase space distribution and longitudinal distribution of a water-bag beam. For this distribution,  $\rho_0(z) = 2N\sqrt{\hat{z}^2 - z^2} / \pi\hat{z}^2$  and  $\sigma_z = \hat{z} / 2$ .

The impedance, on the other hand, is left general. The case of general  $\psi_0(r)$  will be treated in the next section.

The distribution (6.77) is called the *water-bag model*. Its phase space distribution and projection onto the  $z$ -axis are shown in Figure 6.12. The distribution is normalized so that

$$\int_{-\infty}^{\infty} d\delta \int_{-\infty}^{\infty} dz \psi_0 = \frac{\omega_s}{\eta c} \int_0^{\infty} 2\pi r dr \psi_0 = N. \quad (6.78)$$

Any perturbation on a water-bag beam will have to occur around the edge of the bag, i.e., around  $r = \hat{z}$ . As a result, all  $R_l$ 's are  $\delta$ -functions,

$$R_l(r) \propto \delta(r - \hat{z}). \quad (6.79)$$

The result (6.79) also follows from Eq. (6.76) by inspection if we note that  $\psi'_0 \propto \delta(r - \hat{z})$ . Having obtained Eq. (6.79), the integral equation (6.76) reduces to a set of equations for the coefficients  $\alpha_l$ :

$$(\Omega - l'\omega_s)\alpha_{l'} = i \frac{2Nr_0\eta c^2}{\gamma T_0^2 \omega_s \hat{z}^2} l' \sum_{l''} \alpha_{l''} i^{l'' - l'} \sum_p \frac{Z_0^{\parallel}(\omega')}{\omega'} J_{l'}\left(\frac{\omega' \hat{z}}{c}\right) J_{l''}\left(\frac{\omega' \hat{z}}{c}\right),$$

$$l' = 0, \pm 1, \pm 2, \dots \quad (6.80)$$

We are finally ready to discuss modes. There are infinite number of solutions to Eq. (6.80), each specifying a collective mode. Equation (6.80) is written in terms of running indices  $l'$  and  $l''$ , reserving  $l$  for the mode index. First note that when  $N = 0$ , i.e., in the zero-intensity limit, the solution to

Eq. (6.80) for the  $l$ th mode is

$$\begin{aligned}\alpha_{l'}^{(l)} &= \delta_{ll'}, \quad l' = 0, \pm 1, \pm 2, \dots, \\ \Omega^{(l)} &= l\omega_s,\end{aligned}\tag{6.81}$$

where  $\delta_{ll'} = 1$  if  $l = l'$ , and 0 if  $l \neq l'$ . The  $l$ th mode therefore is described by

$$\psi_l^{(l)} e^{-i\Omega s/c} \propto \underbrace{\delta(r - \hat{z}) e^{il\phi}}_{\text{long. dist.}} \underbrace{e^{-il\omega_s s/c}}_{\text{time dep.}}.\tag{6.82}$$

These are the modes illustrated in Figure 6.1(a). The phase space distributions, as well as their projections onto the  $z$ -axis, without the time dependences, are drawn in Figure 6.13.

Observing at a fixed location, a pickup electrode (or an impedance) will receive a signal that contains an unperturbed contribution from  $\rho_0(z)$ , superimposed on a contribution from  $\rho_l^{(l)}(z)$  if the beam is executing the  $l$ th mode. Figure 6.14 displays the signals as the beam traverses the electrode in several different passages. The signals show  $l$  nodes in the  $z$ -distribution if the beam is executing the  $l$ th mode.

In case the beam intensity is nonzero but still weak, we can find the  $l$ th mode frequency by substituting the zeroth order solution (6.81) into the right hand side of Eq. (6.80) to obtain

$$\Omega^{(l)} - l\omega_s = i \frac{2N r_0 \eta c^2}{\gamma T_0^2 \omega_s \hat{z}^2} l \sum_{p=-\infty}^{\infty} \frac{Z_0^{\parallel}(\omega')}{\omega'} J_l^2 \left( \frac{\omega' \hat{z}}{c} \right),\tag{6.83}$$

where  $\omega' = p\omega_0 + l\omega_s$ .

Some results on instabilities at last! Given the impedance, Eq. (6.83) gives the complex mode frequencies for a water-bag beam with weak intensities. In particular, the real part of  $\Omega^{(l)}$  gives the mode frequency shift  $\Delta\Omega^{(l)}$ ; the imaginary part gives the instability growth rate  $1/\tau^{(l)}$ .

One should be careful in obtaining  $\Delta\Omega^{(l)}$  from Eq. (6.83), because it does not contain all contributions. A potential-well frequency shift term was dropped when we linearized the Vlasov equation back in Eq. (6.71).

The  $l = 0$  mode is a trivial mode with  $\Omega^{(0)} = 0$ . It describes the potential-well distortion mode addressed in Section 6.2 and is not of much interest here. Take next the  $l = 1$  mode for consideration. Let us assume the beam bunch is short enough so that  $\omega' \hat{z}/c \ll 1$ , i.e., the wake field lasts much longer than the bunch length. Then  $J_1(\omega' \hat{z}/c) \approx \omega' \hat{z}/2c$ , and we have recovered from the imaginary part of Eq. (6.83) the Robinson growth rate, Eq. (4.10). The real part of Eq. (6.83) reproduces the second term of the

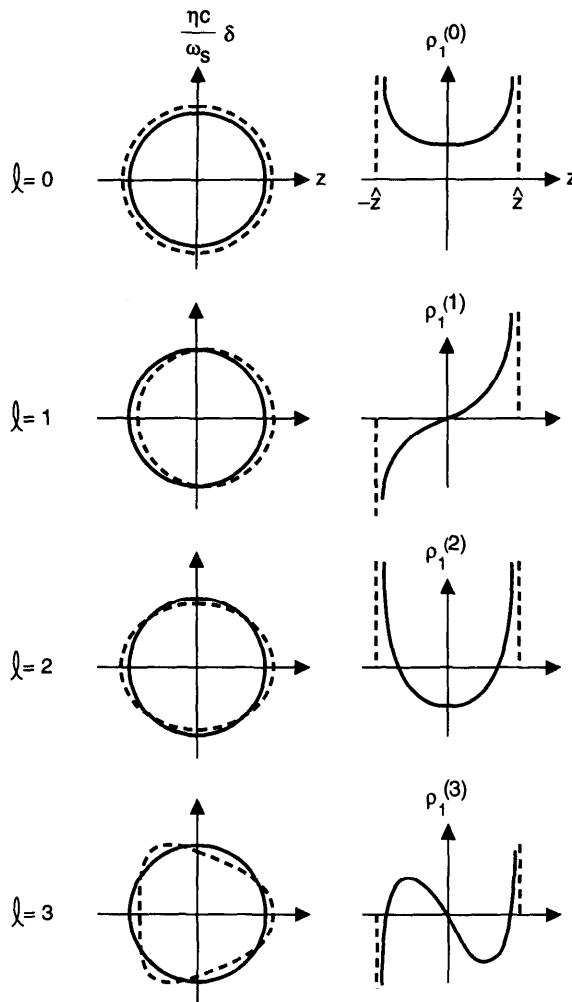


**Figure 6.13.** The phase space distributions (6.82) and corresponding longitudinal projections  $\rho_1^{(l)} \propto \cos(l \cos^{-1} x) / \sqrt{1 - x^2}$ , where  $x = z / \hat{z}$  [see Exercise 6.8(a)], for the modes  $l = 0, 1, 2, 3$ . A water-bag beam with vanishing intensity is assumed. In the phase space distributions on the left, solid curves (circles) are the unperturbed water bag; dashed curves are the perturbed distributions. The  $l = 0$  mode as shown cannot be excited due to charge conservation, although a static mode, corresponding to a potential-well distortion, does exist.

mode frequency shift (4.9). The first term of Eq. (4.9) comes from the potential-well distortion and was addressed in Eq. (6.59).

On the other hand, Eq. (6.83) is much more general than the one-particle results (4.9) and (4.10). It applies to higher order modes  $l > 1$  and arbitrary bunch length  $\hat{z}$ . In particular, when it is applied to the  $l > 1$  cases, a sharp resonator impedance yields Robinson stability criteria for the  $l > 1$  beam

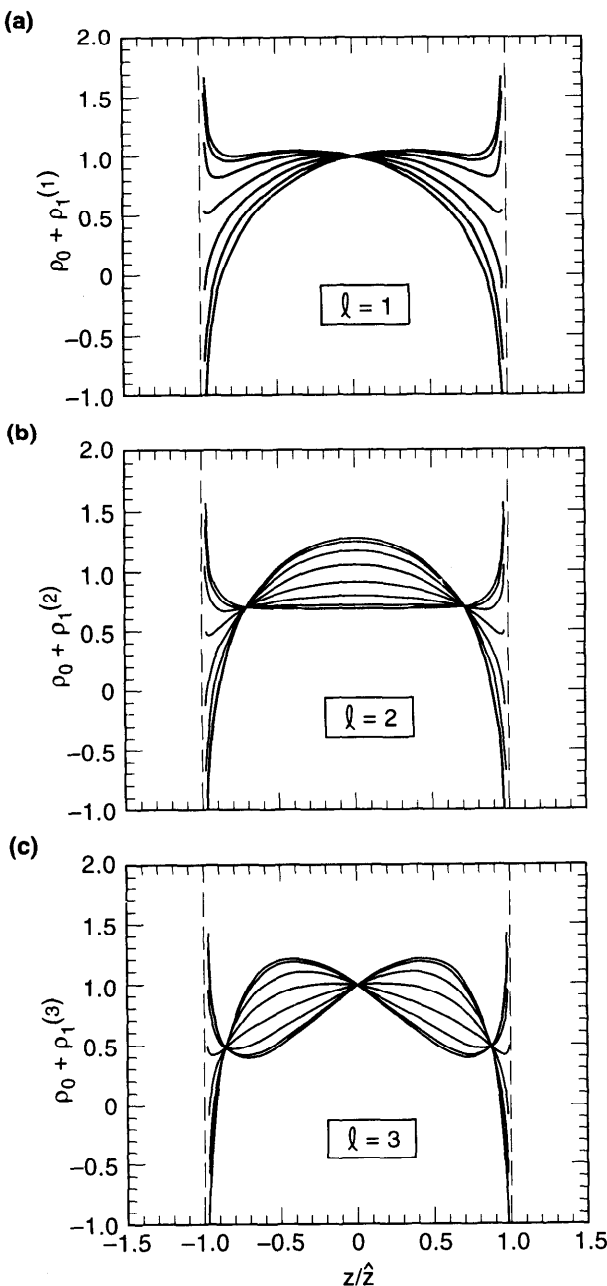


**Figure 6.14.** Signal received by an electrode when the beam is executing the  $\ell$ th longitudinal mode. Signals of several beam passages are superimposed for modes (a)  $\ell = 1$ , (b)  $\ell = 2$ , and (c)  $\ell = 3$ . The number of nodes is equal to  $\ell$ . The divergences at the bunch edge  $z = \pm \hat{z}$  are an artifact of the water-bag model.

oscillation modes. Considering the fundamental rf mode at frequency close to  $\hbar\omega_0$ , the Robinson growth rate for the  $l$ th beam mode is found to be

$$\frac{1}{\tau^{(l)}} = \frac{l}{(l!)^2} \left( \frac{\hbar\omega_0 \hat{z}}{2c} \right)^{2l-2} \frac{Nr_0 \eta \hbar\omega_0}{2\gamma T_0^2 \omega_s} \\ \times [\operatorname{Re} Z_0^{\parallel}(\hbar\omega_0 + l\omega_s) - \operatorname{Re} Z_0^{\parallel}(\hbar\omega_0 - l\omega_s)]. \quad (6.84)$$

For  $l = 1$ , this reduces to the familiar result (4.20). It follows from Eq. (6.84) that the Robinson stability requirement for the higher ( $l > 1$ ) modes is the same as for  $l = 1$ : the rf frequency  $\omega_R$  must be detuned below (above)  $\hbar\omega_0$  when operated above (below) transition. Higher order Robinson growth rates, however, drop off rapidly with increasing mode index  $l$  if the bunch length is much less than the rf wavelength, which is typically the case.

### Exercise 6.8

- (a) Show that for a water-bag beam,

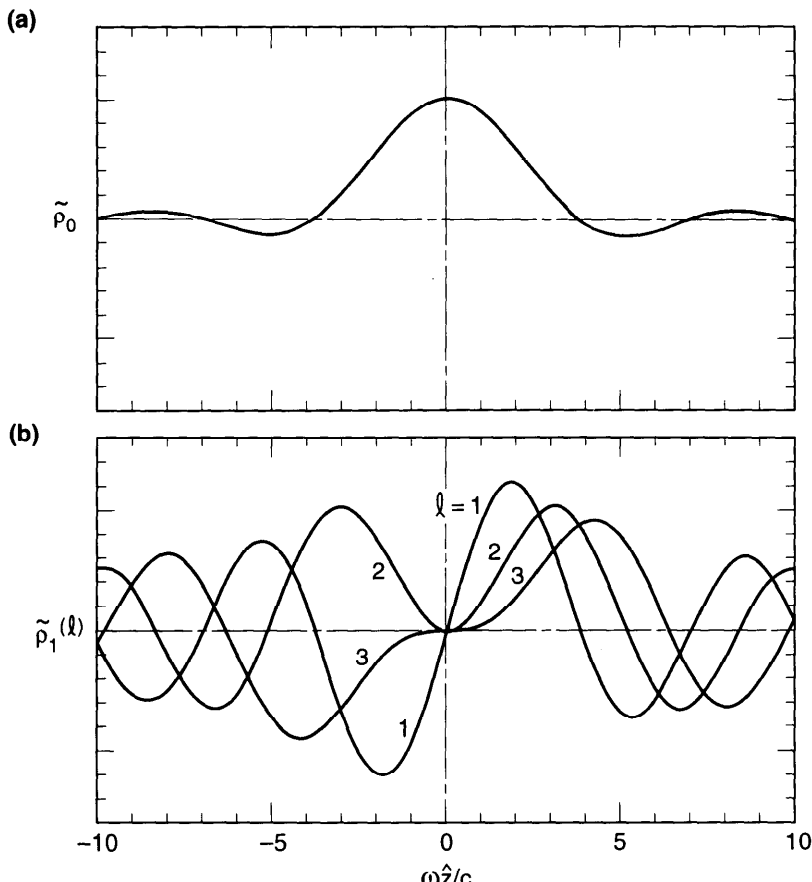
$$\tilde{\rho}_0(\omega) = 2N \frac{c}{\omega \hat{z}} J_1\left(\frac{\omega \hat{z}}{c}\right), \\ \tilde{\rho}_1^{(l)}(\omega) \propto J_l\left(\frac{\omega \hat{z}}{c}\right), \quad (6.85) \\ \rho_1^{(l)}(z) \propto \frac{1}{\sqrt{\hat{z}^2 - z^2}} \cos\left[l \cos^{-1}\left(\frac{z}{\hat{z}}\right)\right].$$

Figure 6.15 shows the frequency spectra  $\tilde{\rho}_0(\omega)$  and  $\tilde{\rho}_1^{(l)}(\omega)$  of the various modes. The density  $\rho_1^{(l)}(z)$  was shown in Figure 6.13. As shown in Figure 6.15, the spectrum shifts towards higher frequencies as the mode index  $l$  increases.

- (b) Using Eq. (6.59), show that the synchrotron frequency shift due to the potential well for a water-bag beam is

$$\Delta\omega_s = \frac{Nr_0 \eta c}{\gamma T_0^2 \omega_s \hat{z}} \sum_{p=-\infty}^{\infty} J_1\left(\frac{p\omega_0 \hat{z}}{c}\right) \operatorname{Im} Z_0^{\parallel}(p\omega_0). \quad (6.86)$$

- (c) Show that in case the wake field is much longer than the bunch length but much shorter than the accelerator circumference, the potential-well term, Eq. (6.86), and the dynamics term, the real part of Eq. (6.83), cancel each other for the  $l = 1$  mode. The dipole mode frequency  $\Omega^{(l=1)}$  therefore does not shift. This property was reflected in Figure 6.2. Physically, this is because as the bunch executes a rigid longitudinal



**Figure 6.15.** (a) Fourier spectrum  $\tilde{\rho}_0(\omega)$  of the unperturbed bunch shape for a water-bag beam. (b) Fourier spectra  $\tilde{\rho}_1^{(l)}(\omega)$  of the lowest three collective modes  $l = 1, 2, 3$ .

dipole motion, the wake field, and therefore the potential well, moves with it. The motion of the beam as a whole is not affected by the wake field. The net result is that the collective dipole mode oscillates at the unperturbed synchrotron frequency up to moderate beam intensities.

**Exercise 6.9** Apply Eq. (6.83) to calculate the complex mode frequencies of a water-bag beam of weak intensity in the presence of a broad-band resonator impedance. Ignore the multiturn and the potential-well distortion effects. Obtain limits for  $\omega_R z/c \gg 1$  and  $\ll 1$ . Use the result to estimate the synchrotron mode frequency shifts for mode  $l$  in the accelerator of Figure 2.19. Note that the incoherent synchrotron frequency shift (for a Gaussian beam) was found in Exercise 6.7. What happens if Eq. (6.83) is applied to the space charge impedance?

**Exercise 6.10** Equation (6.76) has a frequency-domain counterpart. Define

$$\tilde{\rho}_1^{(l)}(p) = \frac{2\pi\omega_s}{\eta c} i^{-l} \int_0^\infty r dr R_l(r) J_l\left(\frac{p\omega_0 + \Omega}{c}r\right) \quad (6.87)$$

so that Eq. (6.75) reads  $\tilde{\rho}_1(\omega') = \sum_l \alpha_l \tilde{\rho}_1^{(l)}(p)$ .

(a) Use Eq. (6.76) to show that

$$(\Omega - l\omega_s) \alpha_l \tilde{\rho}_1^{(l)}(q) = -i \frac{2\pi r_0 c}{\gamma T_0^2} l \sum_{l'} \alpha_{l'} \times \sum_p \frac{Z_0^{\parallel}(p\omega_0 + \Omega)}{p\omega_0 + \Omega} \tilde{\rho}_1^{(l')}(p) F_l(p, q), \quad (6.88)$$

where

$$F_l(p, q) = \int_0^\infty r dr \frac{\psi'_0(r)}{r} J_l\left(\frac{p\omega_0 + \Omega}{c}r\right) J_l\left(\frac{q\omega_0 + \Omega}{c}r\right). \quad (6.89)$$

(b) The problem is analytically soluble for an arbitrary impedance if  $F_l(p, q)$  factorizes so that

$$F_l(p, q) = -T_l(p\omega_0 + \Omega) T_l(q\omega_0 + \Omega). \quad (6.90)$$

Show that the solution to Eq. (6.88) is given by

$$\tilde{\rho}_1^{(l)}(p) \propto i^{-l} T_l(p\omega_0 + \Omega), \quad (6.91)$$

with

$$(\Omega - l\omega_s) \alpha_l = i \frac{2\pi r_0 c}{\gamma T_0^2} l \sum_{l'} \alpha_{l'} i^{l-l'} \times \sum_p \frac{Z_0^{\parallel}(p\omega_0 + \Omega)}{p\omega_0 + \Omega} T_{l'}(p\omega_0 + \Omega) T_l(p\omega_0 + \Omega). \quad (6.92)$$

(c) One factorizable example is that of the water-bag model. Apply the result to the water-bag model to obtain Eqs. (6.79–6.80). Another factorizable example will be given in Eqs. (6.151–6.154).

The Robinson instability described by Eq. (6.84) is an application of Eq. (6.83) to a sharply peaked impedance. It was pointed out in Section 4.1 that a broad-band impedance does not cause instabilities of a one-particle beam.

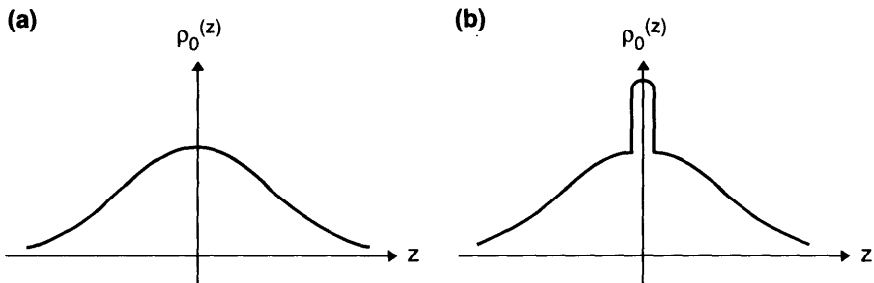


**Figure 6.16.** Two possible unperturbed beam distributions: (a) is a smooth distribution; (b) has a  $\delta$ -function spike at the origin. Depending on the impedance, they may have very different stability criteria, but the significance of the difference is rather limited.

This same conclusion can be reached with the more general Eq. (6.83). For a broad-band impedance, the summation over  $p$  can be approximated by an integral; the real part of the integral vanishes because  $\text{Re } Z_0^{\parallel}(\omega')/\omega'$  is an odd function of  $\omega'$ .

It should be mentioned that the water-bag beam is particularly simple in that one can readily solve for  $R_i(r)$  in Eq. (6.79). The price we pay here is that all radial structures are degenerate and some information has been lost. This will be remedied in the next section. However, one must remember another weakness of the present analysis, namely, the stability obtained here depends on the choice of the unperturbed distribution  $\psi_0$ . Sketched in Figure 6.16 are two possible unperturbed beam distributions. For an impedance that has a significant high frequency tail, one can imagine a situation in which a beam with distribution (a) is stable, while one with distribution (b) is unstable due to the larger overlap between its spectrum and the impedance. But the significance of the instability of distribution (b) is rather limited, because after losing the particles in the spike, the beam stabilizes.

Another important limitation of the linearized Vlasov equation is that it is applicable only at the onset of the instability. Once the instability starts to grow, it no longer applies. In particular, some instabilities may saturate instead of growing indefinitely. Studies of such saturation and of overshoot effects are excluded by the linearized Vlasov treatment and are beyond our present scope.

## 6.4 RADIAL MODES

So far we have solved the linearized Vlasov equation using a highly idealized water-bag model as the unperturbed distribution  $\psi_0$ . For a more realistic distribution, the analysis becomes more involved. In a water-bag model, a

collective mode is described by two mode indices  $m$  and  $l$ . The index  $m$  specifies the transverse behavior of the beam; in the present analysis of longitudinal collective modes, we have  $m = 0$ . The other index  $l$  specifies the *azimuthal* structure of the mode in the longitudinal phase space. In the water-bag model, all perturbation on the beam distribution occurs at the edge of the water bag,  $r = \hat{z}$ ; the azimuthal index  $l$  thus completely specifies the longitudinal structure of the mode. For a general distribution, however, the mode has to be specified by two longitudinal indices  $l$  and  $n$ , where  $n$  is an index describing the *radial* structure of the mode in the longitudinal phase space. This complication will be addressed in this section.

In the limit of zero beam intensity, all radial modes with the same azimuthal index  $l$  but different radial indices  $n$  have the same mode frequency  $\Omega = l\omega_s$ . As the beam intensity is increased slightly, their frequencies shift away from this unperturbed value and modes with different  $n$ 's shift differently, thus breaking the degeneracy. For weak beams, these frequency shifts are much smaller than  $\omega_s$ . In that case, the radial modes will couple if they belong to the same azimuthal family with a given  $l$ , but coupling among radial modes that belong to different azimuthal families can be ignored. For a given  $l$ , Eq. (6.76) for a weak beam then becomes

$$\left( \frac{\Omega}{\omega_s} - l \right) R_l(r) = W(r) \int_0^\infty r' dr' R_l(r') G_l(r, r'), \quad (6.93)$$

where we have introduced a weight function

$$W(r) = -\frac{\omega_s}{N\eta c} \frac{\psi'_0(r)}{r}, \quad (6.94)$$

and a kernel function

$$G_l(r, r') = i \frac{2\pi N r_0 \eta c^2}{\gamma T_0^2 \omega_s^2} l \sum_{p=-\infty}^{\infty} \frac{Z_0^{\parallel}(\omega')}{\omega'} J_l\left(\frac{\omega' r}{c}\right) J_l\left(\frac{\omega' r'}{c}\right), \quad (6.95)$$

where  $\omega' = p\omega_0 + l\omega_s$ .

Equation (6.93), together with Eqs. (6.94–95), is called the *Sacherer integral equation* for the longitudinal ( $m = 0$ ) instabilities. Information on  $\psi_0(r)$  is contained in the weight function; information on  $Z_0^{\parallel}(\omega)$  is contained in the kernel function. Since  $\psi'_0(r)$  tends to be negative, a minus sign is introduced in the definition of  $W(r)$  to make it positive, at least for  $\eta > 0$ .

The Sacherer equation describes an eigensystem. There are an infinite number of solutions of the system, specified by the index  $n = 0, 1, 2, \dots$ . Each solution consists of an eigenvalue  $(\Omega/\omega_s) - l$  and a corresponding eigenfunction  $R_l(r)$ . Note that  $G_l(r, r') = G_l(r', r)$  and that  $G_0(r, r') = 0$ .

To proceed, let us introduce a complete set of orthonormal functions  $\{f_k(r), k = 0, 1, 2, \dots\}$  that satisfies the condition

$$\int_0^\infty r dr W(r) f_k(r) f_{k'}(r) = \delta_{kk'}. \quad (6.96)$$

We then decompose the eigenfunction  $R_l(r)$  according to

$$R_l(r) = W(r) \sum_{k=0}^{\infty} a_k f_k(r). \quad (6.97)$$

Substituting Eq. (6.97) into Eq. (6.93) and using the orthonormality condition (6.96), we obtain an infinite set of equations

$$\left( \frac{\Omega}{\omega_s} - l \right) a_k = \sum_{k'=0}^{\infty} M_{kk'} a_{k'}, \quad k = 0, 1, 2, \dots, \quad (6.98)$$

where

$$M_{kk'} = \int_0^\infty r dr W(r) f_k(r) \int_0^\infty r' dr' W(r') f_{k'}(r') G_l(r, r'). \quad (6.99)$$

For a nontrivial solution to exist, the eigenvalues  $(\Omega/\omega_s) - l$  must satisfy

$$\det \left[ \left( \frac{\Omega}{\omega_s} - l \right) I - M \right] = 0, \quad (6.100)$$

where  $I$  is the identity matrix and  $M$  is the *interaction matrix* with elements given by Eq. (6.99). The infinite number of solutions for the eigenvalue is specified by the radial mode index  $n$  for the given azimuthal index  $l$ .

Substituting Eq. (6.95) into Eq. (6.99) and introducing the quantity

$$g_{lk}(\omega) = \int_0^\infty r dr W(r) f_k(r) J_l\left(\frac{\omega r}{c}\right), \quad (6.101)$$

we obtain the expression

$$M_{kk'} = i \frac{2\pi N r_0 \eta c^2}{\gamma T_0^2 \omega_s^2} l \sum_{p=-\infty}^{\infty} \frac{Z_0^{\parallel}(\omega')}{\omega'} g_{lk}(\omega') g_{lk'}(\omega'). \quad (6.102)$$

The functions  $W(r)$ ,  $f_k(r)$ , and  $g_{lk}(\omega)$  have the dimensionalities  $L^{-4}$ ,  $L$ , and  $L^{-1}$ , respectively. Elements of the interaction matrix  $M$  are dimensionless.

The quantity  $g_{lk}(\omega)$  is related to the Fourier spectrum of the distribution perturbation. This can be seen by following steps similar to Eq. (6.75),

$$\begin{aligned}\tilde{\rho}_l^{(l)}(\omega) &= \int_{-\infty}^{\infty} dz e^{-i\omega z/c} \int_{-\infty}^{\infty} d\delta \psi_l^{(l)} \\ &= \frac{2\pi\omega_s}{\eta c} i^{-l} \alpha_l \sum_{k=0}^{\infty} a_k g_{lk}(\omega),\end{aligned}\quad (6.103)$$

where use has been made of Eqs. (6.72), (6.97), and (6.101).

We have now a well-defined procedure of finding the radial modes for a given unperturbed distribution  $\psi_0(r)$ . To do so, we first obtain the weight function (6.94); a set of orthonormal functions  $\{f_k(r)\}$  is then introduced satisfying Eq. (6.96). The eigenmodes are obtained using Eq. (6.100), where the interaction matrix  $M$  is obtained from Eq. (6.102) with  $g_{lk}(\omega)$  given by Eq. (6.101). This procedure is repeated for each given azimuthal index  $l$ . Coupling among different azimuthal families, which occurs at higher beam intensities than considered here, will be considered in the next section.

First let us consider the highly degenerate water-bag model. In this case we have

$$W(r) = \frac{1}{\pi \hat{z}^3} \delta(r - \hat{z}). \quad (6.104)$$

The orthonormal condition (6.96) allows one and only one value of the radial index:  $k = 0$ , with  $f_0(r) = \sqrt{\pi} \hat{z}$ . This leads to

$$g_{l0}(\omega) = \frac{1}{\sqrt{\pi} \hat{z}} J_l \left( \frac{\omega \hat{z}}{c} \right). \quad (6.105)$$

The distribution perturbation is proportional to the Fourier transform of Eq. (6.105) and is related to the Chebyshev polynomials  $T_l(x) = \cos(l \cos^{-1} x)$  by

$$\tilde{\rho}_l^{(l)} \propto \frac{T_l(x)}{\sqrt{1-x^2}}. \quad (6.106)$$

where  $x = z/\hat{z}$ . [See Eq. (6.85).] These modes are referred to as the *Chebyshev modes*.

Substituting Eq. (6.105) into Eq. (6.102) gives the element of the  $1 \times 1$  matrix

$$M_{00} = i \frac{2Nr_0\eta c^2}{\gamma T_0^2 \omega_s^2 \hat{z}^2} l \sum_{p=-\infty}^{\infty} \frac{Z_0^{\parallel}(\omega')}{\omega'} J_l^2 \left( \frac{\omega' \hat{z}}{c} \right). \quad (6.107)$$

This gives an eigenvalue that coincides with Eq. (6.83).

## Parabolic Model

As a model more realistic than the water bag, consider the distribution

$$\psi_0(r) = \frac{3N\eta c}{2\pi\omega_s\hat{z}^3} \sqrt{\hat{z}^2 - r^2}, \quad r < \hat{z}. \quad (6.108)$$

The coefficient on the right hand side is the result of the normalization (6.78). The corresponding unperturbed longitudinal distribution is parabolic,

$$\rho_0(z) = \frac{3N}{4\hat{z}^3} (\hat{z}^2 - z^2), \quad |z| < \hat{z}, \quad (6.109)$$

and the rms bunch length is  $\sigma_z = \hat{z}/\sqrt{5}$ . This model is called the *parabolic model*.<sup>21</sup> The weight function is

$$W(r) = \frac{3}{2\pi\hat{z}^3} \frac{1}{\sqrt{\hat{z}^2 - r^2}}, \quad r < \hat{z}. \quad (6.110)$$

The orthonormal functions with weight function (6.110) are given by the Jacobi polynomials  $P_k^{(\alpha, \beta)}(x)$  evaluated at  $x = 1 - (2r^2/\hat{z}^2)$ . The closed form expressions are

$$f_k(r) = \hat{z} \sqrt{\frac{4\pi}{3}} \frac{(l + 2k + \frac{1}{2})k!\Gamma(l + k + \frac{1}{2})}{(l + k)!\Gamma(k + \frac{1}{2})} \left(\frac{r}{\hat{z}}\right)^l P_k^{(l, -1/2)}\left(1 - \frac{2r^2}{\hat{z}^2}\right), \quad (6.111)$$

where  $\Gamma(x)$  is the gamma function. Some properties of the Jacobi polynomials are given in Table 6.2.<sup>20</sup>

Substituting Eq. (6.111) into Eq. (6.101) and making use of the properties listed in Table 6.2 give

$$g_{lk}(\omega) = \frac{1}{\hat{z}} \sqrt{\frac{3}{2\pi}} \frac{(l + 2k + \frac{1}{2})\Gamma(k + \frac{1}{2})\Gamma(l + k + \frac{1}{2})}{k!(l + k)!} \frac{J_{l+2k+1/2}(\omega\hat{z}/c)}{\sqrt{\omega\hat{z}/c}}. \quad (6.112)$$

The longitudinal distribution of the disturbance  $\rho_1(z)$  of this mode is related to the Fourier transform of  $g_{lk}(\omega)$  according to Eq. (6.103). Again

<sup>21</sup>Note that what is parabolic is  $\rho_0(z)$ . This is in contrast to the water-bag model, for which what resembles a “water bag” is  $\psi_0(r)$ , not  $\rho_0(z)$ .

Table 6.2. Some properties of Jacobi polynomials

---

|   |   |
|---|---|
| $P_k^{(\alpha, \beta)}(x) = \frac{(-1)^k}{2^k k!} (1-x)^{-\alpha} (1+x)^{-\beta} \frac{d^k}{dx^k} [(1-x)^{\alpha+k} (1+x)^{\beta+k}]$   | $P_k^{(0,0)}(x) = P_k(x)$ = Legendre polynomial   |
| $\int_{-1}^1 dx (1-x)^\alpha (1+x)^\beta P_k^{(\alpha, \beta)}(x) P_{k'}^{(\alpha, \beta)}(x) = \frac{2^{\alpha+\beta+1} \Gamma(\alpha+k+1) \Gamma(\beta+k+1)}{k! (\alpha+\beta+2k+1) \Gamma(\alpha+\beta+k+1)} \delta_{kk'}$ |   |
| $\int_0^\infty \sqrt{x} dx J_{l+2k+1/2}(x) J_l(xy) = \frac{\sqrt{2} k!}{\Gamma(k + \frac{1}{2})} \frac{y^l}{\sqrt{1-y^2}} P_k^{(l, -1/2)}(1-2y^2) H(1- y )$   |   |
|   | $\int_{-\infty}^\infty dx e^{ixy} \frac{J_{k+1/2}(x)}{\sqrt{x}} = i^k \sqrt{2\pi} P_k(y)$ |
| $P_0^{(0, -1/2)} = 1,$  | $P_1^{(0, -1/2)} = \frac{1}{4}(3x+1)$   |
|   | $P_2^{(0, -1/2)} = \frac{1}{32}(35x^2 + 10x - 13)$  |
| $P_0^{(1, -1/2)} = 1,$  | $P_1^{(1, -1/2)} = \frac{1}{4}(5x+3)$   |
|   | $P_2^{(1, -1/2)} = \frac{1}{32}(63x^2 + 42x - 9)$   |
| $P_0^{(2, -1/2)} = 1,$  | $P_1^{(2, -1/2)} = \frac{1}{4}(7x+5)$   |
|   | $P_2^{(2, -1/2)} = \frac{1}{32}(99x^2 + 90x + 3)$   |
| $P_0 = 1,$  | $P_1 = x$   |
|   | $P_2 = \frac{1}{2}(3x^2 - 1)$   |
|   | $P_3 = \frac{1}{2}(5x^3 - 3x)$  |

---

using Table 6.2, we find

$$\rho_1^{(l, k)} \propto \int_{-\infty}^\infty d\omega e^{i\omega z/c} g_{lk}(\omega) \propto P_{l+2k}\left(\frac{z}{\hat{z}}\right), \quad (6.113)$$

where  $P_{l+2k}(x)$  is the Legendre polynomial of order  $l+2k$ .

Substituting Eq. (6.112) into Eq. (6.102) gives the elements of the interaction matrix  $M$ . In case the impedance is sharply peaked around the frequency  $\omega \approx \pm h\omega_0$ , we may keep only the terms  $p = \pm h$  in the summation of Eq. (6.102). If we further assume that the bunch length is much shorter than the range of the wake fields, i.e.,  $h\omega_0 \hat{z}/c \ll 1$ , the most prominent radial mode is that given by the matrix element  $M_{00}$  (because it is the largest matrix element), for which the mode frequency is

$$\Omega - l\omega_s \approx M_{00}\omega_s. \quad (6.114)$$

In particular, the instability growth rate, provided by the imaginary part of  $\Omega$ ,

is given by

$$\frac{1}{\tau^{(l)}} = \frac{3\sqrt{\pi}}{4(l-1)!\Gamma(l+\frac{3}{2})} \left( \frac{h\omega_0 \hat{z}}{2c} \right)^{2l-2} \frac{Nr_0 \eta h \omega_0}{2\gamma T_0^2 \omega_s} \\ \times [\operatorname{Re} Z_0^{\parallel}(h\omega_0 + l\omega_s) - \operatorname{Re} Z_0^{\parallel}(h\omega_0 - l\omega_s)]. \quad (6.115)$$

The Robinson growth rate (6.115) for the parabolic model is slightly different from Eq. (6.84) for the water-bag model. For the dipole  $l = 1$  mode, however, it does give the same result, and both reduce to Eq. (4.20). This is expected, because a short bunch executing dipole motion behaves as a point bunch and the details of  $\psi_0$  cannot matter. Furthermore, the Robinson stability criterion of the positioning of the impedance peak relative to  $h\omega_0$  remains the same for all  $l$ .

An interesting case occurs when the impedance is purely inductive with inductance  $iZ_0^{\parallel}/\omega = \text{const}$ , independent of  $\omega$ . If we further assume  $\omega_0 \hat{z}/c \ll 1$ , i.e., the bunch is much shorter than the accelerator circumference and the impedance is broad-band, we may approximate the summation over  $p$  by an integral,

$$\sum_{p=-\infty}^{\infty} \rightarrow \int_{-\infty}^{\infty} \frac{d\omega'}{\omega_0}. \quad (6.116)$$

Table 6.2 and Eq. (6.102) then give

$$M_{kk'} = T_1 \frac{3}{2\pi} \frac{l\Gamma(k + \frac{1}{2})\Gamma(l+k + \frac{1}{2})}{k!(l+k)!} \delta_{kk'}, \quad (6.117)$$

where we have introduced a dimensionless parameter that consists essentially of the beam current multiplied by the impedance, divided by the beam rigidity,

$$T_1 = \frac{Nr_0 \eta c^3}{\gamma T_0 \omega_s^2 \hat{z}^3} \left( i \frac{Z_0^{\parallel}}{\omega} \right). \quad (6.118)$$

The matrix  $M$  is *diagonal*. For a purely inductive impedance, the eigenmodes are readily solved by our choice of Jacobi polynomials as the base polynomials. The eigenmodes are the *Legendre modes*,

$$\Omega^{(l,n)} = (l + M_{nn})\omega_s, \\ \rho_l^{(l,n)}(z) \propto P_{l+2n}\left(\frac{z}{\hat{z}}\right), \\ \tilde{\rho}_l^{(l,n)}(\omega) \propto \frac{J_{l+2n+1/2}(\omega \hat{z}/c)}{\sqrt{\omega \hat{z}/c}}, \quad (6.119)$$

where  $l$  and  $n$  are the azimuthal and radial mode indices, respectively. The

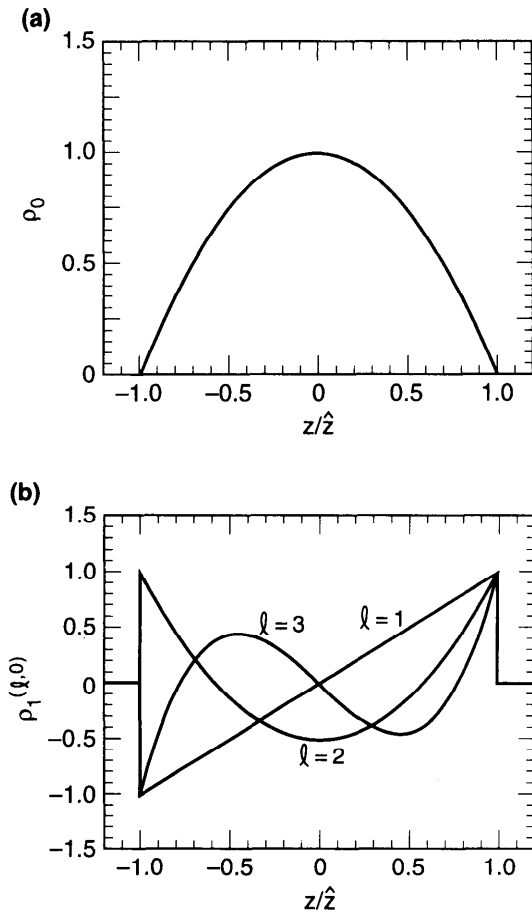


**Figure 6.17.** (a) Parabolic bunch distribution; (b) eigenmodes of a parabolic bunch when the impedance is purely inductive and broad-band. The modes shown have indices  $l = 1, 2, 3$  and  $n = 0$ . These figures are to be compared with Figures 6.12 and 6.13 for the water-bag model.

Legendre modes are associated with a parabolic model for  $\psi_0$ . Some of the lower modes are shown in Figure 6.17, and their frequency spectra are shown in Figure 6.18. Modes with the same value of  $l + 2n$  [for example, the mode  $(l = 0, n = 1)$  and the mode  $(l = 2, n = 0)$ ] have the same projection onto the longitudinal  $z$ -axis, although they have very different mode frequencies. In the longitudinal phase space, the Legendre modes can be constructed by combining the above information,

$$\psi_1^{(l, n)}(r, \phi) e^{-i\Omega s/c} \propto \underbrace{\frac{(r/\hat{z})^l}{\sqrt{1 - (r/\hat{z})^2}} P_n^{(l, -1/2)} \left(1 - \frac{2r^2}{\hat{z}^2}\right)}_{\text{radial dist.}} \underbrace{e^{il\phi}}_{\text{azim. dist.}} \underbrace{e^{-i\Omega^{(l, n)} s/c}}_{\text{time dep.}}. \quad (6.120)$$

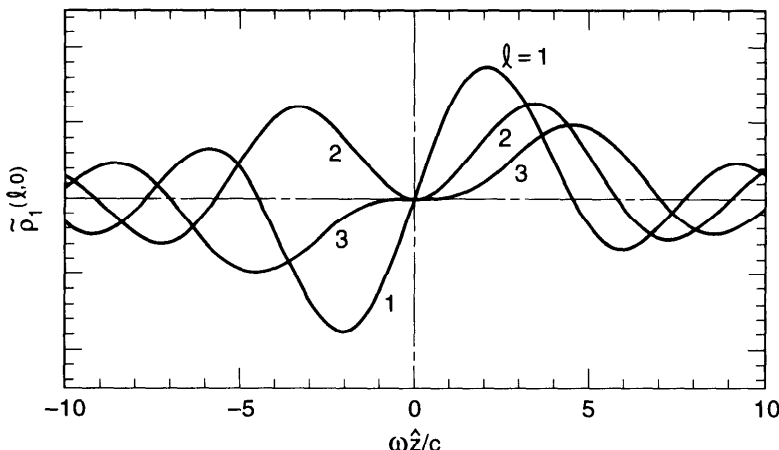


**Figure 6.18.** Fourier spectra of the modes shown in Figure 6.17(b). This figure can be compared with Figure 6.15(b) for the water-bag model.

Note that the matrix elements  $M_{nn}$ , and therefore the mode frequencies, are real. It follows that in the present case there are no collective instabilities, only mode frequency shifts. This is in contrast to the case of a sharp impedance for which the Robinson mechanism is a source of instability as seen in Eq. (6.115). The only collective instability so far is the Robinson type which involves long range wake fields. This conclusion has been reached already in the previous section; what is new here is that it continues to hold when coupling among the radial modes within one azimuthal family is included.

Given  $l$ , the most prominent radial mode—the one that has the largest complex frequency shift—is that with  $n = 0$ . It has

$$\Omega^{(l,0)} - l\omega_s \approx M_{00}\omega_s = \frac{3}{2\sqrt{\pi}} \frac{\Gamma(l + \frac{1}{2})}{(l-1)!} T_1 \omega_s. \quad (6.121)$$

Note that this frequency shift increases with the mode index  $l$ ; for large  $l$ , it grows indefinitely as  $\sqrt{l}$ . This means the higher azimuthal modes are important in this model; the most prominent mode would have a radial mode index  $n = 0$ , but its azimuthal mode index  $l$  diverges and is undefined. This importance of high frequency modes is an unsatisfactory consequence of the assumption that the impedance is proportional to  $\omega$  indefinitely.

Figure 6.19 shows the mode frequencies as functions of the parameter  $T_1$ . One observes three sets of frequencies clustered around  $\Omega = \omega_s$ ,  $2\omega_s$ , and  $3\omega_s$ , corresponding to the azimuthal mode indices  $l = 1, 2$ , and  $3$ , respectively. The five leading radial modes ( $n = 0$  to 4) are shown for each azimuthal family. In the analysis we have assumed that the mode frequency shifts are much smaller than  $\omega_s$  so that coupling among azimuthal modes

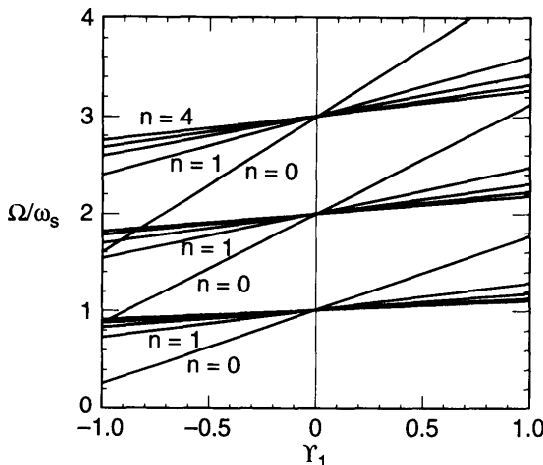


**Figure 6.19.** Mode frequencies versus the beam intensity parameter  $\Upsilon_1$ . A parabolic bunch and a purely inductive impedance have been assumed. Although the figure exhibits the range up to  $|\Upsilon_1| = 1$ , the range of applicability of the analysis is restricted to  $|\Upsilon_1| \ll 1$  so that the mode frequency shifts are much less than  $\omega_s$ . The mode frequency shifts increase with the mode index  $n$ .

can be ignored. This assumption gives rise to the fact that all mode frequencies in Figure 6.19 depends linearly on  $\Upsilon_1$ . As we will see in the next section, inclusion of coupling (at higher beam intensities) among the azimuthal modes causes these dependences to deviate from linearity.

As mentioned before, one has to be careful when applying the frequency shift results (6.119) and (6.121) because a potential-well distortion term has been dropped. To demonstrate this in the present model, consider the mode with  $l = 1$  and  $n = 0$ . The mode frequency shift, according to Eq. (6.121), is

$$\Omega^{(1,0)} - \omega_s = \frac{3}{4} \Upsilon_1 = \frac{3N r_0 \eta c^3}{4\gamma T_0 \omega_s \hat{z}^3} \left( i \frac{Z_0^{\parallel}}{\omega} \right). \quad (6.122)$$

This shift is exactly equal and opposite to the shift in  $\omega_s$  due to the potential-well distortion, Eq. (6.56), if one identifies  $S = -(iZ_0^{\parallel}/\omega)c^2$ . When the potential-well effect is included, therefore, the mode frequency  $\Omega^{(1,0)}$  does not shift with beam intensity for weak beam intensities. The physical reason for this phenomenon was given in Exercise 6.8(c).

**Exercise 6.11** Although the interplay between potential-well distortion and the dynamics of collective modes<sup>22</sup> is ignored in the analysis, one could

<sup>22</sup>K. Oide, *AIP Proc. 230, Nonlinear Dynamics and Particle Acceleration*, Tsukuba, 1990, p. 266; K. Oide, *Proc. 4th Advanced ICFA Workshop on Collective Effects in Short Bunches*, 1990, KEK Report 90-21, p. 64.

consider an approximate description, valid to first order in beam intensity, by simply adding the two contributions algebraically. Show that, with a space charge impedance (2.80), the frequency of the  $l$ th mode, including the contribution from the potential-well distortion, is approximately

$$\begin{aligned}\Delta\nu^{(l,0)} &= \frac{\Omega^{(l,0)} - l\omega_s}{\omega_0} \\ &\approx l \frac{3Nr_0\eta R^2}{2\beta^2\gamma^3\hat{z}^3\nu_s} \left( \ln \frac{b}{a} + \frac{1}{2} \right) \left[ 1 - \frac{2}{\sqrt{\pi}} \frac{\Gamma(l + \frac{1}{2})}{l!} \right],\end{aligned}\quad (6.123)$$

where the first term in the square brackets gives the contribution from the potential-well distortion  $l\Delta\nu_s$ , where  $\Delta\nu_s$  is the incoherent synchrotron tune shift calculated in Eq. (6.56). More explicitly, show that

$$\Delta\nu^{(1,0)} \approx 0, \quad \Delta\nu^{(2,0)} \approx \frac{1}{2}\Delta\nu_s, \quad \Delta\nu^{(3,0)} \approx \frac{9}{8}\Delta\nu_s. \quad (6.124)$$

## Gaussian Model

The same procedure for the parabolic model can also be followed for a Gaussian model,

$$\begin{aligned}\psi_0(r) &= \frac{N\eta c}{2\pi\sigma^2\omega_s} e^{-r^2/2\sigma^2}, \\ \rho_0(z) &= \frac{N}{\sqrt{2\pi}\sigma} e^{-z^2/2\sigma^2},\end{aligned}\quad (6.125)$$

where  $\sigma$  is the rms bunch length. The corresponding weight function is

$$W(r) = \frac{1}{2\pi\sigma^4} e^{-r^2/2\sigma^2}. \quad (6.126)$$

The orthonormal polynomials are found in terms of generalized Laguerre polynomials  $L_k^{(l)}(x)$  as

$$f_k(r) = \sigma \sqrt{\frac{2\pi k!}{(l+k)!}} \left( \frac{r}{\sqrt{2}\sigma} \right)^l L_k^{(l)} \left( \frac{r^2}{2\sigma^2} \right). \quad (6.127)$$

Some properties of generalized Laguerre polynomials are listed in Table 6.3.

Table 6.3. Some properties of generalized Laguerre polynomials

---


$$L_k^{(l)}(x) = \sum_{m=0}^k (-1)^m \frac{(l+k)!}{(k-m)!(l+m)!} \frac{x^m}{m!}$$

$$\int_0^\infty dx e^{-x} x L_k^{(l)}(x) L_k^{(l)}(x) = \frac{(l+k)!}{k!} \delta_{kk'}$$

$$\int_0^\infty dx x^{l+1} e^{-\beta x^2} J_l(xy) L_k^{(l)}(\alpha x^2) = \frac{(\beta - \alpha)^k}{2^{l+1} \beta^{l+k+1}} y^l e^{-y^2/4\beta} L_k^{(l)} \left[ \frac{\alpha y^2}{4\beta(\alpha - \beta)} \right]$$

$$L_0^{(0)} = 1, \quad L_1^{(0)} = 1 - x$$

$$L_2^{(0)} = 1 - 2x + \frac{1}{2}x^2$$

$$L_3^{(0)} = 1 - 3x + \frac{3}{2}x^2 - \frac{1}{6}x^3$$

$$L_0^{(1)} = 1, \quad L_1^{(1)} = 2 - x$$

$$L_2^{(1)} = 3 - 3x + \frac{1}{2}x^2$$

$$L_3^{(1)} = 4 - 6x + 2x^2 - \frac{1}{6}x^3$$

$$L_0^{(2)} = 1, \quad L_1^{(2)} = 3 - x$$

$$L_2^{(2)} = 6 - 4x + \frac{1}{2}x^2$$


---

It follows that

$$g_{lk}(\omega) = \frac{1}{\sigma \sqrt{2\pi k!(l+k)!}} \left( \frac{\omega \sigma}{\sqrt{2c}} \right)^{l+2k} e^{-\omega^2 \sigma^2 / 2c^2} \quad (6.128)$$

and

$$M_{kk'} = i \frac{Nr_0 \eta c^2}{\gamma T_0^2 \omega_s^2 \sigma^2} \frac{l}{\sqrt{k!k'!(l+k)!(l+k')!}}$$

$$\times \sum_{p=-\infty}^{\infty} \frac{Z_0^{||}(\omega')}{\omega'} e^{-\omega'^2 \sigma^2 / c^2} \left( \frac{\omega'^2 \sigma^2}{2c^2} \right)^{l+k+k'}, \quad (6.129)$$

where  $\omega' = p\omega_0 + l\omega_s$ . The longitudinal distribution of the mode is related through Eq. (6.103) to the Fourier transform of  $g_{lk}(\omega)$ ,

$$\int \frac{d\omega}{2\pi} e^{i\omega z/c} g_{lk}(\omega) \propto e^{-z^2/2\sigma^2} H_{l+2k} \left( \frac{z}{\sqrt{2}\sigma} \right), \quad (6.130)$$

where  $H_{l+2k}(x)$  is the Hermite polynomial of order  $l+2k$ . The indices  $l$  and  $k$  appear as the combination  $l+2k$ , just as in the Legendre modes (6.119).

For an impedance sharply peaked around  $\omega \approx \pm h\omega_0$  and a short bunch with  $h\omega_0\sigma/c \ll 1$ , the Robinson growth rate for the most prominent radial

mode can be estimated by  $M_{00}$  as

$$\begin{aligned}\frac{1}{\tau^{(l)}} &= \text{Im}(\Omega - l\omega_s) \approx \text{Im}(M_{00}\omega_s) \\ &= \frac{1}{(l-1)!} \left( \frac{h\omega_0\sigma}{\sqrt{2c}} \right)^{2l-2} \frac{Nr_0\eta h\omega_0}{2\gamma T_0^2\omega_s} \\ &\quad \times [\text{Re } Z_0^{\parallel}(h\omega_0 + l\omega_s) - \text{Re } Z_0^{\parallel}(h\omega_0 - l\omega_s)].\end{aligned}\quad (6.131)$$

Just as in the water-bag and parabolic models, this reduces to the familiar result when  $l = 1$ , and the same Robinson stability criterion applies for all  $l$ .

In the case of a purely inductive impedance, we have

$$M_{kk'} = T_2 \frac{l(2l+2k+2k'-1)!!}{4^{l+k+k'} \sqrt{k!k'!(l+k)!(l+k')!}}, \quad (6.132)$$

where

$$T_2 = \frac{Nr_0\eta c^3}{2\sqrt{\pi}\gamma T_0\omega_s^2\sigma^3} \left( i \frac{Z_0^{\parallel}}{\omega} \right). \quad (6.133)$$

This time the matrix  $M$  is no longer diagonal, although the elements  $M_{kk'}$  remain real. The generalized Laguerre polynomials do not happen to be the eigenmodes for the Gaussian model for the purely inductive impedance. For a given azimuthal mode  $l$ , the eigenmode frequencies are obtained numerically by truncating the matrix to an appropriate dimension. The results are exhibited in Figure 6.20. One observes again that mode frequencies depart from their unperturbed values  $l\omega_s$  linearly in  $T_2$ , and that all radial modes are stable. The only instability at this point is still of the Robinson type.

**Exercise 6.12** Consider a resistive-wall impedance (2.76), make the broad-band approximation<sup>23</sup> (6.116), and ignore the potential-well distortion.

(a) Show that for the water-bag model,

$$\Omega - l\omega_s = \frac{Nr_0\eta c^2}{\pi\gamma\omega_sb\hat{z}^2} \sqrt{\frac{c}{\hat{z}\sigma}} \frac{l\Gamma(l+\frac{1}{4})}{[\Gamma(\frac{3}{4})]^2\Gamma(l+\frac{3}{4})}, \quad (6.134)$$

which increases as  $\sqrt{l}$  for large  $l$ .

(b) Use Table 6.1 to obtain a closed form expression for  $M_{kk'}$  for a parabolic beam. Calculate numerically the eigenmode frequencies as

<sup>23</sup>The broad-band approximation is justified here even for the resistive-wall impedance, because there is no singularity at  $\omega \rightarrow 0$  in these applications.

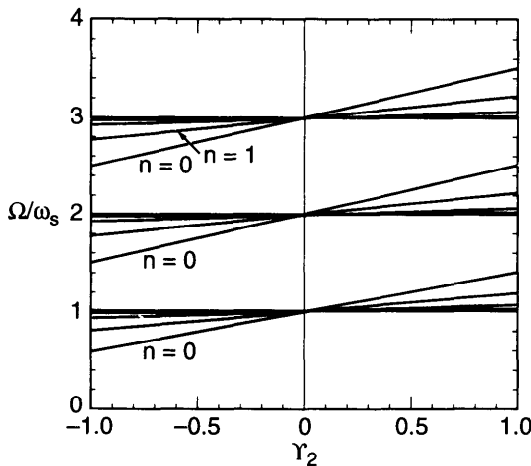


**Figure 6.20.** Mode frequencies versus the beam intensity parameter  $\gamma_2$ , for a Gaussian bunch and a purely inductive impedance.

functions of

$$\Upsilon_3 = \frac{3}{16\pi} \frac{Nr_0\eta c^2}{\gamma\omega_s^2 b\hat{z}^2} \sqrt{\frac{c}{\sigma\hat{z}}} . \quad (6.135)$$

The result is shown in Figure 6.21. How does the frequency shift  $\Omega - l\omega_s$  depend on the mode index  $l$  as  $l$  increases? For a given  $l$ , is the frequency of the leading radial mode well approximated by  $\Omega - l\omega_s \approx M_{00}\omega_s$ ? In Eqs. (6.134–6.135),  $\sigma$  is the conductivity of the resistive wall.

Ignoring coupling among different azimuthal modes, we have now dealt with three bunch distribution models: the water-bag, the parabolic, and the Gaussian models. The eigenmodes for the water-bag model were found to be Chebyshev modes (6.106) regardless of the impedance. For the parabolic model, we do not have a closed form expression of the eigenmodes in general, but for a broad-band, purely inductive impedance, the eigenmodes are given by the Legendre modes (6.119). For the Gaussian model, we did not find closed form expression of the eigenmodes even for a purely inductive impedance. However, a convenient choice of the base functions had led to the Hermite modes (6.130).

### Effective Impedance

Given the impedance  $Z_0^\parallel$  and the unperturbed beam distribution  $\psi_0$ , the beam stability problem is solved by analyzing the eigensystem as described so

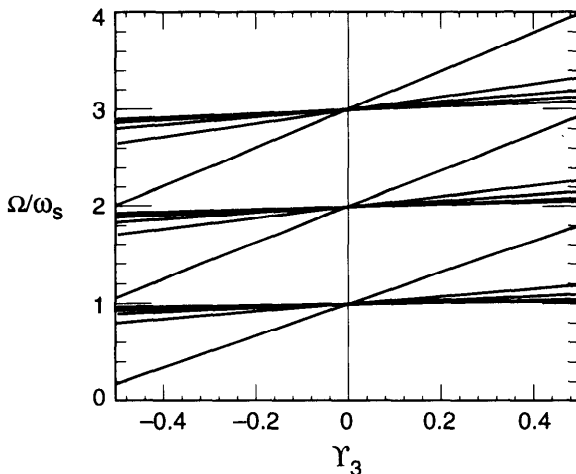


**Figure 6.21.** Mode frequencies of a parabolic beam in the presence of a resistive-wall impedance.

far. This, however, is a tedious procedure, particularly because  $Z_0^{\parallel}$  may have a frequency dependence much more complicated than a purely inductive impedance, and  $\psi_0$  may not be as simple as the parabolic model. In practice, therefore, one often compromises and, instead of results of detailed eigenanalysis, asks only for a rough idea of the instability picture. Questions raised are typically of immediate relevance to the accelerator at hand, such as which modes are most likely to be affected by the given impedance, and what are the orders of magnitude of the growth rates and frequency shifts of these modes. These questions can be addressed, in a short-cut manner, using a quantity called the *effective impedance*.<sup>24</sup>

The procedure followed in this section resembles closely the perturbation technique used in quantum mechanics. Indeed, the interaction matrix element  $M_{kk'}$  in Eq. (6.102) can be expressed in a quantum mechanical notation as

$$\left\langle l, k \left| \frac{Z_0^{\parallel}}{\omega} \right| l, k' \right\rangle \equiv \sum_p \frac{Z_0^{\parallel}(\omega')}{\omega'} g_{lk}(\omega') g_{lk'}(\omega'), \quad (6.136)$$

where one recalls the notation  $\omega' = p\omega_0 + l\omega_s$ . The reason that the impedance samples the frequency at  $\omega'$  was given in Eq. (4.19).

If the problem has been diagonalized so that the eigenmodes have been found and  $\tilde{\rho}_l^{(l,n)}(\omega) \propto i^{-l} g_{ln}(\omega)$  are known, then by Eq. (6.102) we can write

<sup>24</sup>F. Sacherer, IEEE Tran. Nucl. Sci. NS-24, 1393 (1977); B. Zotter, CERN Report ISR-TH/78-16 (1978); B. Zotter, CERN Report ISR-TH/80-03 (1980); K. Balewski and R. D. Kohaupt, DESY Report 90-152 (1990).

the mode frequency as

$$\Omega^{(l,n)} - l\omega_s = M_{nn}\omega_s \\ = \frac{2\pi N r_0 \eta c^2}{\gamma T_0^2 \omega_s} l i \left( \frac{Z_0^{\parallel}}{\omega} \right)_{\text{eff}} \sum_{p=-\infty}^{\infty} |g_{ln}(\omega')|^2, \quad (6.137)$$

where we have introduced an effective impedance

$$\left( \frac{Z_0^{\parallel}}{\omega} \right)_{\text{eff}} = \frac{\sum_{p=-\infty}^{\infty} \frac{Z_0^{\parallel}(\omega')}{\omega'} |\tilde{\rho}_1^{(l,n)}(\omega')|^2}{\sum_{p=-\infty}^{\infty} |\tilde{\rho}_1^{(l,n)}(\omega')|^2}, \quad (6.138)$$

which depends on the mode indices  $l$  and  $n$ .<sup>25</sup> The quantity  $(Z_0^{\parallel}/\omega)_{\text{eff}}$  is essentially the weighted average of the impedance over the bunch mode spectral power  $|\tilde{\rho}_1^{(l,n)}|^2$ . Whether a particular mode is driven significantly by the impedance is determined by the degree to which the impedance overlaps the mode spectrum.

If the problem has not been diagonalized, but one has the situation where the most prominent radial mode has the frequency  $\Omega^{(l)} \approx (l + M_{00})\omega_s$ , or if one is interested only in an order-of-magnitude estimate of the complex mode frequency shifts, one may still apply Eqs. (6.137–6.138), even without explicitly finding the eigenmodes. Although not rigorous, Eqs. (6.139–6.143) below are often used in practical applications.

Take the parabolic bunch for example. We have diagonalized the problem for the special case of a purely inductive impedance. For a general impedance, Eq. (6.137) gives, for the most prominent radial mode,

$$\Omega^{(l)} - l\omega_s \approx \frac{3}{2\sqrt{\pi}} \frac{\Gamma(l + \frac{1}{2})}{(l-1)!} \frac{N r_0 \eta c^3}{\gamma T_0 \omega_s \hat{z}^3} i \left( \frac{Z_0^{\parallel}}{\omega} \right)_{\text{eff}}, \quad (6.139)$$

where

$$\left( \frac{Z_0^{\parallel}}{\omega} \right)_{\text{eff}} = \frac{\sum_{p=-\infty}^{\infty} \frac{Z_0^{\parallel}(\omega')}{\omega'} h_l(\omega')}{\sum_{p=-\infty}^{\infty} h_l(\omega')}, \quad (6.140)$$

<sup>25</sup> Expressions (6.137–6.138) are not very useful for the water-bag model because the summation in Eq. (6.137)—and, equivalently, the denominator in Eq. (6.138)—diverges. The sharp cutoff in the water-bag distribution has introduced a large high frequency contribution. This divergence does not occur for the more realistic parabolic or the Gaussian distribution.

and, from Eq. (6.112),

$$h_l(\omega) = \frac{[J_{l+1/2}(\omega\hat{z}/c)]^2}{|\omega\hat{z}/c|}. \quad (6.141)$$

Because we are addressing the most prominent radial mode, the effective impedance of Eq. (6.140) depends on the mode index  $l$  but not the radial mode index  $n$ . Also, the effective impedance describes the effect of impedance on beam dynamics. It is not the same as the raw impedance we have been used to up to now. In particular, the effective impedance depends on the beam properties, while the raw impedance does not.

As mentioned, Eq. (6.112) is the mode spectrum only for a purely inductive impedance. In obtaining Eq. (6.139), however, we have insisted that the same eigenmode spectra apply even for the arbitrary impedance under consideration, and we have made the broad-band approximation (6.116) when we performed the summation over  $p$  in Eq. (6.137). For a purely inductive impedance, Eq. (6.139) becomes (6.121), as it should.

The real and the imaginary parts of  $(Z_0^{\parallel}/\omega)_{\text{eff}}$  give the growth rate and the frequency shift of the mode under consideration. For a broad-band impedance,  $(Z_0^{\parallel}/\omega)_{\text{eff}}$  is purely imaginary because  $\text{Re } Z_0^{\parallel}(\omega)$  is an even function of  $\omega$ ; the growth rate vanishes and there is no instability.

A similar procedure can be followed for a Gaussian beam. We obtain

$$\Omega^{(l)} - l\omega_s \approx \frac{1}{2\pi} \frac{\Gamma(l + \frac{1}{2})}{2^l(l-1)!} \frac{Nr_0\eta c^3}{\gamma T_0 \omega_s \sigma^3} i \left( \frac{Z_0^{\parallel}}{\omega} \right)_{\text{eff}}, \quad (6.142)$$

where the effective impedance is given by Eq. (6.140) with

$$h_l(\omega) = \left( \frac{\omega\sigma}{c} \right)^{2l} e^{-\omega^2\sigma^2/c^2}. \quad (6.143)$$

More justification of Eqs. (6.142–6.143), at least for short Gaussian bunches, can be found in Exercise 6.14.

**Exercise 6.13** Perform one of the following two calculations numerically: (a)  $(Z_0^{\parallel}/\omega)_{\text{eff}}$  for a parabolic bunch and a broad-band resonator impedance; (b) the same for a Gaussian bunch. The real part of  $(Z_0^{\parallel}/\omega)_{\text{eff}}$  vanishes. Which azimuthal mode is driven most strongly? How does the sign of  $(Z_0^{\parallel}/\omega)_{\text{eff}}$  depend on the azimuthal mode index  $l$ ? Relate the answers to the overlap between the impedance and the mode spectra. The result for a Gaussian bunch is shown in Figure 6.22. The overlap consideration is illustrated in Figure 6.23. Compare result with that obtained for a waterbag model in Exercise 6.9.

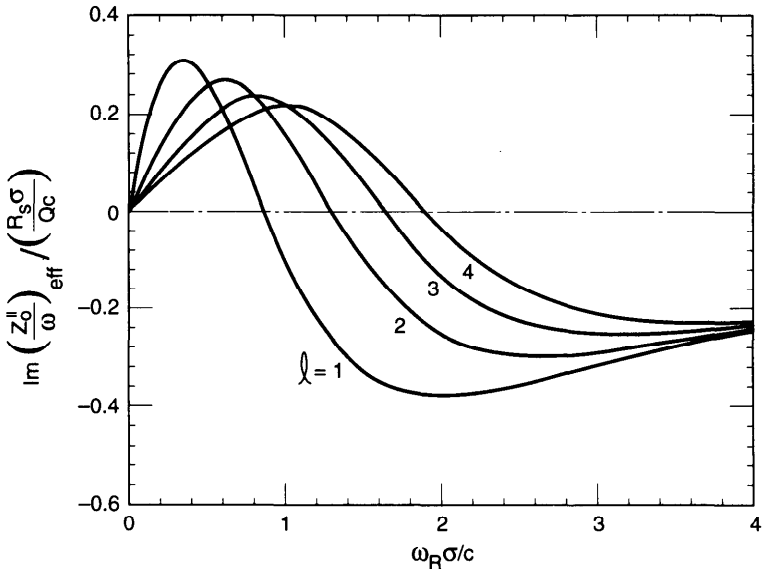


**Figure 6.22.** The effective impedance seen by a Gaussian bunch when the impedance is that of a broad-band resonator. The graph shows  $\text{Im}(Z_0^{\parallel}/\omega)_{\text{eff}}/(R_S\sigma/Qc)$  as a function of  $\omega_R\sigma/c$  for  $l = 1, 2, 3$ , and  $4$  and  $Q = 1$ . The behavior can be understood by relating it to the overlapping between the impedance  $Z_0^{\parallel}(\omega)/\omega$  and the mode spectra  $h_l(\omega)$  as illustrated in Figure 6.23.

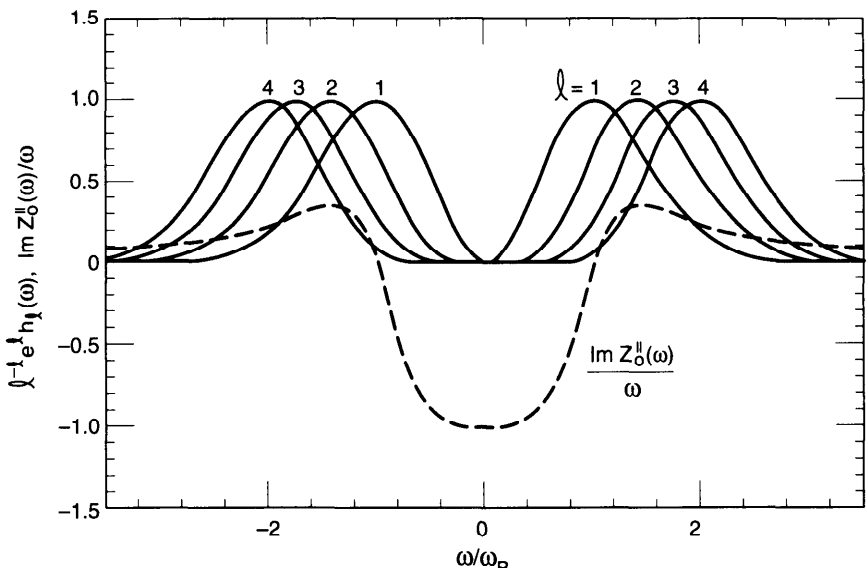


**Figure 6.23.** The effective impedance  $\text{Im}(Z_0^{\parallel}/\omega)_{\text{eff}}$  is obtained from the overlap integral between  $Z_0^{\parallel}(\omega)/\omega$  and  $h_l(\omega)$ . The solid curves are  $h_l(\omega)$  for a Gaussian beam and  $l = 1, 2, 3, 4$  (normalized so that they have the same value at their respective maxima). The dashed curve is  $\text{Im } Z_0^{\parallel}(\omega)/\omega$  for a broad-band resonator. The frequency extent of the impedance is  $\omega_R$ . The frequency extent of the mode spectra is related to  $\sigma$ , with the spectral peak of the  $l$ th mode located at  $\omega = \sqrt{l}c/\sigma$ . For the parameters chosen, with  $c/\sigma = \omega_R$  and  $Q = 1$ , the  $l = 1$  and  $2$

The ideas of the effective impedance and the broad-band resonator model, Eqs. (2.121) and (2.128), can be combined into a useful package for practical applications. Take for example an electron accelerator with  $N = 10^{11}$ ,  $\eta = 0.02$ ,  $b = \sigma = 5$  cm,  $\omega_s = 1.9 \times 10^5$  s $^{-1}$ ,  $E = 7$  GeV and a broad-band resonator impedance with  $Q = 1$  and  $R_s = 720$   $\Omega$  (one deep cavity every 25 m,  $Z_0^{\parallel}/n = R_s b/R = 0.75$   $\Omega$ ). Figure 6.22 gives  $(Z_0^{\parallel}/n)_{\text{eff}} = 0.10 Z_0^{\parallel}/n$  for  $l = 1$  and  $-0.15 Z_0^{\parallel}/n$  for  $l = 2$ , according to which one obtains the mode tune shifts of  $\Delta\nu_s^{(l)} = 0.7 \times 10^{-5}$  for  $l = 1$  and  $-0.8 \times 10^{-5}$  for  $l = 2$ .

## 6.5 AZIMUTHAL MODES

In Section 6.3 we derived for the water-bag model the collective mode frequency (6.83) for a weak beam. We then obtained the Robinson instability growth rate (6.84) and pointed out that the only instability that the weak beam allows is of the Robinson type. In other words, instability occurs only when the impedance consists of sharp peaks like those sketched in Figure 2.27 below cutoff, or equivalently, when the wake field lasts longer than the revolution period. In case the impedance is broad-band, we concluded at the time that all modes are necessarily stable.

This conclusion was not changed when we included the radial modes in Section 6.4.<sup>26</sup> The beam intensity considered is weak, so that the mode frequency shifts are small compared with  $\omega_s$  and we could ignore the coupling among modes of different azimuthal families. The only instability found there is still of the Robinson type. If we further increase the beam intensity, however, the frequency shifts become comparable to  $\omega_s$ , so that coupling among azimuthal modes must be considered. Such a phenomenon, referred to as “mode coupling,”<sup>27</sup> “mode mixing,” or “turbulence” in the literature, can lead to instabilities other than the Robinson type.

To demonstrate this *mode coupling instability*, consider first a water-bag beam (ignoring the radial modes) and a broad-band impedance for which the approximation (6.116) holds—the Robinson instability is therefore excluded. From Eq. (6.80), the eigenvalue  $\Omega/\omega_s$  is determined by the condition

$$\det\left(\frac{\Omega}{\omega_s} I - M\right) = 0, \quad (6.144)$$

<sup>26</sup>Recall that the water-bag model does not allow the study of the radial modes. What we demonstrated in Section 6.4 says that the lack of radial structure of the modes is not the cause of this conclusion.

<sup>27</sup>The “mode” here refers to the azimuthal modes. Coupling of radial modes was already considered in Section 6.4.

where  $I$  is a unit matrix and  $M$  is a matrix with elements

$$M_{ll'} = l\delta_{ll'} + i \frac{Nr_0\eta c^2}{\pi\gamma T_0\omega_s^2\hat{z}^2} li^{l-l'} \int_{-\infty}^{\infty} d\omega \frac{Z_0^{\parallel}(\omega)}{\omega} J_l\left(\frac{\omega\hat{z}}{c}\right) J_{l'}\left(\frac{\omega\hat{z}}{c}\right). \quad (6.145)$$

By applying Eq. (6.116), we have, in effect, ignored the multturn effects. Written out explicitly,  $M$  is a real matrix; it has the form

$$M = \begin{bmatrix} \dots & & & & & \\ \dots & & & & & \\ & 2 + I & R & I & R & I \\ & R & 1 + I & R & I & R \\ & 0 & 0 & 0 & 0 & 0 \\ & R & I & R & -1 + I & R \\ & I & R & I & R & -2 + I \\ & & & & & \dots \\ & & & & & \dots \end{bmatrix}, \quad (6.146)$$

where the  $l = 0$  elements all vanish; the  $I$ 's and  $R$ 's are real quantities, all different from one another, with  $I$  coming only from  $\text{Im } Z_0^{\parallel}$  and  $R$  coming only from  $\text{Re } Z_0^{\parallel}$ . All  $R$ 's and  $I$ 's are proportional to the beam intensity  $N$ . If we drop all the off-diagonal mode coupling terms, we will obtain the weak beam result (6.83). The off-diagonal elements are antisymmetric, i.e.,  $M_{-l, -l'} = -M_{l, l'}$ .

It follows from the structure of the interaction matrix  $M$  that the mode coupling instability results from an interplay between the real and the imaginary parts of the impedance, with the leading contribution in the product form  $RI$  and quadratic in  $N$ . Note also that  $\Omega = 0$  is always a solution; this is the mode that describes the static potential-well distortion.

Equation (6.145) assumes a broad-band impedance. Mode coupling also has an effect for sharp impedances.<sup>28</sup> Consider the case when the beam is happily Robinson damped by proper tuning of a sharp impedance whose resonant frequency is close to  $\hbar\omega_0$ . Instability can still occur at higher beam intensities due to the mode coupling mechanism, thus spoiling the Robinson damping. However, we will not pursue this possibility.

Let us proceed again with an illustrative example. Consider the broad-band impedance

$$Z_0^{\parallel}(\omega) = R_0 \left| \frac{\omega_0}{\omega} \right|^{1/2} [1 + \text{sgn}(\omega)i], \quad (6.147)$$

where  $R_0$  is a real positive constant. This impedance corresponds to the

<sup>28</sup>Tai-sen F. Wang, Part. Accel. 34, 105 (1990).

diffraction model (2.145) and has the associated wake function  $W'_0(z) \propto |z|^{-1/2}$ . The matrix elements of  $M$  are

$$M_{ll'} = l\delta_{ll'} - lC_{ll'}\Upsilon, \quad (6.148)$$

with

$$C_{ll'} = \frac{\frac{1}{2}\Gamma\left(\frac{l+l'-\frac{1}{2}}{2}\right)}{\Gamma\left(\frac{l'-l+\frac{5}{2}}{2}\right)\Gamma\left(\frac{l+l'+\frac{5}{2}}{2}\right)\Gamma\left(\frac{l-l'+\frac{5}{2}}{2}\right)} \times \begin{cases} (-1)^{(l-l')/2} & \text{if } l-l' \text{ is even,} \\ (-1)^{(l-l'-1)/2} & \text{if } l-l' \text{ is odd,} \end{cases} \quad (6.149)$$

where we have defined a dimensionless parameter

$$\Upsilon = \frac{Nr_0\eta R_0}{\gamma\omega_s^2} \left( \frac{c}{T_0\hat{z}} \right)^{3/2} \quad (6.150)$$

and use has been made of Table 6.1.

We have evaluated the eigenvalues  $\Omega/\omega_s$  numerically as functions of  $\Upsilon$ ; the results for the lowest few modes are shown in Figure 6.24. Unlike Figures 6.19–6.21, each azimuthal family in Figure 6.24 has only one radial mode because of the radial degeneracy of the water-bag model. At  $\Upsilon = 0$ , the mode frequencies are simply multiples of  $\omega_s$ . As  $\Upsilon$  increases, the mode frequencies shift. Also unlike Figures 6.19–6.21, the frequency shifts here are not linear in  $\Upsilon$ . As  $\Upsilon$  reaches the critical value  $\Upsilon_{th} \approx 1.45$ , two of the mode frequencies become equal, and when  $\Upsilon > \Upsilon_{th}$ , they become imaginary and the beam is unstable. The parameter  $\Upsilon_{th}$  thus defines the instability threshold of the beam. Note that the instability growth rate increases sharply as soon as  $\Upsilon$  exceeds  $\Upsilon_{th}$ , in the sense that a slight increase in beam intensity beyond the threshold leads to a growth rate comparable to  $\omega_s$ . This is a general property of the mode coupling instabilities.

The matrix (6.148) has infinite dimensions. The eigenvalues in Figure 6.24 are evaluated numerically with the matrix truncated. For the truncation procedure to converge, the beam spectrum, as well as the impedance, must not have long tails at high frequencies. For a water-bag model, the impedance at high frequencies must decrease sufficiently rapidly with increasing frequency. The impedance (6.147) [and also (6.215) and (6.224) in later illustrations] is chosen with these considerations in mind.

The purely inductive, the space charge, and the resistive-wall impedances thus cannot be treated by this approach for the water-bag model. The lack of

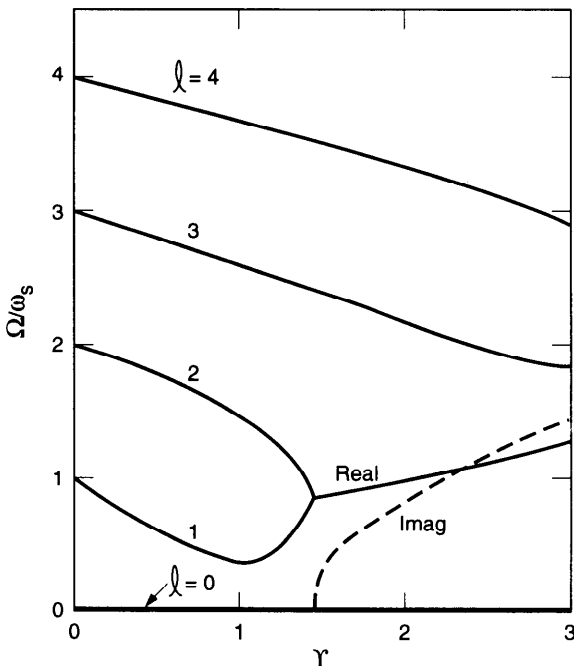


**Figure 6.24.** Longitudinal mode frequencies  $\Omega / \omega_s$  versus the parameter  $\Upsilon$  for a water-bag beam with the impedance (6.147). Instability occurs when  $\Upsilon > \Upsilon_{\text{th}} \approx 1.45$  and the  $l = 1$  and  $l = 2$  mode-frequency lines merge. The solid curves give the real part of the mode frequencies; the dashed curve gives the imaginary part (magnitude only) of the  $l = 1$  and  $l = 2$  mode frequencies above threshold. There is always a static mode with  $\Omega = 0$ . The spectra for  $l < 0$  are mirror images with respect to the  $\Omega = 0$  line. Effects of potential-well distortion have been ignored; otherwise the  $l = 1$  mode frequency would not shift, at least for small  $\Upsilon$ .

convergence is also reflected by the fact that the mode frequency shift increases with the azimuthal index  $l$  as discussed in the previous section. [See Eqs. (6.121) and (6.134).] In case the truncation procedure does not converge, the formalism based on the expansion (6.72) breaks down. Better convergence may be obtained by expanding  $\psi_1$  in the Cartesian coordinates  $z$  and  $\delta$  instead of the present polar coordinates  $r$  and  $\phi$ . The beam behaves more like an unbunched beam. The mode coupling instability treated here for bunched beams then makes a transition to become the microwave instability treated in Section 5.4 for unbunched beams.

We already know that the  $l = 0$  mode is always static; its frequency  $\Omega = 0$  does not move as the beam intensity is varied. We also know that for moderate beam intensities, the dipole  $l = 1$  mode frequency does not move either, as it should when the bunch executes a rigid longitudinal motion and the wake field pattern moves with the bunch—mathematically, this is due to a cancellation between the potential-well and the dynamical contributions, as

discussed in Exercises 6.8 and 6.11. In Figure 6.24, the instability occurs as the  $l = 1$  and the  $l = 2$  modes merge when  $\Upsilon = 1.45$ , but that is when the potential-well contribution has been ignored. If included, the  $l = 1$  mode frequency would not move as shown. This means the longitudinal mode coupling instability is forced to involve high order modes of order  $|l| \geq 2$ , making the convergence issue more pronounced. This situation, as we will see in Section 6.7, is quite different from the transverse situation when the main effects are carried out by the  $l = 0$  and the  $l = -1$  modes in a clean manner. Longitudinal mode coupling is intrinsically more complex than its transverse counterpart.

### Gaussian and Parabolic Models

So far we have been considering the water-bag model. Similar treatment can be applied to the Gaussian model (6.125) except that analytic expressions are available only for short bunches. To proceed, consider the function  $F_l(p, q)$  of Eq. (6.89). For a Gaussian beam, we have

$$\begin{aligned} F_l(p, q) = & -\frac{N\eta c}{2\pi\sigma^2\omega_s} \exp\left[-\frac{\sigma^2}{2c^2}(p\omega_0 + \Omega)^2 - \frac{\sigma^2}{2c^2}(q\omega_0 + \Omega)^2\right] \\ & \times I_l\left[\frac{\sigma^2}{c^2}(p\omega_0 + \Omega)(q\omega_0 + \Omega)\right], \end{aligned} \quad (6.151)$$

where  $I_l(x)$  is the Bessel function. For short bunches, the argument in the Bessel function is  $\ll 1$ ,  $F_l(p, q)$  factorizes as prescribed in Eq. (6.90), with

$$T_l(\omega) = \sqrt{\frac{N\eta c}{2\pi l!\sigma^2\omega_s}} \left(\frac{\omega\sigma}{\sqrt{2}c}\right)^l e^{-\sigma^2\omega^2/2c^2}. \quad (6.152)$$

This  $T_l(\omega)$  is related to the  $k = 0$  component of the spectrum  $g_{lk}(\omega)$  of Eq. (6.128) by  $T_l(\omega) = g_{l0}(\omega)\sqrt{N\eta c/\omega_s}$ . This indicates that for short bunches, the  $k = 0$  component describes the most prominent radial mode.

As worked out in Exercise 6.10, a factorizable  $F_l(p, q)$  means the problem is soluble (a condition which is sufficient but not necessary); the solution is given by Eqs. (6.91–6.92). Equation (6.91), when Fourier transformed, gives the distribution perturbation [see Eq. (6.130)],

$$\rho_1^{(l)}(z) \propto e^{-z^2/2\sigma^2} H_l\left(\frac{z}{\sqrt{2}\sigma}\right), \quad (6.153)$$

where  $H_l(x)$  is the Hermite polynomial. Equation (6.92) can be written in the

matrix form (6.144) to give the mode frequency  $\Omega$ , where

$$M_{ll'} = l\delta_{ll'} + i \frac{Nr_0\eta c^2}{2\pi\gamma T_0\omega_s^2\sigma^2} \frac{l^{l-l'}}{\sqrt{l!l'!}} \times \int_{-\infty}^{\infty} d\omega \frac{Z_0^{\parallel}(\omega)}{\omega} e^{-\sigma^2\omega^2/\sigma^2} \left( \frac{\sigma\omega}{\sqrt{2}c} \right)^{l+l'}. \quad (6.154)$$

Equation (6.154) is the Gaussian model counterpart of Eq. (6.145). Radial modes are ignored in this treatment.

**Exercise 6.14** If mode coupling can be ignored, we may keep only the diagonal terms of the matrix  $M$ . Show that for a short Gaussian beam, this procedure reproduces the expression (6.142) in terms of the effective impedance.

**Exercise 6.15** Specialize the result (6.154) to the space charge impedance. Perform a numerical calculation to construct the mode frequency diagram like Figure 6.24. Do the higher order modes converge in this model?

**Exercise 6.16** In analogy to the result (6.154) for a Gaussian beam, show that the mode frequency  $\Omega$  for a parabolic beam satisfies Eq. (6.144) with

$$M_{ll'} = l\delta_{ll'} + i \frac{3Nr_0\eta c^2}{2\gamma T_0\omega_s^2\hat{z}^2} l^{l-l'} \sqrt{\frac{\Gamma(l+\frac{3}{2})\Gamma(l'+\frac{3}{2})}{\pi l!l'!}} \times \int_{-\infty}^{\infty} d\omega \frac{Z_0^{\parallel}(\omega)}{\omega} \frac{J_{l+1/2}(\omega\hat{z}/c)J_{l'+1/2}(\omega\hat{z}/c)}{\omega\hat{z}/c}. \quad (6.155)$$

Show that for a purely inductive impedance, the matrix  $M$  is diagonal and the eigenmode frequencies are given by Eq. (6.121). The beam is stable in this case even in the presence of mode coupling.

We have now obtained results for three bunch distributions—the waterbag, parabolic, and Gaussian models—under the following two circumstances: (a) when the beam intensity is weak so that coupling among the azimuthal modes can be ignored; (b) when the azimuthal modes are coupled, but only one radial mode (the most prominent mode) is considered per azimuthal family. The full problem, of simultaneous consideration of all azimuthal and radial modes, is considered to be beyond our scope. It is interesting to note that the special case of a parabolic bunch and a purely inductive impedance has been diagonalized in both circumstances mentioned above [see Eqs. (6.117) and (6.155)], but the same analysis does not diagonalize the full problem.

## Bunch Lengthening

One consequence of mode coupling instability is the *bunch lengthening* effect, often observed in circular accelerators for electrons.<sup>29</sup> The exact mechanism of the bunch lengthening phenomenon is a research topic.<sup>30</sup> One possible explanation is offered by the mode coupling instability.<sup>31</sup> As mentioned before, a proper explanation will invoke the higher order modes  $|l| \geq 2$  and to assure their proper convergence, but as an illustration of this idea, let us consider Figure 6.24. Suppose a beam of “natural” bunch length  $\hat{z}_0$  and intensity  $N$  is stored in the accelerator. If the intensity is  $T < T_{th}$ , the beam will keep its length  $\hat{z}_0$  and little will happen. But if  $T > T_{th}$ , the instability takes over and the bunch starts to lengthen. An inspection of Eq. (6.150) indicates that as the beam lengthens,  $T$  drops and when  $T$  drops below  $T_{th}$ , the beam becomes stable again. In equilibrium, one might presume that the beam will be lengthened just enough so that  $T$  stays at the instability threshold. When this happens, we have

$$\hat{z} = \frac{c}{T_0} \left( \frac{Nr_0\eta R_0}{\gamma\omega_s^2 T_{th}} \right)^{2/3}. \quad (6.156)$$

The behavior of bunch length as a function of beam intensity therefore looks like Figure 6.25(a). For the impedance (6.147), the curve above the bunch lengthening threshold has  $\hat{z} \propto N^{2/3}$ . Below the threshold, we have shown a slight potential-well bunch shortening.

The change of bunch distribution due to potential-well distortion and that due to mode coupling instability are distinctly different. In the former case, the energy distribution of the beam (we consider an electron beam) is unaffected. In the latter case, the synchrotron oscillation brings the changes in  $\hat{z}$  rapidly into proportional changes in  $\hat{\delta}$ . As a result, the energy spread of the beam behaves like that shown in Figure 6.25(b). Below the bunch lengthening threshold,  $\hat{\delta}$  is constant; above the threshold,  $\hat{\delta} \propto N^{2/3}$ .

We have been using the impedance (6.147) as an illustration. It turns out that, in general, for a given accelerator with an arbitrary impedance, the

<sup>29</sup>F. Amman, IEEE Trans. Nucl. Sci. **NS-16**, No. 3, 1073 (1969); ADONE Group, IEEE Trans. Nucl. Sci. **NS-18**, 217 (1971); B. Richter, IEEE Trans. Nucl. Sci. **NS-20**, 752 (1973).

<sup>30</sup>For more references, see P. Channell and A. M. Sessler, Nucl. Instr. Meth. **136**, 473 (1976); A. Renieri, Frascati Report LNF-76/11R (1976); P. B. Wilson, K. Bane, and K. Satoh, IEEE Trans. Nucl. Sci. **NS-28**, 2525 (1981); T. Weiland, DESY Report 81/088 (1981); R. Siemann, Nucl. Instr. Meth. **203**, 57 (1982); Toshio Suzuki, Yongho Chin, and Kohtaro Satoh, Part. Accel. **13**, 179 (1983); T. Suzuki, Part. Accel. **14**, 91 (1983); Kohji Hirata, Part. Accel. **22**, 57 (1987); R. Meller, Proc. IEEE Part. Accel. Conf., Washington, 1987, p. 1155; K. Hirata, S. Petracca, and F. Ruggiero, Phys. Rev. Lett. **66**, 1693 (1991); Toshio Suzuki, AIP Proc. **249**, Phys. Part. Accel., 1992, Vol. 1, p. 491.

<sup>31</sup>F. Sacherer, IEEE Trans. Nucl. Science **NS-24**, No. 3, 1393 (1977); A. W. Chao and J. Gareyte, SLAC Report SPEAR-197/PEP-224 (1976) and Part. Accel. **25**, 229 (1990).

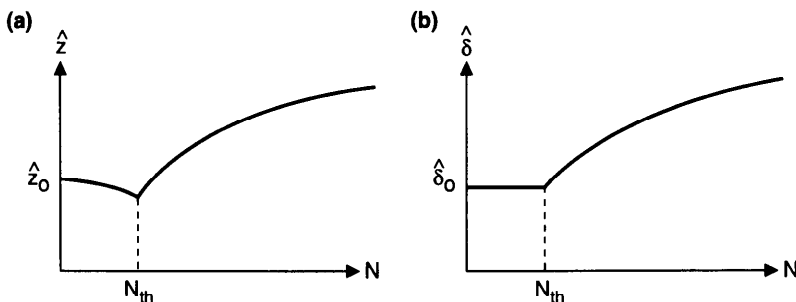


**Figure 6.25.** Bunch length  $\hat{z}$  and energy spread  $\hat{\delta}$  as functions of beam intensity  $N$  for circular electron accelerators, assuming the mode coupling instability is the underlying mechanism of bunch lengthening. Below a certain bunch lengthening threshold  $N_{th}$ ,  $\hat{z}$  changes (shortens in the case shown) due to potential-well distortion, while  $\hat{\delta}$  stays constant. Above  $N_{th}$ , both  $\hat{z}$  and  $\hat{\delta}$  increase with  $N$ . If the impedance is given by Eq. (6.147),  $\hat{z}$  and  $\hat{\delta}$  are proportional to  $N^{2/3}$  in the region  $N > N_{th}$ .

bunch length  $\hat{z}$  above threshold depends only on the single parameter

$$\xi = \frac{\eta I_{av}}{\nu_s^2 E}. \quad (6.157)$$

In other words, the accelerator may be operated with various possible values of the average beam current  $I_{av} = Ne/T_0$ , slippage factor  $\eta$  (which is about equal to the momentum compaction factor  $\alpha$  for most electron accelerators), synchrotron tune  $\nu_s = \omega_s/\omega_0$ , and beam energy  $E$ , but the bunch length above the lengthening threshold depends only on these factors combined as specified by Eq. (6.157). This behavior is called the *scaling law*, and  $\xi$  is the *scaling parameter*.<sup>32</sup> Equation (6.156), of course, obeys the scaling. Figure 6.26 shows some experimental data for the storage ring SPEAR.<sup>33</sup> The scaling property of these data is apparent.

There is more. An inspection of Eq. (6.145) shows that if the impedance behaves like

$$Z_0^{\parallel}(\omega) \propto \omega^a, \quad (6.158)$$

then the bunch length above the lengthening threshold will behave like

$$\hat{z} \propto \xi^{1/(2+a)}. \quad (6.159)$$

For example, the impedance (6.147) has  $a = -\frac{1}{2}$ , and thus  $\hat{z} \propto \xi^{2/3}$  in Eq.

<sup>32</sup>A. W. Chao and J. Gareyte, Part. Accel. **25**, 229 (1990); M. Month and E. Messerschmidt, IEEE Trans. Nucl. Sci. **NS-24**, 1208 (1977).

<sup>33</sup>P. B. Wilson et al., IEEE Trans. Nucl. Sci. **HS-24**, 1211 (1977).

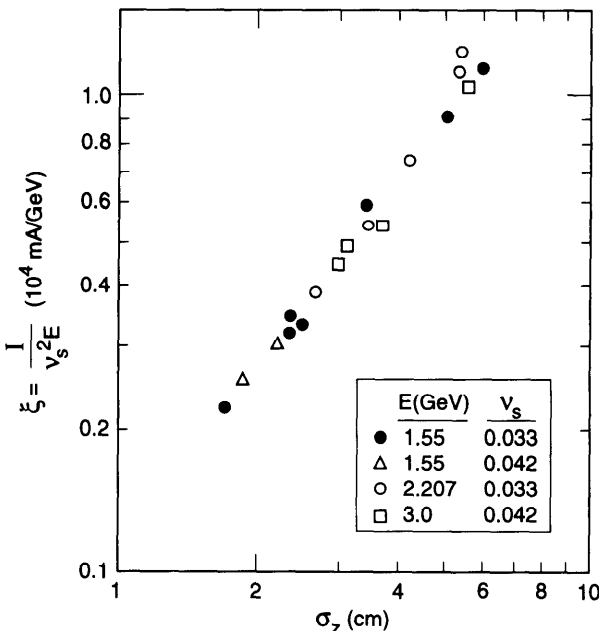


**Figure 6.26.** Bunch length versus the scaling parameter for the electron storage ring SPEAR. Data are taken above the lengthening threshold. The momentum compaction factor  $\alpha$  was kept constant in these experiments, and  $\sigma_z$  is the rms bunch length.

(6.156). Figure 6.26 indicates that for SPEAR,  $\sigma_z \propto \xi^{0.76}$ , from which we deduce that  $a = -0.68$  in the frequency range of interest, which covers from  $c/\sigma_z$  to a few times  $c/\sigma_z$ . With  $\sigma_z$  ranging from 1 to 6 cm, the corresponding frequency  $f = \omega/2\pi$  ranges from approximately 1 to several GHz. The impedance is therefore a moderately decreasing function of  $\omega$  in this frequency range for SPEAR.

Consider an accelerator whose integrated impedance over its circumference resembles that of a resonator impedance with  $\omega_R \sim c/b$ , where  $b$  is the vacuum chamber pipe radius. A long bunch with  $\sigma_z \gg b$  samples the impedance at low frequencies where the parameter is approximately proportional to  $\omega$  and  $a \approx 1$ . The bunch length above threshold, according to Eq. (6.159), scales with the beam intensity as  $\sigma_z \propto N^{1/3}$ . For short bunches with  $\sigma_z \ll b$ , the impedance  $\sim \omega^{-1}$  and  $a \approx -1$ , and we find  $\sigma_z \propto N$ . For the SPEAR case,  $\sigma_z$  is slightly shorter than  $b$ , and we have  $a \approx -0.68$  and  $\sigma_z \propto N^{0.76}$ . Figure 6.27 gives a qualitative sketch of this behavior.

The same scaling behavior is displayed by the microwave instabilities of unbunched beams. To see this, consider the stability criterion (5.136) derived by imposing Landau damping on the longitudinal microwave instability of unbunched beams, but extrapolated to bunched beams. Assuming the bunch length, in the unstable regime, is such that it maintains equality of the two

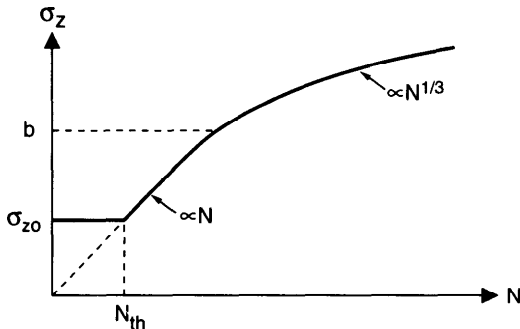


**Figure 6.27.** The solid curve is a sketch of how the bunch length is expected to behave for a broad-band resonator impedance. Below the threshold,  $N < N_{th}$ ,  $\sigma_z = \sigma_{z0}$  is unperturbed by the wake fields. Above the threshold,  $\sigma_z \propto N$  if  $\sigma_z \ll b$  and  $\sigma_z \propto N^{1/3}$  if  $\sigma_z \gg b$ , where  $b$  is the vacuum chamber pipe radius.

sides of Eq. (5.136), we obtain the bunch length above threshold

$$\Delta z_{1/2} = 0.91 \left( \frac{Nr_0\eta c^3}{\gamma T_0 \omega_s^2} \left| \frac{Z_0^\parallel}{\omega} \right| \right)^{1/3}. \quad (6.160)$$

Since this holds for  $|Z_0^\parallel/\omega| = \text{const}$ , we have  $a = 1$ , and therefore the bunch length scales as  $\xi^{1/3}$ .

As a further illustration, consider the example of potential-well distortion we worked out for the impedance (6.35). One result obtained in that example—the one based on Eq. (6.44), applicable for electrons—was that when the wake strength parameter  $D > 2/3^{3/2}$ , the beam cannot stay in a state that maintains an unperturbed energy spread. This consideration also yields Eq. (6.160), except that the numerical factor 0.91 now becomes  $3^{5/6}/2^{2/3} = 1.57$ . Yet another similar situation occurs in Exercise 6.4.

## 6.6 TRANSVERSE MODES

By the transverse modes here, we mean those modes with  $m = 1$ , i.e., the beam has a dipole moment (pointing, say, in the vertical  $y$ -direction) in the transverse plane. This dipole moment is not necessarily constant longitudinally from the bunch head to the bunch tail. Instead, it may go positive and negative and, depending on the longitudinal mode number  $l$ , its longitudinal structure may be simple or complicated as sketched in Figure 6.1(b).

What we will do in this section is to study these transverse modes. Note that, although they are called the *transverse* modes, the transverse structure of these modes is simple (after all, how complicated can a dipole be?), and our main task is, in fact, to find their *longitudinal* structure. This section is

the transverse  $m = 1$  counterpart of Sections 6.3 and 6.4 for the longitudinal  $m = 0$  case.

It may seem that the problem is going to be much more complicated than the longitudinal case; the Vlasov equation, for example, now needs to take into account both the transverse and the longitudinal phase spaces. Fortunately, however, the transverse structure of the beam is simple and can be found with ease. The strategy is that, after factoring out the transverse dimension from the Vlasov equation, we are left with an equation very similar to the  $m = 0$  case; the analysis developed for the longitudinal case can then be followed straightforwardly for the transverse case as well.

The phase space distribution  $\psi(y, p_y, z, \delta, s)$  satisfies the Vlasov equation

$$\frac{\partial\psi}{\partial s} + y' \frac{\partial\psi}{\partial y} + p'_y \frac{\partial\psi}{\partial p_y} + z' \frac{\partial\psi}{\partial z} + \delta' \frac{\partial\psi}{\partial \delta} = 0, \quad (6.161)$$

where a prime means taking the derivative with respect to  $s$ . The dynamics of the beam is contained in the single-particle equations of motion

$$\begin{aligned} y' &= p_y, \\ p'_y &= -\left(\frac{\omega_\beta}{c}\right)^2 y + \frac{1}{E} F_y(z, s), \\ z' &= -\eta\delta, \\ \delta' &= \frac{1}{\eta}\left(\frac{\omega_s}{c}\right)^2 z + \frac{y}{E} \frac{\partial F_y(z, s)}{\partial z}. \end{aligned} \quad (6.162)$$

The quantity  $F_y$  is the transverse wake force generated by the dipole moment of the beam,  $E$  is the particle energy, and  $\omega_\beta$  and  $\omega_s$  are the unperturbed betatron and synchrotron frequencies.

In Eq. (6.162), we have included a wake field term in the  $\delta'$ -equation. It comes from the fact that a dipole moment generates not only a transverse deflecting force, but also a longitudinal retarding force. It also follows from the requirement that the system be Hamiltonian. Equation (6.162), in fact, is a consequence of the Hamiltonian

$$H = \frac{1}{2}\left(\frac{\omega_\beta}{c}\right)^2 y^2 + \frac{1}{2}p_y^2 - \frac{1}{2\eta}\left(\frac{\omega_s}{c}\right)^2 z^2 - \frac{\eta}{2}\delta^2 - \frac{y}{E}F_y(z, s). \quad (6.163)$$

In what follows, however, the term in question will be dropped; the system is therefore, strictly speaking, non-Hamiltonian. Thus, the betatron motion is affected by the wake, but the synchrotron motion is treated as unperturbed.

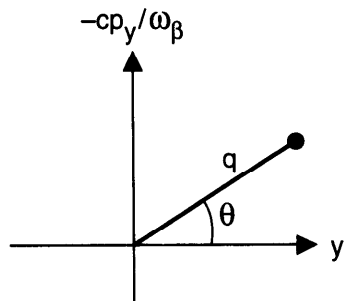


**Figure 6.28.** Coordinates in the betatron phase space.

This is a good approximation provided the synchro-betatron resonance conditions  $\omega_\beta \pm l\omega_s = n\omega_0$  are avoided and the transverse beam size has not grown too large.<sup>34</sup>

We now transform the longitudinal and the transverse coordinates into their polar forms defined by Eq. (6.62) and

$$\begin{aligned} y &= q \cos \theta, \\ p_y &= -\frac{\omega_\beta}{c} q \sin \theta. \end{aligned} \quad (6.164)$$

The transverse phase space coordinates are shown in Figure 6.28. Equation (6.161) then becomes

$$\frac{\partial \psi}{\partial s} + \frac{\omega_\beta}{c} \frac{\partial \psi}{\partial \theta} + \frac{1}{E} F_y(z, s) \frac{\partial \psi}{\partial p_y} + \frac{\omega_s}{c} \frac{\partial \psi}{\partial \phi} = 0. \quad (6.165)$$

The unperturbed stationary distribution of the beam is a function only of  $r$  and  $q$ . On top of the unperturbed distribution, we will consider a small perturbation that describes a transverse dipole oscillation mode. The distribution is therefore written as

$$\psi = f_0(q) g_0(r) + f_1(q, \theta) g_1(r, \phi) e^{-i\Omega s/c}, \quad (6.166)$$

where  $\Omega$  is the mode frequency, the unperturbed distributions  $f_0$  and  $g_0$  are considered to be given, and  $f_1$  and  $g_1$  describe the transverse and longitudi-

<sup>34</sup>The synchro-betatron coupling was discussed in the context of a two-particle model in Section 4.3. For more references, see Ronald M. Sundelin, IEEE Trans. Nucl. Sci. **NS-26**, 3604 (1979); T. Suzuki, Nucl. Instr. Meth. **A241**, 89 (1985); F. Ruggiero, Part. Accel. **20**, 45 (1986); Y. H. Chin, CERN Report SPS/85-33 (DI-MST) (1985); T. Suzuki, CERN Report LEP-TH/87-55 (1987). See also Exercise 6.18 below.

nal beam structures of the mode. As we did for the longitudinal instabilities, our job now is to look for self-consistent solutions for  $\Omega$ ,  $f_1$ , and  $g_1$ .

In writing down Eq. (6.166), we have implicitly assumed that the center of the unperturbed bcam coincides with the accelerator pipe axis. Effects associated with a distorted beam trajectory (i.e., a distorted closed orbit) are excluded from our study.

We next introduce an important complication that comes from the head-tail effect discussed in Section 4.5. What happens is that the betatron frequency is not a constant; it depends on  $\delta$  through the chromaticity  $\xi$ . The quantity  $\omega_\beta$  in Eq. (6.165) is therefore replaced by  $\omega_\beta(1 + \xi\delta)$ . Substituting Eq. (6.166) into Eq. (6.165) and linearizing with respect to the perturbation, keeping in mind that  $F_y$  is already first order, we find the linearized equation

$$\left[ -i\frac{\Omega}{c}f_1g_1 + \frac{\omega_\beta}{c}(1 + \xi\delta)\frac{\partial f_1}{\partial\theta}g_1 + \frac{\omega_s}{c}f_1\frac{\partial g_1}{\partial\phi} \right] e^{-i\Omega s/c} - \frac{c}{E\omega_\beta} \sin\theta F_y f'_0 g_0 = 0. \quad (6.167)$$

As mentioned before, the transverse structure  $f_1$  is easy to find. Indeed, since it describes a dipole motion, we anticipate a solution

$$f_1(q, \theta) = -Df'_0(q)e^{i\theta}, \quad (6.168)$$

where  $D$  is the dipole displacement of this distribution:

$$\frac{\int q dq \int d\theta y f_1}{\int q dq \int d\theta f_0} = -D \frac{\pi \int q^2 dq f'_0(q)}{2\pi \int q dq f_0(q)} = D. \quad (6.169)$$

This dipole motion is sketched in Figure 6.29.

Substituting Eq. (6.168) into Eq. (6.167), one obtains a reduced Vlasov equation that involves only longitudinal coordinates:

$$\left[ i(\Omega - \omega_\beta - \xi\omega_\beta\delta)g_1 - \omega_s \frac{\partial g_1}{\partial\phi} \right] De^{-i\Omega s/c} + i\frac{c^2}{2E\omega_\beta} F_y g_0 = 0. \quad (6.170)$$

In obtaining Eq. (6.170), the factor  $\sin\theta$  in Eq. (6.167) has been replaced by  $e^{i\theta}/2i$ . Rigorously, one needs both  $e^{i\theta}$  and  $e^{-i\theta}$  components, but the  $e^{-i\theta}$  component can be ignored if the frequency shift due to the wake field is small compared with the betatron frequency  $\omega_\beta$ .

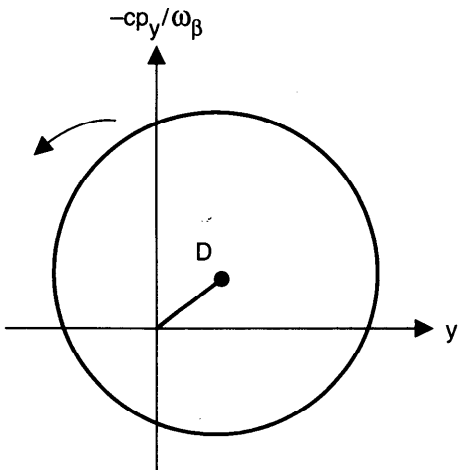


**Figure 6.29.** Dipole motion in the transverse phase space. The unperturbed distribution  $f_0(q)$  is displaced by a distance  $D$ . The displaced distribution then rotates around the origin.

We need to find  $F_y$ . The dipole moment of the beam, observed as location  $s$  as a function of  $z$ , is

$$De^{-i\Omega s/c} \int_{-\infty}^{\infty} d\delta g_1(r, \phi) = De^{-i\Omega s/c} \rho_1(z). \quad (6.171)$$

The deflecting force is then obtained by summing the wake field over all previous revolutions:

$$F_y(z, s) = -\frac{De^2}{cT_0} \int_{-\infty}^{\infty} dz' \sum_{k=-\infty}^{\infty} \rho_1(z') e^{-i\Omega[(s/c) - kT_0]} W_1(z - z' - kcT_0), \quad (6.172)$$

where  $W_1$  is the transverse wake function integrated over the accelerator circumference  $cT_0$ . The longitudinal counterpart of this expression is Eq. (6.66). As before, the distribution  $\rho_1(z)$  is what is observed at the fixed location of the impedance and is not the snapshot distribution.

Going to the frequency domain, Eq. (6.172) reads

$$F_y(z, s) = i \frac{De^2}{cT_0^2} e^{-i\Omega s/c} \sum_{p=-\infty}^{\infty} \tilde{\rho}_1(\omega') Z_1^\perp(\omega') e^{i\omega' z/c}, \quad (6.173)$$

where  $\omega' = p\omega_0 + \Omega$ , and  $Z_1^\perp(\omega)$  is the total transverse impedance in the accelerator.

Substituting Eq. (6.173) into Eq. (6.170), the factor  $De^{-i\Omega s/c}$  drops out; we get

$$i(\Omega - \omega_\beta - \omega_\beta \xi \delta) g_1 - \omega_s \frac{\partial g_1}{\partial \phi} - \frac{cr_0}{2\gamma\omega_\beta T_0^2} g_0 \sum_p \tilde{\rho}_1(\omega') Z_1^\perp(\omega') e^{i\omega' z/c} = 0. \quad (6.174)$$

We next Fourier expand  $g_1$  as

$$g_1(r, \phi) = \sum_{l=-\infty}^{\infty} \alpha_l R_l(r) e^{il\phi} e^{i\xi\omega_\beta z/c\eta}. \quad (6.175)$$

This expansion is in analogy to Eq. (6.72) except for the difference that, due to the chromaticity, we now have an additional head-tail phase factor. The same factor appeared in our two-particle treatment in Section 4.5. As mentioned there, it has the remarkable property that it depends only on  $z$ , and not on  $\delta$ . From here on, the treatment is very similar to what we did for the longitudinal case.

Substituting Eq. (6.175) into Eq. (6.174), we find the chromaticity term is canceled nicely except for the phase factor, and we have

$$i \sum_{l'} (\Omega - \omega_\beta - l'\omega_s) \alpha_{l'} R_{l'}(r) e^{il'\phi} - \frac{r_0 c}{2\gamma\omega_\beta T_0^2} g_0(r) e^{-i\xi\omega_\beta z/c\eta} \sum_p \tilde{\rho}_1(\omega') Z_1^\perp(\omega') e^{i\omega' z/c} = 0. \quad (6.176)$$

Multiplying the result by  $e^{-il\phi}$  and integrating over  $\phi$  from 0 to  $2\pi$ , we get an infinite set of equations,

$$i(\Omega - \omega_\beta - l\omega_s) \alpha_l R_l(r) = \frac{r_0 c}{2\gamma\omega_\beta T_0^2} i^l g_0(r) \times \sum_{p=-\infty}^{\infty} \tilde{\rho}_1(\omega') Z_1^\perp(\omega') J_l \left( \frac{\omega'}{c} r - \frac{\xi\omega_\beta}{c\eta} r \right), \\ l = 0, \pm 1, \pm 2, \dots \quad (6.177)$$

Furthermore, similarly to Eq. (6.75), we have

$$\tilde{\rho}_1(\omega') = 2\pi \frac{\omega_s}{c\eta} \sum_{l=-\infty}^{\infty} \int_0^\infty r dr \alpha_l R_l(r) i^{-l} J_l \left( \frac{\omega'}{c} r - \frac{\xi\omega_\beta}{c\eta} r \right). \quad (6.178)$$

Combining Eqs. (6.177–6.178) gives

$$\begin{aligned} (\Omega - \omega_\beta - l\omega_s)\alpha_l R_l(r) &= -i \frac{\pi r_0 \omega_s}{\gamma \omega_\beta T_0^2 \eta} g_0(r) \sum_{l'=-\infty}^{\infty} \int_0^{\infty} r' dr' \alpha_{l'} R_{l'}(r') i^{l-l'} \\ &\quad \times \sum_{p=-\infty}^{\infty} Z_{l'}^{\perp}(\omega') J_l\left(\frac{\omega' - \omega_\xi}{c} r\right) J_{l'}\left(\frac{\omega' - \omega_\xi}{c} r'\right), \end{aligned} \quad (6.179)$$

where

$$\omega' \equiv p\omega_0 + \omega_\beta + l\omega_s. \quad (6.180)$$

Note that in spite of the head-tail phase, the beam signal observed at a fixed location (at the impedance) is  $\omega'$ , independent of the chromaticity. The effect of the chromaticity is only to cause a shift in the Bessel function spectrum,

$$\omega' \rightarrow \omega' - \omega_\xi, \quad \text{where} \quad \omega_\xi \equiv \frac{\xi \omega_\beta}{\eta}. \quad (6.181)$$

To proceed further, we will assume a simple model of the unperturbed longitudinal distribution, namely,

$$\begin{aligned} g_0(r) &= \frac{N\eta c}{2\pi\omega_s \hat{z}} \delta(r - \hat{z}), \\ \rho_0(z) &= \frac{N}{\pi\sqrt{\hat{z}^2 - z^2}}, \quad z < |\hat{z}|. \end{aligned} \quad (6.182)$$

In this distribution, shown in Figure 6.30, particles populate an elliptical shell in the phase space. This is called a hollow beam model, or an *air-bag* model.

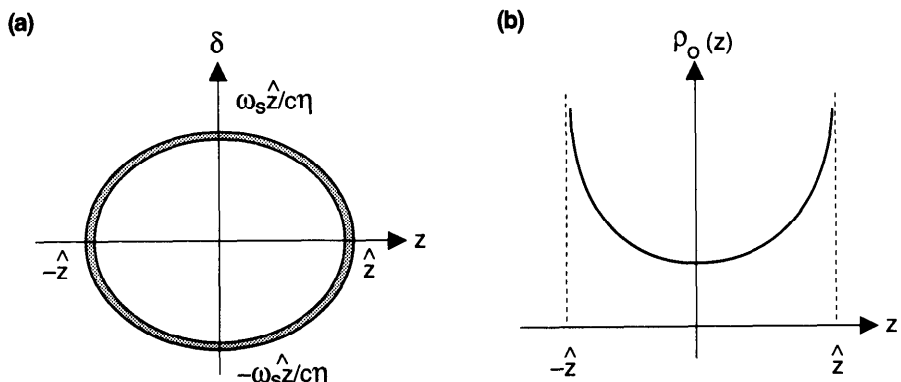


**Figure 6.30.** (a) Phase space distribution and (b) longitudinal distribution of an air-bag beam. For this distribution,  $\sigma_{rms} = \hat{z} / \sqrt{2}$ .

The advantage of using the air-bag model is obvious: all  $R_l$ 's degenerate into  $\delta(r - \hat{z})$ , i.e., we have  $R_l(r) \propto \delta(r - \hat{z})$ , and consequently Eq. (6.179) reduces to

$$\begin{aligned} (\Omega - \omega_\beta - l' \omega_s) \alpha_{l'} &= -i \frac{Nr_0 c}{2\gamma T_0^2 \omega_\beta} \sum_{l''} \alpha_{l'} i^{l'-l''} \\ &\quad \times \sum_p Z_1^\perp(\omega') J_{l'} \left( \frac{\omega' - \omega_\xi}{c} \hat{z} \right) J_{l''} \left( \frac{\omega' - \omega_\xi}{c} \hat{z} \right), \\ l' &= 0, \pm 1, \pm 2, \dots \end{aligned} \quad (6.183)$$

A mode is now specified by the frequency  $\Omega^{(l)}$  and the set of coefficients  $\alpha_l^{(l)}$ , where  $l$  is the mode index. In the absence of the wake field, the right hand side of Eq. (6.183) vanishes; the  $l$ th mode is described by

$$\begin{aligned} \alpha_l^{(l)} &= \delta_{ll'}, \\ \Omega^{(l)} &= \omega_\beta + l \omega_s. \end{aligned} \quad (6.184)$$

The distribution of this mode is given by

$$\underbrace{f'_0(q) e^{i\theta}}_{\text{trans. dist.}} \underbrace{\delta(r - \hat{z}) e^{il\phi}}_{\text{long. dist.}} \underbrace{e^{i\xi\omega_\beta z/c\eta}}_{\text{head-tail phase factor}} \underbrace{e^{-i(\omega_\beta + l\omega_s)s/c}}_{\text{time dep.}}. \quad (6.185)$$

These modes, without the head-tail phase factor, are those sketched in Figure 6.1(b).

The mode (6.185) gives rise to a dipole moment. Observed at a fixed location such as a pickup electrode or an impedance, we have

$$\text{dipole moment} \propto \frac{1}{\sqrt{\hat{z}^2 - z^2}} \cos \left[ l \cos^{-1} \left( \frac{z}{\hat{z}} \right) \right] \cos \left( \Omega^{(l)} \frac{s}{c} - \chi \frac{z}{\hat{z}} \right), \quad (6.186)$$

where we have defined a *head-tail phase*<sup>35</sup>

$$\chi = \frac{\omega_\xi \hat{z}}{c} = \frac{\xi \omega_\beta \hat{z}}{c\eta}. \quad (6.187)$$

As we will see,  $\chi$  plays a crucial role in the mechanism of transverse collective instabilities. As a result, the chromaticity  $\xi$  often needs to be controlled carefully. The fact that  $\chi \propto 1/\eta$  is another indication of the fact that transition crossing (when  $\eta \approx 0$ ) when accelerating an intense beam in a synchrotron is an involved process.

A superposition of the signal (6.186) at several beam passages is shown in Figure 6.31 for different modes and different values of  $\chi$ . For mode  $l$ , there

<sup>35</sup>Remember that  $\hat{z}$  is half the total bunch length.

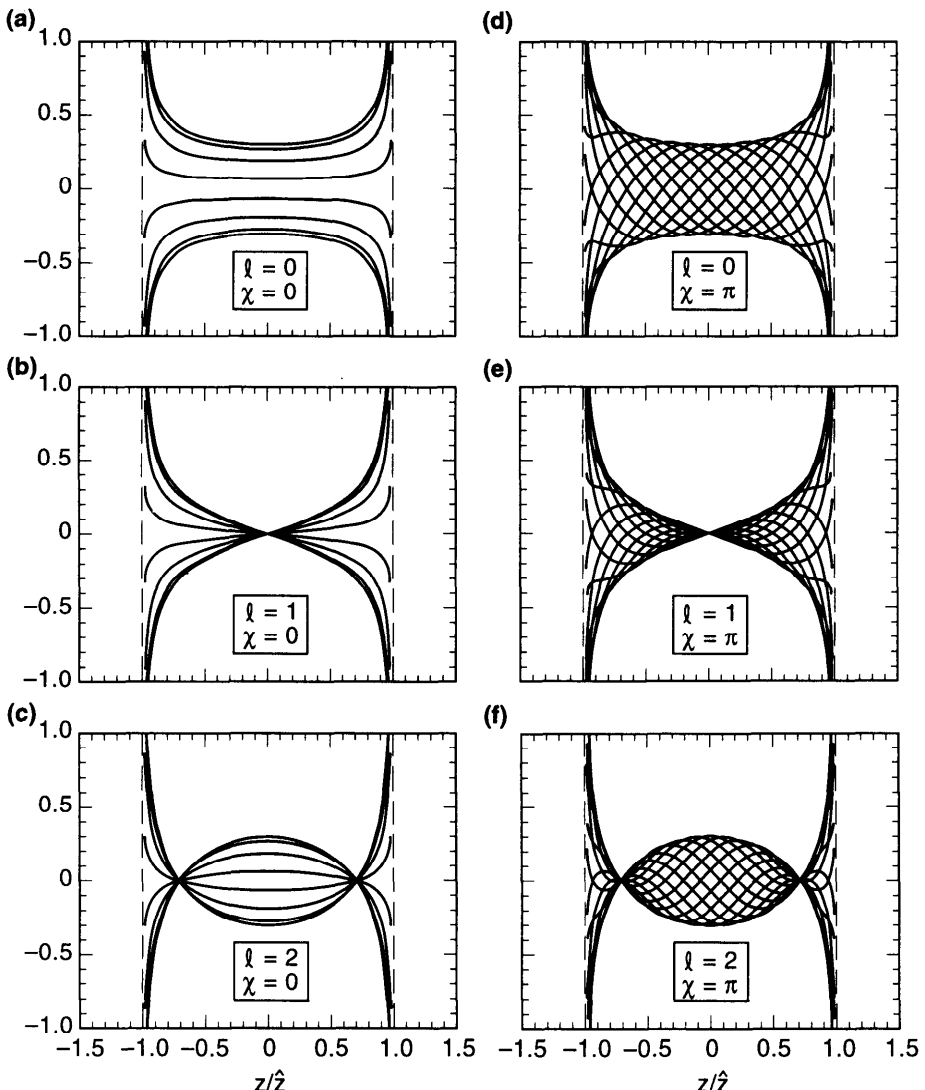


**Figure 6.31.** Dipole moment observed by a pickup electrode as an air-bag beam executes a collective mode  $\ell$ . Several signals observed at different beam passages are superimposed. In (a) to (c), the head-tail phase  $\chi = 0$ ; in (d) to (f),  $\chi = \pi$ . The beam is assumed to have a vanishing intensity.

are  $\ell$  nodes in the signal pattern. The locations of these nodes are not affected by a nonzero  $\chi$ , although the signal away from the nodes becomes more complex.

The signal (6.186) diverges at the bunch edges  $z = \pm \hat{z}$  because of the air-bag distribution assumed. The real beam is not likely to have an air-bag distribution. Figure 6.32 shows the beautiful mode patterns observed at the

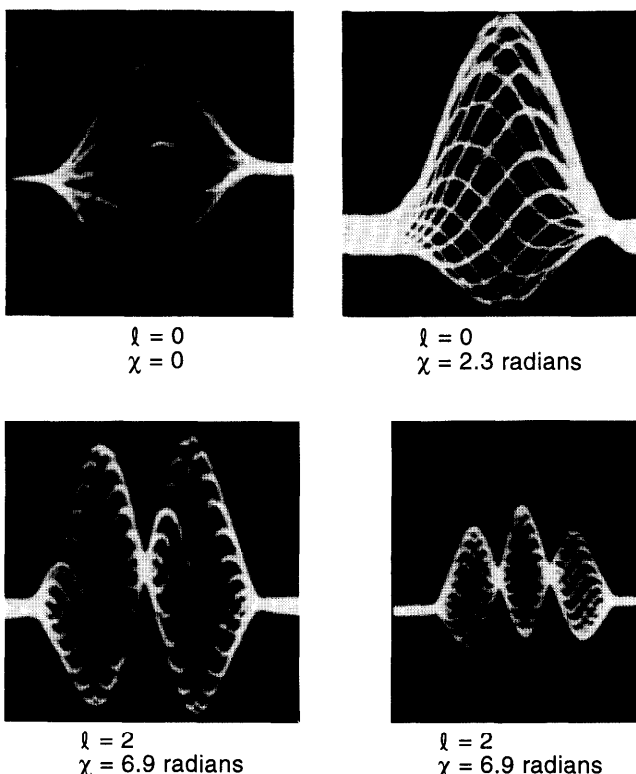


**Figure 6.32.** Transverse beam oscillation modes observed at the CERN PS Booster. The head-tail phase  $\chi$  is properly defined for the observed bunch shape. (Courtesy Jacques Gareyte, 1992).

CERN Proton Synchrotron Booster.<sup>36</sup> These patterns are to be compared with those of Figure 6.31.

For a weak beam, the mode frequency shifts are small compared with  $\omega_s$ ; one can obtain the first order perturbation by substituting the unperturbed solution Eq. (6.184) into the right hand side of Eq. (6.183) to obtain

$$\Omega^{(l)} - \omega_\beta - l\omega_s = -i \frac{Nr_0 c}{2\gamma T_0^2 \omega_\beta} \sum_{p=-\infty}^{\infty} Z_1^\perp(\omega') J_l^2 \left( \frac{\omega' z}{c} - \chi \right). \quad (6.188)$$

Again, the real part of this expression gives the mode frequency shift, and the imaginary part gives the instability growth rate.

**Exercise 6.17** Consider an air-bag beam executing the mode (6.185). Show that the center of charge of the beam as a whole has an oscillation

<sup>36</sup>J. Gareyte and F. Sacherer, *Proc. 9th Int. Conf. on High Energy Accel.*, Stanford, 1974, p. 341.

amplitude proportional to  $J_l(\chi)$ . Therefore, if  $\chi = 0$ , a pickup electrode will see only the  $l = 0$  mode, but all modes show up if  $\chi \neq 0$ .

### Exercise 6.18

- (a) The wake term in the  $\delta'$ -equation of Eq. (6.162) was dropped. To see the significance of this term, let us keep it but drop the wake term in the  $p'_y$ -equation instead. Follow closely the development of this section, assuming  $f_0$  Gaussian and  $g_0$  water bag. Show that

$$f_1 = \frac{D}{\sigma_y^2} f_0(q) q e^{i\theta} \quad (6.189)$$

and that  $(\Omega - \omega_\beta - l' \omega_s) \alpha_{l'}$  equals

$$i \frac{Nr_0 \eta \hat{z}}{\gamma T_0^2 \omega_s} \left( \frac{\sigma_y}{\hat{z}} \right)^2 l' \sum_{l''} \alpha_{l'} i^{l''-l'} \sum_p \omega' Z_1^\perp(\omega') \left[ \frac{J_{l'}(x) J_{l''}(x)}{x} \right]_{x=(\omega' \hat{z}/c) - \chi}. \quad (6.190)$$

Compare with (6.183). Show that this wake effect can be ignored if  $\sigma_y$  is small compared with  $\sqrt{\omega_s/\eta\omega_\beta}$  times the bunch length  $\hat{z}$ .

- (b) If there is a longitudinal impedance  $Z_0^\parallel$  present, one can also compare the above result with Eq. (6.80). Show that the effect can be ignored if  $Z_1^\perp(\omega)$  is much less than  $cZ_0^\parallel(\omega)/\omega\sigma_y^2$ . If  $Z_0^\parallel(\omega)$  is related to  $Z_1^\perp(\omega)$  through Eq. (2.107), then the criterion becomes  $\sigma_y \ll b$ . Both the conditions  $\sigma_y \ll \hat{z}\sqrt{\omega_s/\eta\omega_\beta}$  and  $\sigma_y \ll b$  are fulfilled in most accelerators.

### Exercise 6.19

There is a frequency-domain version of Eq. (6.179). Follow similar steps as in Exercise 6.10 to establish

$$\begin{aligned} & (\Omega - \omega_\beta - l \omega_s) \alpha_l \tilde{\rho}_1^{(l)}(q) \\ &= -i \frac{\pi r_0 \omega_s}{\gamma \omega_\beta T_0^2 \eta} \sum_{l'} \alpha_{l'} \sum_p Z_1^\perp(p \omega_0 + \Omega) \tilde{\rho}_1^{(l')}(p) F_l(p, q), \end{aligned} \quad (6.191)$$

where

$$F_l(p, q) = \int_0^\infty r dr g_0(r) J_l \left( \frac{q \omega_0 + \Omega - \omega_\xi}{c} r \right) J_l \left( \frac{p \omega_0 + \Omega - \omega_\xi}{c} r \right). \quad (6.192)$$

If  $F_l(p, q)$  factorizes like Eq. (6.90), show that the solution to Eq. (6.191) is given by Eq. (6.91) and

$$\begin{aligned} (\Omega - \omega_\beta - l\omega_s)\alpha_l &= -i \frac{\pi r_0 \omega_s}{\gamma \omega_\beta T_0^2 \eta} \sum_{l'} \alpha_{l'} i^{l-l'} \\ &\times \sum_p Z_1^\perp(p\omega_0 + \Omega) T_{l'}(p\omega_0 + \Omega) T_l(p\omega_0 + \Omega). \end{aligned} \quad (6.193)$$

Apply these results to the air-bag model to obtain Eq. (6.183).

We will return to Eq. (6.188) and continue the discussion of transverse collective instabilities in the next section. In the rest of this section, we will discuss the radial modes by following steps very similar to those of Section 6.4. Consider a weak beam, whose mode frequency shift from the unperturbed values  $\omega_\beta + l\omega_s$  is small compared with  $\omega_s$ , so that modes with different azimuthal indices  $l$  do not couple.

For a given  $l$ , introduce a weight function

$$W(r) = \frac{\omega_s}{N\eta c} g_0(r) \quad (6.194)$$

and a kernel function

$$G_l(r, r') = -i \frac{\pi N r_0 c}{\gamma T_0^2 \omega_\beta \omega_s} \sum_{p=-\infty}^{\infty} Z_1^\perp(\omega') J_l\left(\frac{\omega' - \omega_\xi}{c} r\right) J_l\left(\frac{\omega' - \omega_\xi}{c} r'\right). \quad (6.195)$$

We obtain the *Sacherer's integral equation* for  $m = 1$ ,

$$\left( \frac{\Omega - \omega_\beta}{\omega_s} - l \right) R_l(r) = W(r) \int_0^\infty r' dr' R_l(r') G_l(r, r'). \quad (6.196)$$

We next form a set of functions  $\{f_k(r), k = 0, 1, 2, \dots\}$  that satisfy the orthonormality condition (6.96) with the present choice of weight function. The frequencies of the radial modes are determined by the eigenvalue condition

$$\det \left[ \left( \frac{\Omega - \omega_\beta}{\omega_s} - l \right) I - M \right] = 0. \quad (6.197)$$

The interaction matrix  $M$  is given by

$$M_{kk'} = -i \frac{\pi N r_0 c}{\gamma T_0^2 \omega_\beta \omega_s} \sum_{p=-\infty}^{\infty} Z_1^\perp(\omega') g_{lk}(\omega' - \omega_\xi) g_{lk'}(\omega' - \omega_\xi), \quad (6.198)$$

where  $\omega' = p\omega_0 + \omega_\beta + l\omega_s$  and  $\omega_\xi = \xi\omega_\beta/\eta$ . The function  $g_{lk}(\omega)$  has the expression (6.101). In contrast to the longitudinal case, the weight function has the dimension  $L^{-2}$ , and  $f_k$ ,  $g_{lk}$ , and  $M_{kk'}$  are dimensionless.

Consider a bunch with a uniform longitudinal distribution  $\rho_0(z)$ ,

$$\begin{aligned} g_0(r) &= \frac{N\eta c}{2\pi\omega_s \hat{z}} \frac{1}{\sqrt{\hat{z}^2 - r^2}}, \quad r < \hat{z}, \\ \rho_0(z) &= \frac{N}{2\hat{z}}, \quad |z| < \hat{z}, \\ \sigma_z &= \frac{\hat{z}}{\sqrt{3}}. \end{aligned} \quad (6.199)$$

The weight function

$$W(r) = \frac{1}{2\pi\hat{z}\sqrt{\hat{z}^2 - r^2}} \quad (6.200)$$

is very close to that of the parabolic model solved in Section 6.4. It follows that, for the present case,

$$\begin{aligned} f_k(r) &= \sqrt{4\pi} \frac{(l+2k+\frac{1}{2})k!\Gamma(l+k+\frac{1}{2})}{(l+k)!\Gamma(k+\frac{1}{2})} \\ &\times \left(\frac{r}{\hat{z}}\right)^l P_k^{(l, -1/2)} \left(1 - \frac{2r^2}{\hat{z}^2}\right), \\ g_{lk}(\omega) &= \sqrt{\frac{1}{2\pi}} \frac{(l+2k+\frac{1}{2})\Gamma(k+\frac{1}{2})\Gamma(l+k+\frac{1}{2})}{k!(l+k)!} \\ &\times \frac{J_{l+2k+1/2}(\omega\hat{z}/c)}{\sqrt{\omega\hat{z}/c}}. \end{aligned} \quad (6.201)$$

If we further assume the impedance  $Z_1^\perp(\omega) = \text{const}$ , independent of  $\omega$ , and make the broad-band approximation (6.116), the problem is readily

diagonalized. The matrix elements are

$$M_{kk'} = -\frac{Nr_0c^2}{4\pi\gamma T_0\omega_\beta\omega_s\hat{z}}iZ_1^\perp \frac{\Gamma(k + \frac{1}{2})\Gamma(l + k + \frac{1}{2})}{k!(l+k)!}\delta_{kk'}. \quad (6.202)$$

Note that the chromaticity does not play a role here. This is because the constant impedance does not respond to a shift of spectrum dictated by the chromaticity. The eigenmodes are the Legendre modes

$$\begin{aligned} \Omega^{(l,n)} &= \omega_\beta + l\omega_s + M_{nn}\omega_s, \\ \rho_1^{(l,n)} &\propto P_{l+2n}\left(\frac{z}{\hat{z}}\right), \\ \psi_1^{(l,n)} e^{-i\Omega s/c} &\propto f'(q)e^{i\theta} \frac{(r/\hat{z})^l}{\sqrt{1-(r/\hat{z})^2}} P_n^{(l+1/2)}\left(1 - \frac{2r^2}{\hat{z}^2}\right) \\ &\times e^{il\phi} e^{i\omega_\xi z/c} e^{-i\Omega^{(l,n)} s/c}. \end{aligned} \quad (6.203)$$

One can also study the Hermite modes of a Gaussian model. The relevant quantities are

$$\begin{aligned} g_0(r) &= \frac{N\eta c}{2\pi\sigma^2\omega_s} e^{-r^2/2\sigma^2}, \\ W(r) &= \frac{1}{2\pi\sigma^2} e^{-r^2/2\sigma^2}, \\ f_k(r) &= \sqrt{\frac{2\pi k!}{(l+k)!}} \left(\frac{r}{\sqrt{2}\sigma}\right)^l L_k^{(l)}\left(\frac{r^2}{2\sigma^2}\right), \\ g_{lk}(\omega) &= \frac{1}{\sqrt{2\pi k!(l+k)!}} \left(\frac{\omega\sigma}{\sqrt{2}c}\right)^{l+2k} e^{-\omega^2\sigma^2/2c^2}, \\ \tilde{g}_{lk}(z) &\propto e^{-z^2/2\sigma^2} H_{l+2k}\left(\frac{z}{\sqrt{2}\sigma}\right). \end{aligned} \quad (6.204)$$

Given  $l$  and  $Z_1^\perp(\omega)$ , the radial modes are in general obtained by solving the eigenvalue problem (6.197) with the interaction matrix (6.198).

In the same spirit as Eqs. (6.139–6.143), one can also define an effective impedance even if the problem has not been diagonalized, i.e.,

$$(Z_1^\perp)_{\text{eff}} = \frac{\sum_{p=-\infty}^{\infty} Z_1^\perp(\omega') h_l(\omega' - \omega_\xi)}{\sum_{p=-\infty}^{\infty} h_l(\omega' - \omega_\xi)}. \quad (6.205)$$

One notable difference from Eq. (6.140) is of course the beam spectral shift (6.181) due to the chromaticity.

For a uniform beam model (6.199),  $h_l(\omega)$  is given by Eq. (6.141), and the complex mode frequency shift is given by

$$\Omega^{(l)} - \omega_\beta - l\omega_s \approx -\frac{1}{4\sqrt{\pi}} \frac{\Gamma(l + \frac{1}{2})}{l!} \frac{Nr_0 c^2}{\gamma T_0 \omega_\beta \hat{z}} i(Z_1^\perp)_{\text{eff}}. \quad (6.206)$$

For a Gaussian beam, we have  $h_l(\omega)$  given by Eq. (6.143) and

$$\Omega^{(l)} - \omega_\beta - l\omega_s \approx -\frac{1}{4\pi} \frac{\Gamma(l + \frac{1}{2})}{2^l l!} \frac{Nr_0 c^2}{\gamma T_0 \omega_\beta \sigma} i(Z_1^\perp)_{\text{eff}}. \quad (6.207)$$

Equations (6.205–6.207) are handy expressions for order-of-magnitude estimates. Take for example a Gaussian beam with  $N = 10^{11}$ ,  $\gamma = 10$ ,  $T_0 = 3 \mu\text{s}$ ,  $\nu_\beta = \omega_\beta/\omega_0 \approx 12$ , and  $\sigma = 10 \text{ cm}$ . If there is reason to believe that  $i(Z_1^\perp)_{\text{eff}} = 1 \text{ M}\Omega/\text{m}$ ,<sup>37</sup> Eq. (6.207) gives mode tune shifts of  $-0.0013$  for  $l = 0$  and  $-0.00033$  for  $l = 1$ . The  $l = 0$  mode frequency shift can be compared with  $\omega_s/2$ . When the shift becomes comparable to  $\omega_s/2$ , the strong head-tail instability is likely to set in.

**Exercise 6.20** The most prominent transverse mode is likely to be the one with  $l = 0$ . Consider the  $l = 0$  mode of a point bunch. Let the chromaticity  $\xi = 0$ . Use Eq. (6.206) to show that the mode frequency shift is given by

$$\Omega^{(0)} - \omega_\beta \approx -\frac{Nr_0 c}{2\gamma T_0^2 \omega_\beta} i \sum_{p=-\infty}^{\infty} Z_1^\perp(\omega'). \quad (6.208)$$

The same result is obtained for a Gaussian bunch using Eq. (6.207) as should be obtained for a point bunch. The expression (6.208) was obtained before in Eqs. (4.27–4.28) using a one-particle model.

Like its longitudinal counterpart, the effective impedance (6.205) involves the overlap integral between the impedance  $Z_1^\perp(\omega)$  and the beam spectra  $h_l(\omega)$ —except that  $l = 0$  is now an allowed mode and that there is the spectral shift (6.181)—as illustrated in Figure 6.33. One consequence of the spectral shift (6.181) is that the real part of  $(Z_1^\perp)_{\text{eff}}$  no longer vanishes even for broad-band impedances. The mode frequency therefore acquires an imaginary part, and if  $\text{Re}(Z_1^\perp)_{\text{eff}} < 0$ , the beam can become unstable. Inspection of the  $l = 0$  member of Figure 6.33(b) indicates that this mode becomes

<sup>37</sup>For example, one may have the information from elsewhere that the longitudinal impedance has  $(Z_0^\parallel/n)_{\text{eff}} = 8.8 \Omega$ . By applying Eq. (2.108) to the effective impedances and knowing  $b = 5 \text{ cm}$ , one obtains  $(Z_1^\perp)_{\text{eff}} = 1 \text{ M}\Omega/\text{m}$ , provided  $\xi = 0$ .

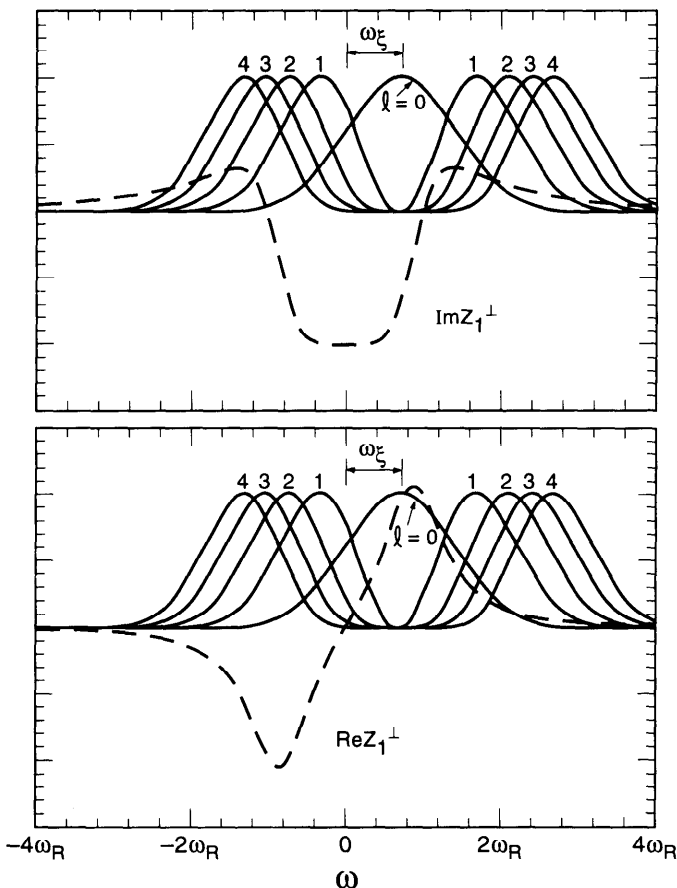


**Figure 6.33.** Solid curves are the spectra  $h_l(\omega - \omega_\xi)$  of a Gaussian beam (normalized so that they have the same value at their respective maxima). Dashed curves are the broad-band impedance  $Z_1^\perp(\omega)$ : (a) imaginary part; (b) real part. The parameters are such that  $c/\sigma = \omega_R$ ,  $\omega_\xi = 0.7\omega_R$ , and  $Q = 1$ . The real part of  $(Z_1^\perp)_{\text{eff}}$  vanishes if  $\xi = 0$  due to symmetry. When  $\xi \neq 0$ , however,  $\text{Re}(Z_1^\perp)_{\text{eff}} \neq 0$  and there can be instability growth.

unstable if  $\omega_\xi = \xi\omega_\beta/\eta$  is negative. This confirms again the head-tail stability criterion that for the  $l = 0$  mode to be stable, one needs to have  $\xi > 0$  above transition and  $\xi < 0$  below transition.

**Exercise 6.21** With a broad-band resonator impedance and a Gaussian beam, show that for a short bunch,  $\sigma \ll c/\omega_R$ ,

$$\frac{1}{\tau^{(0)}} \approx - \frac{Nr_0\sigma^2\omega_R\omega_\xi}{\gamma T_0\omega_\beta b^2} \frac{R_S}{Q}. \quad (6.209)$$

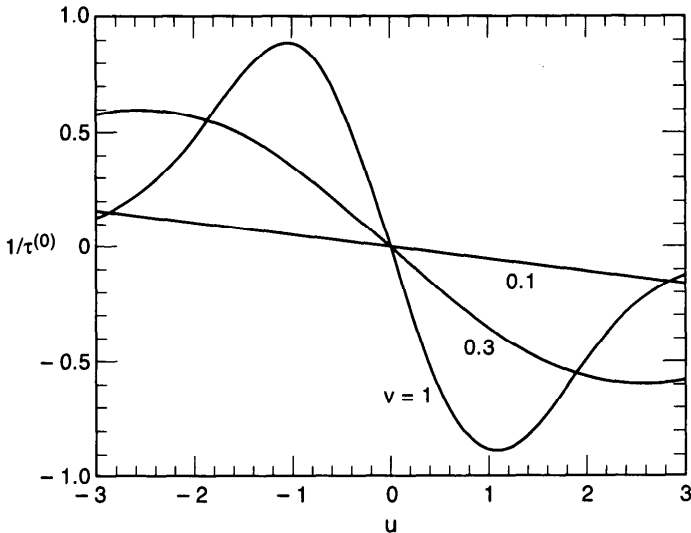


**Figure 6.34.** Growth rate  $1/\tau^{(0)}$  (normalized by  $Nr_0c^2R_S/2\pi\gamma T_0\omega_\beta b^2$ ) for the  $l = 0$  mode versus  $u = \omega_\xi/\omega_R$ . A  $Q = 1$  resonator impedance and a Gaussian bunch are assumed. Results are given for three values of  $v = \omega_R\sigma/c$ . Equation (6.209) gives an approximate expression when  $v \ll 1$ .

Compare the result with that for the water-bag model. Compute  $1/\tau^{(0)}$  numerically as a function of  $\omega_\xi/\omega_R$ . Show that the worst growth rate occurs when  $\omega_\xi \approx -\omega_R$ . Some results can be found in Figure 6.34.

The dependence of  $(Z_1^\perp)_{\text{eff}}$  on the chromaticity provides a way to measure  $Z_1^\perp$  as a function of  $\omega$ , particularly for proton synchrotrons that go through transition during acceleration with long bunches. Consider the  $l = 0$  mode, whose spectrum centers around  $\omega = \omega_\xi = \xi\omega_\beta/\eta$ . The effective impedance is approximately given by  $Z_1^\perp(\omega_\xi)$  if the bunch length is longer than the range of the wake field. It follows from Eqs. (6.206–6.207) that

$$\Omega^{(0)} - \omega_\beta \approx -\frac{Nr_0c^2}{4\gamma T_0\omega_\beta} i Z_1^\perp(\omega_\xi) \begin{cases} \frac{1}{\hat{z}}, & \text{uniform beam,} \\ \frac{1}{\sqrt{\pi}\sigma}, & \text{Gaussian beam.} \end{cases} \quad (6.210)$$

Measuring the frequency shift and the growth rate of the  $l = 0$  mode of a long bunch therefore provides information on the imaginary and the real parts of the transverse impedance  $Z_1^\perp$ . This impedance measuring technique was used at the CERN Proton Synchrotron.<sup>36</sup> By varying the chromaticity  $\xi$

and the slippage factor  $\eta$ ,  $Z_1^\perp$  as a function of frequency can be measured. The reachable frequency range can be expanded by choosing to operate the accelerator close to transition when  $\eta$  is small. The resolution of the technique requires  $\xi\omega_\beta/\eta \geq c/\sigma_z$ .

## 6.7 TRANSVERSE INSTABILITIES

In this section, we will study the transverse collective instabilities, ignoring the radial modes. Our starting point is Eq. (6.188), developed in the previous section for a weak air-bag beam using the Vlasov technique. Equation (6.188) gives the complex mode frequency for mode  $l$ . For example, the  $l = 0$  mode describes a rigid beam mode in which the entire beam bunch, from head to tail, has the same dipole moment. Consider a point bunch,  $\hat{z} = 0$ ; the only mode that this bunch can have is the  $l = 0$  mode, and its mode frequency is

$$\Omega^{(0)} - \omega_\beta = -i \frac{Nr_0c}{2\gamma T_0^2 \omega_\beta} \sum_{p=-\infty}^{\infty} Z_1^\perp(p\omega_0 + \omega_\beta). \quad (6.211)$$

This result has been obtained before in Eq. (4.25) using a one-particle model. As pointed out there, Eq. (6.211) leads to the transverse Robinson instability if the impedance has sharp peaks with widths  $\Delta\omega \lesssim [\omega_\beta]$ , where  $[\omega_\beta]$  is the betatron frequency modulo the revolution frequency  $\omega_0$ . It also leads to the resistive-wall instability summarized by Eqs. (4.34–4.35).

**Exercise 6.22** Consider an impedance sharply peaked at  $\omega \approx \pm h\omega_0$ . Use Eq. (6.188) to show that the transverse Robinson growth rate for the  $l$ th mode is

$$\frac{1}{\tau^{(l)}} \approx -\frac{Nr_0c}{2\gamma T_0^2 \omega_\beta} \left[ \operatorname{Re} Z_1^\perp(h\omega_0 + \Delta) J_l^2 \left( h\omega_0 \frac{\hat{z}}{c} - \chi \right) - \operatorname{Re} Z_1^\perp(h\omega_0 - \Delta) J_l^2 \left( h\omega_0 \frac{\hat{z}}{c} + \chi \right) \right], \quad (6.212)$$

where  $\Delta = [\omega_\beta] + l\omega_s$ . The two terms in the square brackets are weighted differently according to the head-tail phase  $\chi$  defined by Eq. (6.187). When  $\hat{z} = 0$ , Eq. (4.31) is recovered.

### Head-Tail Instability

Equation (6.188) is more general than Eq. (6.211) in two ways. First, it can be applied to the  $l \neq 0$  modes as well, and second, it contains the chromaticity information that leads to the head-tail instability. As demonstrated in Eq.

(6.212), a sharply peaked impedance would introduce transverse Robinson instabilities in the  $l \neq 0$  modes. What is more interesting, however, is the head-tail instability. To study that, let us consider a broad-band impedance (single-turn wake field), so that the summation in Eq. (6.188) can be approximated by an integral over  $p$ . The growth rate then reads

$$\frac{1}{\tau^{(l)}} = -\frac{Nr_0c}{4\pi\gamma T_0\omega_\beta} \int_{-\infty}^{\infty} d\omega' \operatorname{Re} Z_1^\perp(\omega') J_l^2\left(\omega' \frac{\hat{z}}{c} - \chi\right). \quad (6.213)$$

The quantity  $\operatorname{Re} Z_1^\perp(\omega')$  is odd in  $\omega'$ . If  $\chi = 0$ , the integral (6.213) vanishes and there will be no instability. One then obtains the familiar situation when the chromaticity  $\xi = 0$  (and therefore  $\chi = 0$ ), namely, the only instability of weak beams is of the Robinson type. This, however, is no longer true if  $\xi \neq 0$ . For finite but small  $\chi$ , Eq. (6.213) becomes, to first order in  $\chi$ ,

$$\frac{1}{\tau^{(l)}} \approx \frac{Nr_0c}{\pi\gamma T_0\omega_\beta} \chi \int_0^{\infty} d\omega \operatorname{Re} Z_1^\perp(\omega) J_l\left(\frac{\omega \hat{z}}{c}\right) J'_l\left(\frac{\omega \hat{z}}{c}\right), \quad (6.214)$$

where  $J'_l$  is the derivative of the Bessel function  $J_l$ .

The physical reason there is no instability for short range wakes when  $\chi = 0$  can be related to the mode patterns, shown in Figure 6.31(a)–(c). In this case, the beam displacement at any point along the bunch is either in phase or out of phase with the displacement at any other point along the bunch. The wake force a particle experiences can therefore only be in phase or out of phase with its displacement, thus lacking the  $90^\circ$  phase component required for instability. Such a  $90^\circ$  phase can be provided by the head-tail phase when  $\chi \neq 0$ , as Figure 6.31(d)–(f) shows.

As an illustration, let us consider an impedance that gives rise to a constant wake (4.37), namely,

$$Z_1^\perp(\omega) = W_0 \left[ \frac{1}{\omega} - i\pi\delta(\omega) \right]. \quad (6.215)$$

The integration in Eq. (6.214) can be performed using Table 6.1, yielding the head-tail instability growth rate<sup>38</sup>

$$\frac{1}{\tau^{(l)}} = \frac{Nr_0cW_0}{\gamma T_0\omega_\beta} \chi \frac{2}{\pi^2(4l^2 - 1)}. \quad (6.216)$$

One can compare Eq. (6.216) with the result (4.99) obtained using the two-particle model. The present expression is clearly superior in that it gives

<sup>38</sup>The same result was obtained in M. Sands, SLAC Report TN-69-8 (1969).

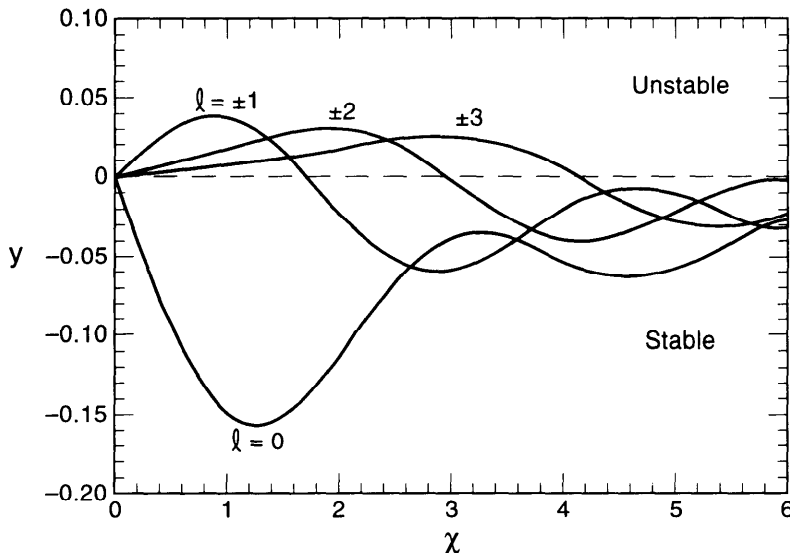


**Figure 6.35.** The growth rate  $1/\tau^{(l)}$  versus the head-tail phase  $\chi$  for the impedance (6.215), for  $|l| = 0, 1, 2, 3$ . The vertical axis  $y$  is  $1/\tau^{(l)}$ , normalized by  $Nr_0cW_0/\gamma T_0\omega_\beta$ . For  $\chi < 0$ ,  $\tau^{-1}$  can be obtained using the fact that it is an odd function of  $\chi$ .

the growth rate for all modes. By associating the + and the - modes with the  $l = 0$  and the  $l = 1$  modes, respectively, the two-particle model predicts that the growth and damping rates of the two modes are equal in magnitude, with  $1/\tau^{(0)} = -1/\tau^{(1)}$ . In the present, more accurate, treatment, we find  $1/\tau^{(1)}$  is suppressed by a factor of 3 relative to the  $l = 0$  mode. The two-particle model thus overestimates the effect on the  $l = 1$  mode—the air-bag model is obviously more realistic than the two-particle model. Nevertheless, because of its sharp edges, even the air-bag model is likely to have overestimated the effect of the higher order modes.

According to Eq. (6.216), the  $l = 0$  mode is unstable if  $\chi < 0$ , and the higher order modes are unstable if  $\chi > 0$ .<sup>39</sup> Strictly speaking, the beam is stable only when  $\chi = 0$  exactly. In practice, however, since the  $l = 0$  mode has the largest growth rate,  $\chi$  is often chosen to be small but slightly positive if the head-tail instability is a problem. This means the chromaticity  $\xi$  is typically chosen to be small but slightly positive above transition and slightly negative below transition. One should keep in mind, however, that this behavior is model dependent. If the impedance is different from Eq. (6.215) or if  $\chi$  is not small compared with unity, this conclusion may change. Figure 6.35 shows the growth rates  $1/\tau^{(l)}$  versus  $\chi$  for  $l = 0, \pm 1, \pm 2$ , and  $\pm 3$ , assuming an air-bag beam and that the impedance is given by Eq. (6.215). Equation (6.216) gives only the linear portion of these curves for small  $\chi$ .

<sup>39</sup>Remember that  $W_0$  must be positive by the property of wake functions.

**Exercise 6.23** From Eq. (6.213), show that

$$\sum_{l=-\infty}^{\infty} \frac{1}{\tau^{(l)}} = 0. \quad (6.217)$$

This result is valid for arbitrary impedance and arbitrary chromaticity. See footnote 6 of this chapter for the significance of Eq. (6.217).

**Exercise 6.24** The imaginary part of the impedance (6.215) gives rise to a mode frequency shift. Show that

$$\Delta\Omega^{(l)} = -\frac{Nr_0cW_0}{4\gamma T_0\omega_\beta} J_l^2(\chi). \quad (6.218)$$

All shifts are negative. If  $\chi = 0$ , the only mode that suffers a frequency shift is  $l = 0$ . Compare this  $\chi = 0$  result with the two-particle strong head-tail result shown in Figure 4.8. The beam becomes unstable when the  $l = 0$  mode frequency shifts by  $\omega_s$  and becomes equal to that of the  $l = -1$  mode. Estimate the strong head-tail instability threshold this way. Compare the result with that of the two-particle model, Eq. (4.46), and that of Exercise 6.25 below.

It may be instructive to examine the structure of Eqs. (6.216) and (6.218) for the  $l = 0$  mode, at least when  $\chi = 0$ . From Table 2.2, the wake force integrated over the accelerator circumference is  $\sim Ne^2W_0\langle x \rangle$ . For  $l = 0$ , the beam bunch acts as a rigid charge distribution, and this wake force can be interpreted as an equivalent quadrupole magnet of gradient

$$\frac{1}{B\rho} \frac{\partial B_y}{\partial x} \sim -\frac{Nr_0W_0}{\gamma C}. \quad (6.219)$$

The corresponding mode tune shift is given by Eq. (1.15):

$$\frac{\Delta\Omega^{(0)}}{\omega_0} \sim \frac{1}{4\pi} \int_0^C ds \beta_Z \frac{1}{B\rho} \frac{\partial B_y}{\partial x}, \quad (6.220)$$

where  $\beta_Z$  is the  $\beta$ -function at the location of the impedance; it is taken to be  $\omega_0 R / \omega_\beta$  in a smooth accelerator model. Equation (6.220) readily reproduces Eq. (6.218) for  $l = 0$ . Having established  $\Delta\Omega^{(0)}$ , the instability growth rate  $1/\tau^{(0)}$  in Eq. (6.216) is basically just a factor  $\chi$  times  $\Delta\Omega^{(0)}$ . This is because the instability comes from the phase lag between the bunch head and tail, and for small  $\chi$ , the phase factor  $e^{i\chi}$  gives an imaginary part of  $i\chi$ .

## Mode Coupling

As the beam intensity increases, the expression (6.188) breaks down. One has to consider the general case described by Eq. (6.183) and take into consideration the coupling among azimuthal modes. A mode is no longer approximately given by Eqs. (6.184–6.185). Instead, it has to be described as a linear mixture of all the unperturbed modes. This phenomenon has been referred to as “mode coupling,” “mode mixing,” “transverse turbulence,” and “strong head-tail” in the literature.<sup>40</sup> The associated instability mechanism has been illustrated by a two-particle model in Section 4.3.

Let us consider a broad-band impedance and  $\chi = 0$ . We mentioned before that there is no collective instability under these conditions for weak beams. At high intensities, however, the mode coupling effect can cause instability of the air-bag beam. To demonstrate this, Eq. (6.183) is written as

$$\det\left(\frac{\Omega - \omega_\beta}{\omega_s} I - M\right) = 0, \quad (6.221)$$

which has the same form as Eq. (6.144) except for a shift in  $\Omega$  by  $\omega_\beta$ . The matrix elements of  $M$  are

$$M_{ll'} = l\delta_{ll'} - i\frac{Nr_0c}{4\pi\gamma T_0\omega_\beta\omega_s} i^{l-l'} \int_{-\infty}^{\infty} d\omega Z_1^\perp(\omega) J_l\left(\frac{\omega\hat{z}}{c}\right) J_{l'}\left(\frac{\omega\hat{z}}{c}\right). \quad (6.222)$$

The matrix  $M$  has the following form:

$$M = \begin{bmatrix} & & & & \\ & \cdots & & & \\ & & \cdots & & \\ & & & 2 + I & R & I & R & I \\ & & & R & 1 + I & R & I & R \\ & & & I & R & I & R & I \\ & & & R & I & R & -1 + I & R \\ & & & I & R & I & R & -2 + I \\ & & & & & & & \\ & & & & & & & \cdots \\ & & & & & & & \cdots \end{bmatrix}. \quad (6.223)$$

The symbols are the same as those used in Eq. (6.146). The elements of  $M$  are all real. Unlike Eq. (6.146), the  $l = 0$  row does not vanish.

A mode coupling instability was already hinted at in Exercise 6.24, although we ignored the off-diagonal matrix elements there. This exercise will be continued in Exercise 6.25. Here we will introduce another example.

<sup>40</sup>R. D. Kohaupt, *Proc. 11th Int. Conf. High Energy Accelerators*, Geneva, 1980, p. 562; K. Satoh and Y. Chin, *Nucl. Instr. Meth.* **207**, 309 (1983).

Take the impedance

$$Z_1^\perp(\omega) = \frac{2c}{b^2\omega_0} R_0 \left| \frac{\omega_0}{\omega} \right|^{3/2} [\operatorname{sgn}(\omega) + i]. \quad (6.224)$$

This impedance is related to the longitudinal impedance (6.147) through Eq. (2.107) and gives the diffraction model (2.145) if  $R_0$  is properly chosen. The corresponding transverse wake function is

$$W_l(z) = -\frac{8R_0}{b^2} \sqrt{\omega_0 c} |z|^{1/2}. \quad (6.225)$$

Substituting Eq. (6.224) into Eq. (6.222), we find

$$M_{ll'} = l\delta_{ll'} + \frac{\Upsilon'}{2} C_{ll'}, \quad (6.226)$$

where  $C_{ll'}$  are the coefficients given by Eq. (6.149) and  $\Upsilon'$  is a dimensionless parameter defined by

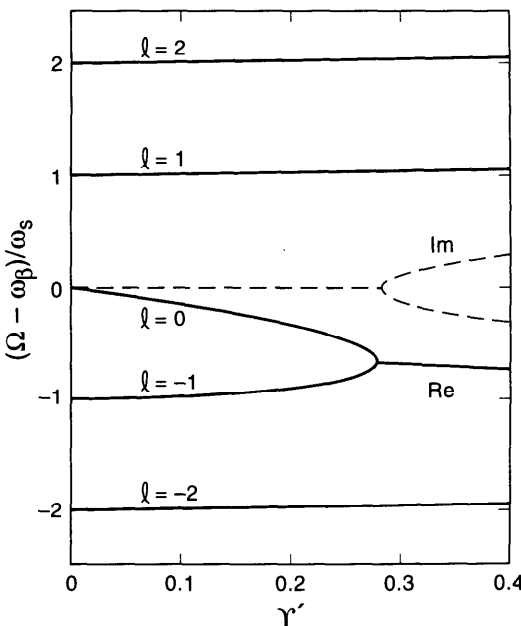
$$\Upsilon' = \frac{Nr_0 c^2 R_0}{\gamma T_0 \omega_\beta \omega_s b^2} \sqrt{\frac{\hat{z}}{cT_0}}. \quad (6.227)$$

Figure 6.36 shows the results of a numerical calculation using Eq. (6.221) and the matrix (6.226). The eigenvalues  $(\Omega - \omega_\beta)/\omega_s$  are plotted versus the transverse strength parameter  $\Upsilon'$  for several modes. At  $\Upsilon' = 0$ , the mode frequencies are located at  $\omega_\beta, \omega_\beta \pm \omega_s, \omega_\beta \pm 2\omega_s, \dots$ . As  $\Upsilon'$  increases, the mode frequencies shift, and at  $\Upsilon' \approx 0.28$ , the two modes  $l = 0$  and  $l = -1$  become degenerate. At this value of  $\Upsilon'$ , the other modes have shifted only slightly. Further increase of  $\Upsilon'$  renders the beam unstable.

The parameter  $\Upsilon'$  can be related to the longitudinal strength parameter  $\Upsilon$ , Eq. (6.150), by

$$\Upsilon' = \Upsilon \left( \frac{\hat{z}}{b} \right)^2 \frac{\omega_s}{\eta \omega_\beta}. \quad (6.228)$$

As a rough estimate of whether the longitudinal or the transverse instabilities dominate the beam behavior, we can compare  $\Upsilon$  and  $\Upsilon'$  relative to their respective threshold values  $\Upsilon_{th} = 1.45$  and  $\Upsilon'_{th} = 0.28$ . If  $\Upsilon'/\Upsilon \gtrsim 0.28/1.45 \approx 0.2$ , the limiting beam instability is probably transverse, while if  $\Upsilon'/\Upsilon \lesssim 0.2$ , the longitudinal instability may have a lower threshold.



**Figure 6.36.** Transverse mode frequencies  $(\Omega - \omega_\beta)/\omega_s$  versus the parameter  $\Upsilon'$  for an air-bag beam with the impedance (6.224). The instability threshold is located at  $\Upsilon'_{th} \approx 0.28$ , where the modes  $l = 0$  and  $-1$  become degenerate. The dashed curves give the imaginary part of the mode frequencies for  $l = 0$  and  $l = -1$ .

As an alternative expression to Eq. (6.228), one can write

$$\frac{\Upsilon'}{\Upsilon} = \frac{2\sigma_z\sigma_\delta\beta_Z}{b^2}, \quad (6.229)$$

where  $\sigma_z$  is the rms bunch length,  $\sigma_\delta = \omega_s\sigma_z/\eta c$  is the rms relative energy spread, and  $\beta_Z$  is the  $\beta$ -function at the location of the transverse impedance. Equation (6.229) is to be compared with Eq. (5.138) derived using unbunched beams. Note that short bunches tend to be more unstable longitudinally, and long bunches transversely. Given the design of an electron storage ring,  $\sigma_z$  and  $\sigma_\delta$  are proportional to the operating beam energy. It follows that the transverse instability tends to be more important at high operating energies, and the longitudinal instability at low energies.

In the present example, the beam is found to be more stable transversely for shorter bunches, since  $\Upsilon' \propto \hat{z}^{1/2}$ . Although this tendency is generally true, its functional dependence is model dependent. For a different impedance,  $\Upsilon'$  would depend on  $\hat{z}$  differently. The scaling with respect to the other parameters, on the other hand, is more robust. For example, for a given accelerator and given bunch length  $\hat{z}$ , the threshold beam intensity

obeys the scaling property

$$N_{\text{th}} \propto \omega_s \omega_\beta E, \quad (6.230)$$

or alternatively,

$$I_{\text{th}} \propto \frac{\nu_s E}{\beta_Z}, \quad (6.231)$$

where  $I_{\text{th}}$  is the threshold beam current, and  $\nu_s = \omega_s/\omega_0$  is the synchrotron tune.

**Exercise 6.25** Show that for an air-bag beam and an impedance (6.215), the matrix  $M$  has the elements

$$M_{ll'} = l\delta_{ll'} + \frac{\Upsilon}{\pi^2} \begin{cases} \frac{4}{\pi(l^2 - l'^2)} & \text{if } l - l' \text{ is odd,} \\ -\pi\delta_{l0}\delta_{l'0} & \text{if } l - l' \text{ is even,} \end{cases} \quad (6.232)$$

where  $\Upsilon$  is the same parameter defined by Eq. (4.42) when we studied the two-particle model using the same impedance. Using the two-particle model, we obtained Figure 4.8. Using the matrix  $M$  above, we obtain Figure 6.37. Note that the two-particle model greatly exaggerates the effect of wake field on the higher order modes.

In Figures 6.36–6.37, the  $l = 0$  mode frequency shifts downward as the beam intensity increases from zero. This is a general behavior for short bunches. The transverse wake force produced by an off-axis beam has the polarity that deflects the beam further away from the pipe axis. This force acts as a defocusing force for the rigid beam mode ( $l = 0$ ), and as a result, its mode frequency shifts downward. Such a downshift of the betatron frequency is routinely observed in electron accelerators.<sup>41</sup> As discussed following Eq. (4.52), the measurement of the betatron frequency shift with beam intensity provides one of the most available handles on the impedance.

In general, the mode frequency shift is determined by the overlap integral between the mode spectrum and  $\text{Im } Z_1^\perp$ . For a resonator impedance and  $\omega_\xi = 0$ , the  $l = 0$  mode samples mainly the low frequency region where  $\text{Im } Z_1^\perp < 0$ . [See Figure 6.33(a).] For a short bunch, the  $l = \pm 1$  mode spectra extend to high frequencies and sample mainly the region where  $\text{Im } Z_1^\perp > 0$ , and their mode frequencies shift up. Instability results when the frequencies

<sup>41</sup>R. D. Kohaupt, IEEE Trans. Nucl. Sci. **NS-26**, 3480 (1979); J. Le Duff et al., Proc. 11th Int. Conf. High Energy Accel., Geneva, 1980, p. 566; D. Rice et al., IEEE Trans. Nucl. Sci. **NS-28**, 2446 (1981); M. P. Level et al., IEEE Trans. Nucl. Sci. **NS-32**, 2215 (1985); M. P. Level, Proc. 4th Advanced ICFA Beam Dynamics Workshop, KEK, 1990, KEK Report 90-21, p. 101.

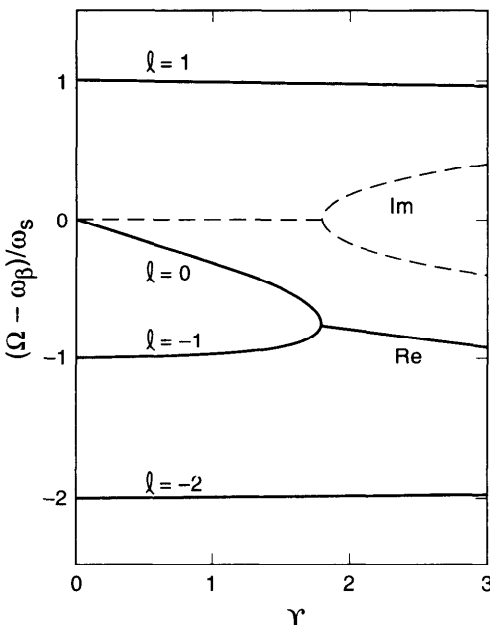


**Figure 6.37.** Transverse mode frequencies  $(\Omega - \omega_\beta) / \omega_s$  versus the parameter  $\gamma$  for an air-bag beam and an impedance (6.215). The instability threshold is located at  $\gamma_{th} \approx 1.8$ . At the threshold, the  $l = 0$  mode frequency has shifted down from  $\omega_\beta$  by  $\sim 0.8\omega_s$ . The dashed curves are the imaginary part of the mode frequencies for  $l = 0$  and  $l = -1$ . This graph can be compared with Figure 4.8 for the two-particle model.

of the  $l = 0$  mode (which shifts down) and the  $l = -1$  mode (which shifts up) meet. These tendencies were reflected in Figure 6.2, which assumed a short bunch. For a long bunch, the  $l = \pm 1$  modes sample the low frequency region and their mode frequencies shift down just like that of the  $l = 0$  mode.

Recall that in the longitudinal case, as the beam becomes unstable, the bunch lengthens essentially without losing beam particles. The same does not happen in the transverse case. As soon as the threshold is crossed, beam particles will be lost, at least according to the linearized theory.

Aside from this apparent difference, however, the transverse and longitudinal instabilities are remarkably parallel. For each longitudinal effect, there is most likely a transverse analogy, and vice versa. For example, we have mentioned that the Robinson instability, originally introduced as a longitudinal effect, has its transverse analog, and that at high beam intensities, both the longitudinal and the transverse cases have the mode coupling instabilities.

One may ask then whether there is a head-tail instability in the longitudinal case and whether there is a transverse counterpart of the potential-well

distortion. The answer to both questions is yes. The *longitudinal head-tail instability*, first suggested by Hereward<sup>42</sup> and possibly observed at the CERN SPS,<sup>43</sup> results from the fact that the phase slippage factor  $\eta$  is not strictly a constant; it depends on the instantaneous energy error  $\delta$  just as the betatron frequency  $\omega_\beta$  does. The longitudinal beam distribution then acquires a head-tail phase, and instability may arise as a result.

One transverse analog of the potential-well distortion has been introduced in Chapter 1, namely, the space charge effect that led to the Laslett tune shifts. Another, perhaps less obvious, effect occurs when the trajectory of the unperturbed beam is off the accelerator pipe axis. Such a displacement of the unperturbed beam may result from a closed orbit error caused by imperfections of the accelerator magnets. The transverse wake field associated with the closed orbit error deflects the bunch tail by a fixed amount every time the beam passes by the impedance. The result is that the beam is distorted into a banana shape and this distortion is static in time when observed at a fixed location.<sup>44</sup>

**Exercise 6.26** Consider a beam bunch stored in a circular accelerator with a closed orbit distortion so that it passes by a broad-band impedance  $Z_1^\perp$  with a transverse displacement  $y_0$ . The head of the bunch follows the distorted closed orbit. The bunch tail, on the other hand, acquires an additional static wake induced kick  $\Delta y'(z)$ , given by Eq. (3.49), every time the bunch passes by the impedance. The bunch tail therefore follows a closed orbit that differs from that of the bunch head by an amount of the order of  $\sqrt{\beta_Z \beta(s)} \Delta y'(z)$ , where  $\beta_Z$  and  $\beta(s)$  are respectively the  $\beta$ -functions at the locations of the impedance and the observation point. The beam becomes banana-shaped in the  $y$ - $z$  plane. Give an approximate expression of the tilt angle between bunch head and bunch tail in terms of the quantity  $Z_0^{\parallel}/n$ .

In the most general description, Eq. (6.76) for  $m = 0$  and (6.179) for  $m = 1$  are part of a grand scheme in which modes with different  $m$ 's and  $l$ 's are all coupled together. To study the beam instability, one then has to solve the eigenvalue problem of a doubly infinite matrix (ignoring radial modes)—if the vacuum pipe were not axially symmetric, this matrix would have been triply infinite—of which we have separately studied only the  $m = 0$  and the  $m = 1$  components. In reality, as long as the mode frequency shifts are small compared with  $\omega_\beta$  (modulo  $\omega_0$ ), the matrix degenerates into blocks, each with a distinct value of  $m$ . If the mode frequency shifts are small even

<sup>42</sup>H. Hereward, Rutherford Lab. Reports RL-74-062, EPIC/MC/48 (1974), and RL-75-021, EPIC/MC/70 (1975). See also B. Chen and A. W. Chao, SSCL Report 606 (1992).

<sup>43</sup>D. Boussard and T. Linnecar, Proc. 2nd Euro. Part. Accel. Conf., Nice, 1990, p. 1560.

<sup>44</sup>A. W. Chao and S. Kheifets, IEEE Trans. Nucl. Sci. NS-30, 2571 (1983).

compared with  $\omega_s$ , further degeneracy occurs and indeed we obtain results like Eqs. (6.83) and (6.188).

## 6.8 MULTIPLE BUNCHES

In the previous sections, we have assumed that there is only one bunch of particles in the accelerator. We will now show that with a slight modification, the analysis can be extended to a beam of  $M$  bunches, provided the bunches are equally spaced and equally populated. The macroparticle treatment of multiple bunches was given in Section 4.6.

Consider first the longitudinal instabilities. A mode of the multibunch beam is described by

$$\psi_n(r, \phi, s) = \psi_0(r) + \psi_1(r, \phi) \exp\left[-i\Omega\left(\frac{s}{c} - \frac{nT_0}{M}\right)\right] \exp\left(2\pi i \frac{\mu n}{M}\right),$$

$$n = 0, 1, \dots, M-1, \quad (6.233)$$

where  $\psi_n$  is the distribution of the  $n$ th bunch observed at a fixed location  $s$ ,<sup>45</sup>  $\psi_0$  is the unperturbed distribution normalized by Eq. (6.78),  $N$  is the number of particles per bunch,  $\psi_1$  is the perturbation distribution (the same for all bunches), and  $\mu$  is the multibunch mode index, which assumes the values  $0, 1, \dots, M-1$ . Successive bunches oscillate with a phase difference of  $2\pi\mu/M$  if the phases are compared at a given time. The mode number  $\mu$  and the phase factor  $\exp(2\pi i \mu n/M)$  have been introduced in Section 4.6.

We will concentrate on the reference bunch, for which  $n = 0$ . The retarding wake voltage seen by particles in this bunch is

$$V(z, s) = e \int_{-\infty}^{\infty} dz' \sum_{k=-\infty}^{\infty} \rho_1(z') \sum_{n=0}^{M-1} W_0\left(z - z' - kC - \frac{nC}{M}\right)$$

$$\times \exp\left[-i\Omega\left(\frac{s}{c} - \frac{nT_0}{M} - kT_0\right) + 2\pi i \frac{\mu n}{M}\right]. \quad (6.234)$$

Compared with Eq. (6.66), this expression contains an additional summation over the  $M$  bunches. The quantity  $\rho_1$  is the projection of  $\psi_1$  onto the  $z$ -axis defined in Eq. (6.64). In the frequency domain, Eq. (6.234) reads

$$V(z, s) = \frac{Me}{T_0} e^{-i\Omega s/c} \sum_{p=-\infty}^{\infty} \tilde{\rho}_1(\omega') e^{i\omega' z/c} Z_0^{\parallel}(\omega'), \quad (6.235)$$

<sup>45</sup> $\psi_n$  is not the snapshot distribution. This explains the extra time-of-flight factor  $\exp(i\Omega n T_0/M)$  in Eq. (6.233).

where

$$\omega' = pM\omega_0 + \mu\omega_0 + \Omega. \quad (6.236)$$

Compared with Eq. (6.67), Eq. (6.235) has an additional factor of  $M$  in front, but the summation over  $p$  is  $M$  times more sparse.

We then follow the procedures of Sections 6.3 to 6.5 to linearize and analyze the Vlasov equation for the  $n = 0$  bunch. For a water-bag beam, for example, we obtain again Eq. (6.83) for weak beams, with the modifications

$$\sum_{p=-\infty}^{\infty} (\ )_{\omega'=p\omega_0+\Omega} \rightarrow M \sum_{p=-\infty}^{\infty} (\ )_{\omega'=pM\omega_0+\mu\omega_0+\Omega}. \quad (6.237)$$

This modification is a general rule for obtaining multibunch results. The same observation was made in Section 4.6.

As discussed following Eq. (4.128), the multibunch Robinson instability occurs mainly for the  $\mu = 0$  mode, and the corresponding growth rate is proportional to the total beam current, not the single-bunch beam current.

For a broad-band impedance (wake range shorter than bunch spacing), the summation over  $p$  is replaced by an integral. The replacement removes the factor of  $M$  in front, and one obtains results identical to the single-bunch results. This is expected, because having a broad-band impedance means the wake force is short ranged and instability is a result of a local interaction among particles in a single bunch.

Treatment of the transverse motion of a multibunch beam is again very similar. The  $n$ th bunch executes the motion

$$\psi_n = f_0(q)g_0(r) + f_1(q, \theta)g_1(r, \phi)\exp\left[-i\Omega\left(\frac{s}{c} - \frac{nT_0}{M}\right)\right]\exp\left(i2\pi\frac{\mu n}{M}\right), \quad (6.238)$$

where  $f_1$  is given by Eq. (6.168). The dipole deflecting force is

$$\begin{aligned} F_y(z, s) = & -\frac{e^2 D}{c T_0} \sum_{k=-\infty}^{\infty} \int_{-\infty}^{\infty} dz' \rho_1(z') \sum_{n=0}^{M-1} \exp\left[-i\frac{\Omega}{c}\left(s - kC - \frac{nC}{M}\right)\right] \\ & \times \exp\left(i2\pi\frac{\mu n}{M}\right) W_1\left(z - z' - kC - \frac{nC}{M}\right). \end{aligned} \quad (6.239)$$

In terms of impedance, we have

$$F_y(z, s) = i \frac{Me^2 D}{c T_0^2} e^{-i\Omega s/c} \sum_{p=-\infty}^{\infty} \tilde{\rho}_1(\omega') e^{i\omega' z/c} Z_1^\perp(\omega'), \quad (6.240)$$

where  $\omega'$  is given by (6.236). The deflecting force therefore observes the rule (6.237). It follows that the mode frequency shifts and growth rates of the  $\mu$ th transverse multibunch mode can all be obtained from the single-bunch results by simply applying the substitution rule (6.237).

## 6.9 UNBUNCHED BEAMS

The discussion so far in this chapter has been for bunched beams. The Vlasov technique can also be applied to unbunched beams. The analysis for unbunched beams, including Landau damping, was given in Sections 5.3 and 5.4. In this section, we will content ourselves with a rederivation, using the Vlasov technique, the main results of Sections 5.3 and 5.4.

First consider the longitudinal case. For an unbunched beam, the single-particle equations of motion are

$$\dot{z} = -\eta c \delta \quad \text{and} \quad \dot{\delta} = -\frac{eV(z, t)}{ET_0}, \quad (6.241)$$

where the retarding voltage  $V(z, t)$  contains only the wake field contributions because there is no rf focusing. The Vlasov equation is

$$\frac{\partial \psi}{\partial t} - \eta c \delta \frac{\partial \psi}{\partial z} - \frac{eV(z, t)}{ET_0} \frac{\partial \psi}{\partial \delta} = 0. \quad (6.242)$$

Let us write the distribution  $\psi(z, \delta, t)$  as an unperturbed term plus an infinitesimal perturbation term,

$$\psi = g_0(\delta) + g_1(\delta) e^{in\Theta} e^{-i\Omega t}, \quad (6.243)$$

where  $n$  is the mode index, and

$$\Theta = \bar{\omega}_0 t + \frac{z}{R}. \quad (6.244)$$

Equations (6.243–6.244) follow from the fact that the quantity  $z$  is defined relative to a reference particle that circulates around the accelerator with the ideal revolution frequency  $\bar{\omega}_0 \equiv c/R$ . The distribution must then be periodic in  $\Theta$  with period  $2\pi$ .

For an unbunched beam, the unperturbed distribution  $g_0$  is a function only of  $\delta$ , normalized by

$$\int_{-\infty}^{\infty} d\delta g_0(\delta) = \frac{N}{2\pi R}. \quad (6.245)$$

The unperturbed uniform beam does not generate longitudinal wake forces. The wake retarding voltage is given by

$$\begin{aligned} V(z, t) &= e \int_{\Theta}^{\infty} R d\Theta' \rho_1 \left( \Theta, t - \frac{R\Theta' - R\Theta}{c} \right) W'_0(R\Theta - R\Theta') \\ &= e \int_{-\infty}^{\infty} d\delta g_1(\delta) \times \int_{\Theta}^{\infty} R d\Theta' e^{in\Theta} e^{-i\Omega[t-(R\Theta'-R\Theta)/c]} W'_0(R\Theta - R\Theta'). \end{aligned} \quad (6.246)$$

In terms of impedance, we have

$$V(z, t) = e c e^{in\Theta} e^{-i\Omega t} Z_0^{\parallel}(\Omega) \int_{-\infty}^{\infty} d\delta g_1(\delta). \quad (6.247)$$

Substitute Eqs. (6.243) and (6.247) into Eq. (6.242) and linearize the result with respect to  $g_1$ . We find

$$g_1(\delta) = i \frac{r_0 c}{\gamma T_0} \frac{g'_0(\delta)}{\Omega - n\bar{\omega}_0(1 - \eta\delta)} Z_0^{\parallel}(\Omega) \int_{-\infty}^{\infty} d\delta' g_1(\delta'). \quad (6.248)$$

Integrate Eq. (6.248) over  $\delta$  on both sides. The factor  $\int d\delta' g_1(\delta')$  drops out. We obtain a dispersion relation

$$1 = i \frac{r_0 c}{\gamma T_0} Z_0^{\parallel}(\Omega) \int d\delta \frac{g'_0(\delta)}{\Omega - n\bar{\omega}_0(1 - \eta\delta)}. \quad (6.249)$$

We learned from the discussions of Landau damping in Chapter 5 that, given the impedance  $Z_0^{\parallel}$  and the unperturbed energy spectrum  $g_0(\delta)$  of the beam, Eq. (6.249) can be used to predict the instability threshold boundary by attaching an infinitesimal positive imaginary part to  $\Omega$ , i.e.,  $\Omega \rightarrow \Omega + i\epsilon$ .

Equation (6.249) is our main result. We can also cast it in a different form as follows. The revolution frequency of a particle with energy error  $\delta$  is

$$\omega_0 = \bar{\omega}_0(1 - \eta\delta). \quad (6.250)$$

Let the  $\omega_0$  spectrum of the beam be  $\rho(\omega_0)$ , normalized by  $\int d\omega_0 \rho(\omega_0) = 1$ . Then we have

$$g_0(\delta) = \frac{N|\eta|\bar{\omega}_0}{2\pi R} \rho(\omega_0). \quad (6.251)$$

Changing variable from  $\delta$  to  $\omega_0$  yields another form of the dispersion

relation,

$$1 = -i \frac{2\pi N r_0 \eta}{\gamma T_0^3} Z_0^{\parallel}(\Omega) \int d\omega_0 \frac{\rho'(\omega_0)}{\Omega - n\omega_0}, \quad (6.252)$$

which is just the result obtained in Eq. (5.118). All results subsequent to Eq. (5.118) then follow. We have thus rederived the longitudinal instability conditions discussed in Section 5.4.

The transverse  $m = 1$  case is similar, except for the complication due to the head-tail phase. If we ignore the longitudinal component of the  $m = 1$  wake force, the Vlasov equation reads

$$\frac{\partial \psi}{\partial t} + \omega_\beta(1 + \xi\delta) \frac{\partial \psi}{\partial \theta} + \frac{c}{E} F_y(z, t) \frac{\partial \psi}{\partial p_y} - c\eta\delta \frac{\partial \psi}{\partial z} = 0. \quad (6.253)$$

The beam distribution  $\psi(q, \theta, z, \delta, t)$  is written as

$$\psi = f_0(q) g_0(\delta) + f_1(q, \theta) g_1(\delta) e^{in\Theta} e^{i\omega_\xi(z + \eta\delta ct)/c} e^{-i\Omega t}, \quad (6.254)$$

where  $\omega_\xi = \xi\omega_\beta/\eta$  is the head-tail frequency. In Eq. (6.254) we have adopted the polar coordinates  $(q, \theta)$  for the transverse phase space and the Cartesian coordinates  $(z, \delta)$  for the longitudinal phase space. Since the distribution is the one observed at a fixed location, the head-tail phase depends on the longitudinal position at a previous time  $z - \dot{z}t = z + \eta\delta ct$  for a particle with energy error  $\delta$ .

The solution for  $f_1$  is given by Eq. (6.168). The transverse deflecting wake force is

$$F_y = -\frac{De^2}{cT_0} \int_{-\infty}^{\infty} d\delta g_1(\delta) \int_{\Theta}^{\infty} R d\Theta' e^{in\Theta + i\omega_\xi(z + \eta\delta ct)} \\ \times e^{-i\Omega(t - (R\Theta' - R\Theta)/c)} W_1(R\Theta - R\Theta'), \quad (6.255)$$

or in terms of impedance,

$$F_y = i \frac{De^2}{T_0} e^{in\Theta + i\omega_\xi(z + \eta\delta ct)} e^{-i\Omega t} Z_1^{\perp}(\Omega) \int_{-\infty}^{\infty} d\delta g_1(\delta). \quad (6.256)$$

Substituting Eqs. (6.168), (6.254), and (6.256) into Eq. (6.253) gives

$$g_1(\delta) = -i \frac{r_0 c^2}{2\gamma T_0 \omega_\beta} Z_1^{\perp}(\Omega) \frac{g_0(\delta)}{\Omega - n\bar{\omega}_0(1 - \eta\delta) - \omega_\beta(1 + \xi\delta)} \int_{-\infty}^{\infty} d\delta' g_1(\delta'). \quad (6.257)$$

An integration over  $\delta$  then yields the dispersion relation

$$1 = -i \frac{r_0 c^2}{2\gamma T_0 \omega_\beta} Z_1^\perp(\Omega) \int d\delta \frac{g_0(\delta)}{\Omega - n\bar{\omega}_0(1 - \eta\delta) - \omega_\beta(1 + \xi\delta)}. \quad (6.258)$$

The only effect of the chromaticity  $\xi$  is to introduce an extra term in the denominator of the integrand on the right hand side. With a  $\delta$ -function energy distribution,  $g_0(\delta) = N\delta(\delta)/2\pi R$ , Eq. (6.258) reduces to Eqs. (5.77–5.78). Otherwise, it describes the Landau damping effect due to an energy spread of the beam.

Changing variable from  $\delta$  to  $\omega \equiv \omega_\beta - (n\bar{\omega}_0\eta - \xi\omega_\beta)\delta$ , and defining  $\rho(\omega)$  to be the spectrum in  $\omega$ , normalized by  $\int d\omega \rho(\omega) = 1$ , we have

$$g_0(\delta) = \frac{N| - n\eta\bar{\omega}_0 + \xi\omega_\beta |}{2\pi R} \rho(\omega) \quad (6.259)$$

and a new dispersion relation

$$1 = -i \frac{Nr_0 c}{2\gamma T_0^2 \omega_\beta} Z_1^\perp(\Omega) \int d\omega \frac{\rho(\omega)}{\Omega - n\bar{\omega}_0 - \omega}, \quad (6.260)$$

which is the same result obtained in Eq. (5.84). We have thus reproduced Section 5.3.

In passing, we have also explicitly shown that the transverse Landau damping is provided by the spread in the combined quantity  $n\omega_0 + \omega_\beta$ , as asserted in Eq. (5.92). Equation (6.260) is more general than Eq. (6.258) in that the spread in  $\omega$  does not have to come from chromatic sources. A spread in  $\omega_\beta$ , for instance, can also be incorporated.

As an application of Eq. (6.258), consider a beam with a Lorentz spectrum in  $\delta$ ,

$$g_0(\delta) = \frac{N\Delta\delta}{2\pi^2 R} \frac{1}{\delta^2 + \Delta\delta^2}. \quad (6.261)$$

The dispersion relation can be solved to give the complex mode frequency shift

$$\Omega - n\bar{\omega}_0 - \omega_\beta = -i \frac{Nr_0 c}{2\gamma T_0^2 \omega_\beta} Z_1^\perp(n\bar{\omega}_0 + \omega_\beta) - i\Delta\delta| - n\bar{\omega}_0\eta + \xi\omega_\beta |, \quad (6.262)$$

where we have assumed the perturbation is weak, so that the impedance is evaluated at the unperturbed frequency  $\Omega = n\bar{\omega}_0 + \omega_\beta$ .

The beam is stable if the imaginary part of  $\Omega$  is negative, or

$$-\frac{Nr_0c}{2\gamma T_0^2\omega_\beta} \operatorname{Re} Z_1^\perp(n\bar{\omega}_0 + \omega_\beta) < \Delta\delta | -n\bar{\omega}_0\eta + \xi\omega_\beta|. \quad (6.263)$$

This result is consistent with Eq. (5.88). A sufficient (but not necessary) condition for beam stability is  $\operatorname{Re} Z_1^\perp(n\bar{\omega}_0 + \omega_\beta) > 0$ , which in turn is satisfied if  $n\bar{\omega}_0 + \omega_\beta > 0$  according to Eq. (2.106). The general fact that the collective mode frequency,  $\operatorname{Re} \Omega$ , is unaffected by Landau damping for a Lorentz spectrum is also evident from Eq. (6.262).

The potentially most dangerous situation occurs when Landau damping is least effective, i.e., when  $-n\bar{\omega}_0\eta + \xi\omega_\beta \approx 0$ . This occurs for the mode with index

$$n \approx \frac{\xi\omega_\beta}{\eta\bar{\omega}_0}. \quad (6.264)$$

It would be desirable to arrange the parameters in such a way that this mode is naturally damped without Landau damping. As just mentioned, this can be accomplished by having  $n\bar{\omega}_0 + \omega_\beta > 0$ , where  $n$  is given by Eq. (6.264). This requires

$$\frac{\xi}{\eta} + 1 > 0. \quad (6.265)$$

The condition (6.265) can be satisfied by arranging the chromaticity  $\xi$  to have the same sign as the slippage factor  $\eta$ , i.e.,  $\xi > 0$  above transition and  $< 0$  below transition. This feature has been mentioned in connection with Eq. (5.93).

Equation (6.263) can be rewritten as

$$-\operatorname{Re} Z_1^\perp(n\bar{\omega}_0 + \omega_\beta) < Z_0 \frac{2\pi R\gamma| -n\eta + \xi\nu_\beta |}{Nr_0\beta_Z} \Delta\delta, \quad (6.266)$$

where  $Z_0 = 4\pi/c = 377$   $\Omega$ ,  $\nu_\beta = \omega_\beta/\omega_0$ , and  $\beta_Z$  is the  $\beta$ -function at the location of the impedance. Equation (6.266) is the equivalent of the expression (5.93) for a Lorentz spectrum.

The beam is stable if the imaginary part of  $\Omega$  is negative, or

$$-\frac{Nr_0c}{2\gamma T_0^2\omega_\beta} \operatorname{Re} Z_1^\perp(n\bar{\omega}_0 + \omega_\beta) < \Delta\delta | -n\bar{\omega}_0\eta + \xi\omega_\beta|. \quad (6.263)$$

This result is consistent with Eq. (5.88). A sufficient (but not necessary) condition for beam stability is  $\operatorname{Re} Z_1^\perp(n\bar{\omega}_0 + \omega_\beta) > 0$ , which in turn is satisfied if  $n\bar{\omega}_0 + \omega_\beta > 0$  according to Eq. (2.106). The general fact that the collective mode frequency,  $\operatorname{Re} \Omega$ , is unaffected by Landau damping for a Lorentz spectrum is also evident from Eq. (6.262).

The potentially most dangerous situation occurs when Landau damping is least effective, i.e., when  $-n\bar{\omega}_0\eta + \xi\omega_\beta \approx 0$ . This occurs for the mode with index

$$n \approx \frac{\xi\omega_\beta}{\eta\bar{\omega}_0}. \quad (6.264)$$

It would be desirable to arrange the parameters in such a way that this mode is naturally damped without Landau damping. As just mentioned, this can be accomplished by having  $n\bar{\omega}_0 + \omega_\beta > 0$ , where  $n$  is given by Eq. (6.264). This requires

$$\frac{\xi}{\eta} + 1 > 0. \quad (6.265)$$

The condition (6.265) can be satisfied by arranging the chromaticity  $\xi$  to have the same sign as the slippage factor  $\eta$ , i.e.,  $\xi > 0$  above transition and  $< 0$  below transition. This feature has been mentioned in connection with Eq. (5.93).

Equation (6.263) can be rewritten as

$$-\operatorname{Re} Z_1^\perp(n\bar{\omega}_0 + \omega_\beta) < Z_0 \frac{2\pi R\gamma | -n\eta + \xi\nu_\beta |}{Nr_0\beta_Z} \Delta\delta, \quad (6.266)$$

where  $Z_0 = 4\pi/c = 377 \Omega$ ,  $\nu_\beta = \omega_\beta/\omega_0$ , and  $\beta_Z$  is the  $\beta$ -function at the location of the impedance. Equation (6.266) is the equivalent of the expression (5.93) for a Lorentz spectrum.